EOCENE TECTONIC CONTROLS ON RESERVOIR DISTRIBUTION

IN VLE196, BLOCK V, LAMAR FIELD, MARACAIBO BASIN, VENEZUELA

A Dissertation

by

BYEONGGOO CHOI

Submitted to the Office of Graduate Studies of
Texas A&M University
in partial fulfillment of the requirements for the degree of

DOCTOR OF PHILOSOPHY

August 2005

Major Subject: Geology

EOCENE TECTONIC CONTROLS ON RESERVOIR DISTRIBUTION

IN VLE196, BLOCK V, LAMAR FIELD, MARACAIBO BASIN, VENEZUELA

A Dissertation

by

BYEONGGOO CHOI

Submitted to the Office of Graduate Studies of
Texas A&M University
in partial fulfillment of the requirements for the degree of

DOCTOR OF PHILOSOPHY

Approved by:

Chair of Committee,	Joel S. Watkins
Committee Members,	Walter B. Ayers, Jr.
	Robert R. Berg
	William R. Bryant
	Steven L. Dorobek
	John H. Spang
Head of Department,	Richard L. Carlson

August 2005

Major Subject: Geology

ABSTRACT

Eocene Tectonic Controls on Reservoir Distribution in VLE196, Block V, Lamar Field, Maracaibo Basin, Venezuela. (August 2005)

Byeonggoo Choi, B.S., Korea University;

M.E., Hanyang University;

M.S., University of Aberdeen

Chair of Advisory Committee: Dr. Joel S. Watkins

Integrated interpretation of three-dimensional seismic and well-logging data reveals a prominent “pop-up” structure associated with the VLE 400 fault on the regional unconformity between the Eocene and Miocene in the VLE 196 field, Maracaibo basin, Venezuela. The VLE 400 fault family, an eastern splay of the left-lateral Icotea fault in the basin, played an important role in hydrocarbon migration and accumulation in the field. Hydrocarbons accumulated to the east of the fault but not to the west. The “pop-up” structure on the Eocene unconformity has a four-way dip closure, straddling the fault and extending to the west of the fault. Structures of the Misoa Formation, which is the main reservoir developed below the unconformity in the basin, differ from the structure of the unconformity. The structure of the Misoa Formation shows a tilted uplift of the eastern block of the fault dipping toward the east caused by thrust tectonic movements. Thrust movement and following strike-slip movements provided

additional accommodation space to the west of the fault and generated expanded thickness of Eocene sediments compared to the area east of the fault. The thickness of the Misoa Formation east and west of the fault shows no significant changes. Expanded sediments overlie the Misoa Formation in the western block in lateral contact with Misoa sediments eastern block act as a lateral seal.

Ductile movement of the Guasare Formation shale contributed to the lateral sealing of the fault against the reservoir rocks in the eastern block. Mobilization of the Guasare Formation modified the structure of overlying formations including the anticline of the Eocene unconformity.

The growth strata provide useful information of reactivation of existing faults, especially subtle movements which are not recognized by conventional seismic interpretation. Growth strata isochrons shows subtle reactivation of the VLE 400 fault family during Miocene time.

DEDICATION

To my parents

Love, Dream and Belief

ACKNOWLEDGMENTS

I would like to thank my committee chair, Dr. Watkins for his advice and guidance through the course of my study. I also want to thank to Dr. Ayers, Dr. Berg, Dr. Bryant, Dr. Dorobek, and Dr. Spang for acting as committee members. This dissertation has greatly benefited from their teaching during classes and editorial comments.

Thanks also to my colleagues and the department faculty and staff for making my time at Texas A&M University a great experience.

I also want to thank British Petroleum for providing me a Petroleum Corporation Fellowship and the Geology and Geophysics Department for a graduate teaching assistantship.

I am grateful to the Korea National Oil Corporation for providing me an opportunity to finish the course. I sincerely thank Mr. O.S. Yi and Mr. M.H. Yi. Thanks also to General Manager, Mr. H.G. Im and colleagues for their kind understanding of my absence during the study.

There are many Korean students who have helped our family to settle down in Texas. Owing to their help, I could concentrate on my study.

Finally, thanks to my mother, mother-in-law and father-in-law for their encouragement and to my wife, Jiyoung, for her patience and love.

TABLE OF CONTENTS

Page

Page

Page

LIST OF FIGURES

FIGURE Page

FIGURE Page

FIGURE Page

FIGURE Page

FIGURE Page

FIGURE Page

1. INTRODUCTION

The purpose of this study is to understand the relationships among structure, stratigraphy, tectonics and petroleum accumulation in one of the most prolific petroleum-producing basin in the world, Maracaibo basin. Its area is twenty percent of that of the North Sea, but the amount of oil in place is more than twice that of the North Sea, or about 261 billion barrels (Talukdar and Marcano, 1994). By volume, the Maracaibo basin is ten times as prolific as the North Sea. However, studies to date of the basin do not reveal the characteristics of the basin, its petroleum system and the basin evolution. A complicated history of changing stress orientation, sediment provenance, and lithology makes understanding tectonic controls of the structure and stratigraphy of the basin difficult.

Studies of two-dimensional (2-D) seismic data have revealed regional structural features (Lugo, 1991), and evaluation of recent three-dimensional (3-D) seismic data has revealed the detailed structural features of the basin (Link et al., 1996; Castillo, 2001; Escalona and Mann, 2003). One of the main structural

---

This dissertation follows the style and format of the Bulletin of the American Association of Petroleum Geologists.

elements of the basin disclosed by previous studies is a series of north-south striking, linear, left-lateral strike-slip faults such as the Urdaneta, the Icotea, the VLE 400 and the Pueblo Viejo faults that developed between the Oca to north and the Bocono right-lateral faults to south. Many oil and gas fields occur around the north-south striking faults, but their origins and roles for hydrocarbon trapping have rarely been studied. Understanding the regional geology and stratigraphy framework of the basin is essential to assess an oil-producing field that was generated by the complicated interaction between growing structures and sediment deposition related to thrust faulting in foreland basin systems that generated complex structural and stratigraphic features.

1.1. Objectives

The purposes of this study are to interpret 3-D seismic reflection data and wireline logging-data from the VLE196-Lamar field, Maracaibo basin, Venezuela and to establish a structural and stratigraphic framework, to identify the controls of the hydrocarbon distribution in the field, with emphasis on the movement of the VLE 400 fault family. Specific objectives are to: 1) determine the structural origin of an anticline “pop-up” straddling the VLE 400 fault family and the evolution of the VLE 400 fault family for its structural framework; 2) determine the role of “unnamed sediments” to the hydrocarbon trapping and controls of the hydrocarbon distribution in the field for the stratigraphic

framework, and 3) determine the role of structure and stratigraphy in hydrocarbon accumulation in the field by mapping individual strata and evaluating depositional trends.

1.2. Method of analysis

Thirty seven square kilometers of 3-D seismic data over the VLE 196-Lamar field and logs from 24 wells were available for the study. Most wells have gamma ray, resistivity and density, and a few wells have neutron and sonic. Schlumberger Geoframe 3.8 software was used for 3-D seismic interpretation and well-to-well correlation. For 3-D seismic interpretation, processed SEG-Y format seismic data were loaded into the workstation. During data loading, the original 32-bit data were scaled to 8-bit to reduce data volume without significant amplitude loss; usually 2 to 3 percent of amplitude was clipped out during data loading. The change of amplitude does not affect the quality of a seismic horizon amplitude map. For the quantitative evaluation, such as porosity, water saturation and sandstone percentage calculations from amplitude of the interpreted seismic horizons, 32-bit data are necessary for the accurate interpretation. Otherwise, 8-bit data are adequate for geological interpretation. A two-monitor UNIX workstation was used for hardware. Two monitors were useful for interpretation, because it is convenient to simultaneously display both a map-view window and a seismic-profile window.

Twelve seismic horizons were mapped and interpreted. Tops of the C-4 and C-5 sandstones were picked from well-to-seismic correlations; other stratal tops were picked on the basis of seismic facies and characteristics. The seismic horizons were picked from peaks of zero-phase data using manual or auto tracking methods depending on to the continuity of horizons. Every fifth seismic profile of inline and crossline (so-called "seed" lines) was interpreted, and then continuous seismic horizons were generated using auto horizon tracking in the volume. Auto tracking method was used where possible. Additional seed lines were interpreted where necessary.

After interpretation of seed lines of seismic horizons, each fault heave was measured and fault polygons were generated. Every inline of the Hz. 6 (the Eocene unconformity) was interpreted to reveal detailed structural features. Some cross lines were interpreted for the Hz. 6, but interpretation of every line generates a continuous horizon surface without cross-line interpretation. Amplitudes were also extracted. Amplitude displays were superimposed on the time structure maps and fault polygons. Isochron maps were generated using simple mathematics. Actually, this procedure does not represent true thickness if the two seismic horizons have structural dip. The thickness simply calculated by subtraction was directly used for an isochron map because it was adequate to show large scale thickness variation related to the tectonic movements.

1.3. Regional geology

The Maracaibo basin, located in western Venezuela is interpreted to be a foredeep in a foreland basin system, is bounded by orogenic belts on the northwest (Perija Range), on the southwest (Santander massif of Colombia), on the southeast (Merida (Venezuela) Andes), and on the northeast (Trujilo Range) (Parnaund et al., 1995; Castillo, 2001) (Figure 1-1). As a foreland basin, this basin is believed to have followed the general evolution stages (Figure 1-2) that provide favorable conditions for a petroleum system from source rocks to reservoir rocks (Cant and Stockmal, 1989), even though specific tectonic and evolution models have not been established.

1.3.1. The Maracaibo basin

The basin was created by rifting and formation of grabens and half-grabens trending northnortheast during the Jurassic period. The basin began to subside below sea level in the early stages of the Cretaceous (Lugo and Mann, 1995). Extensional tectonics continued through the early Late Cretaceous. A marine transgression correlated with eustatic sea-level changes occurred during the Cretaceous. A stable shallow-water carbonate platform developed over the basal trangressive clastic sediments during the late Cretaceous highstand of sea level (Lugo and Mann, 1995). The La Luna Formation, mainly consisting of shallow marine to deep marine carbonates alternating with shales, is the

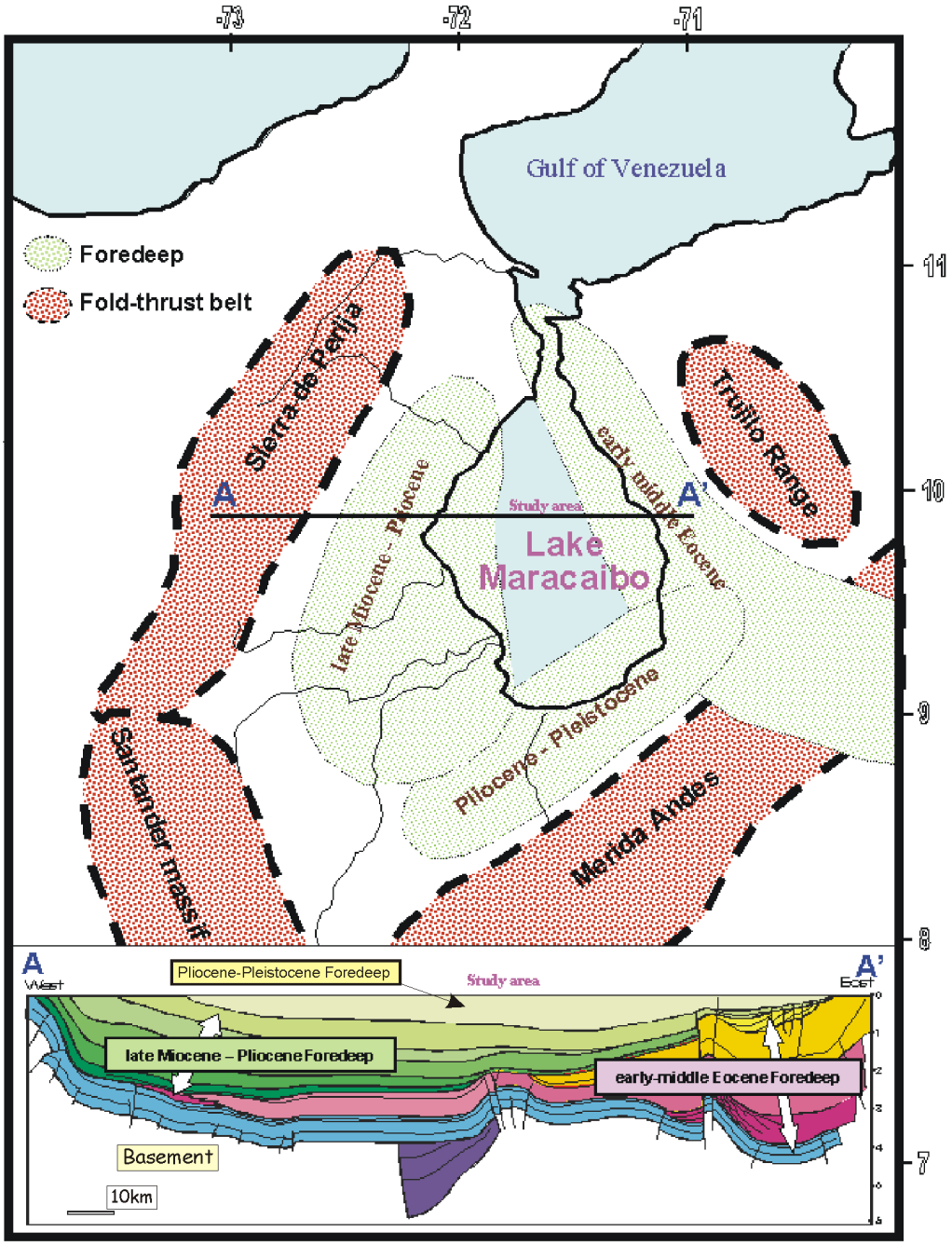

Figure 1-1. Fold-thrust belts and foredeep locations (modified from Parnaud et al., 1995; Castillo, 2001).

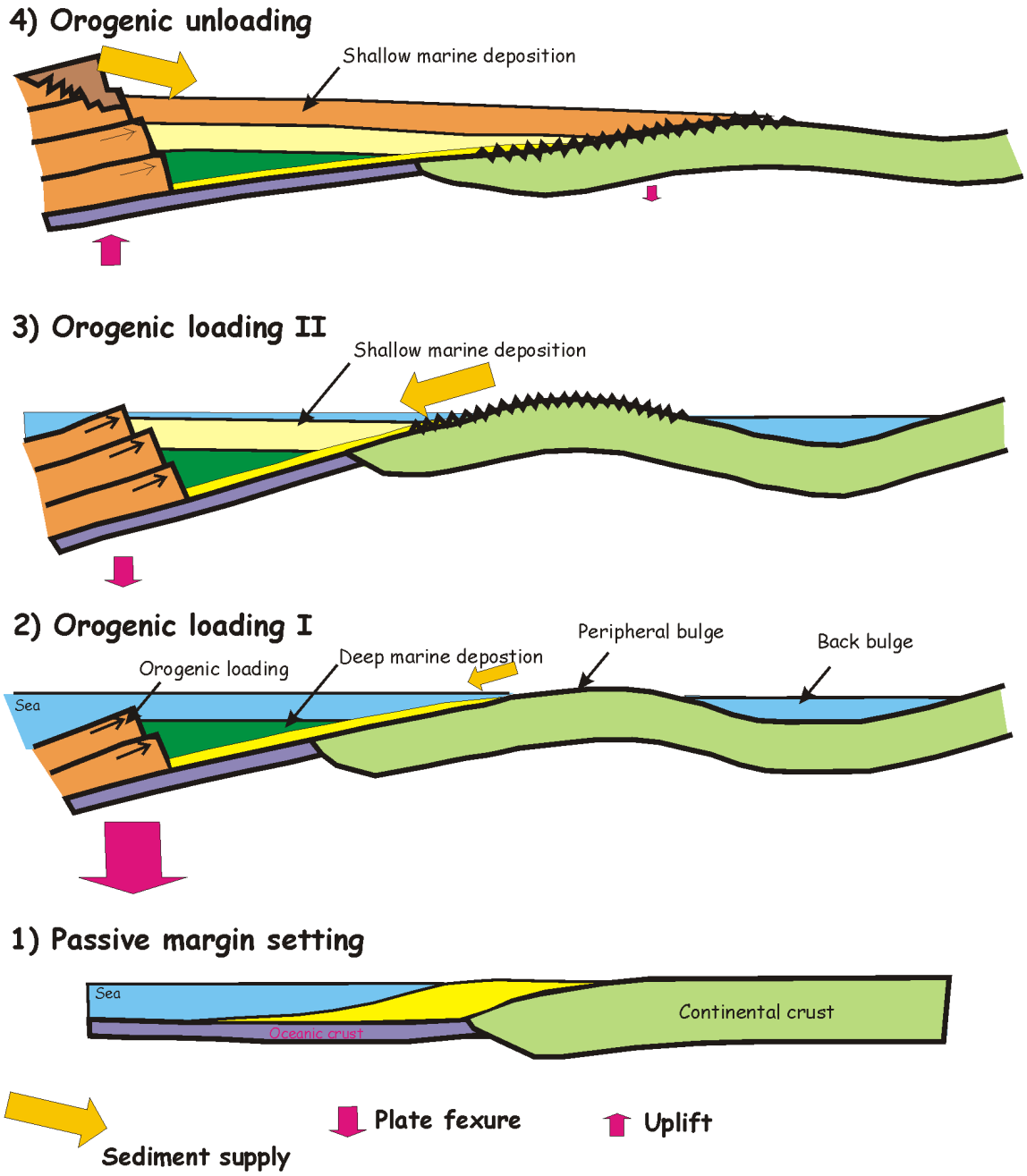

Figure 1-2. Genealized basin evolution model for the Maracaibo basin adapted from an idealized model for terrane accretion and the consequences for the adjacent continental margin (modified from Cant and Stockmal, 1989).

principal source rock in the basin (Lugo and Mann, 1995; Parnaund et al., 1995). Tectonic convergence, characterized by a series of collisions of Caribbean-derived terranes against the passive continental margin, changed the basin from a platform to a foreland basin. During the collisions, three different foreland basin systems developed (Figure 1-1). During the Eocene, up to 7,000 m of the Misoa Formation consisting of retrograde sequences of shallow marine clastic sediments was deposited (Parnaund et al., 1995). Next, Sierra de Perija and its foredeep formed during the late Miocene-Pliocene, and then, the Merida Andes and its foredeep formed during the Pliocene-Pleistocene (Castillo, 2001). The transpressive tectonic episode which provided structural traps in the basin occurred from the middle late Eocene to middle late Miocene and generated a faulted anticlinal trap for hydrocarbon accumulation (Parnaund et al., 1995).

1.3.2. The VLE 400 fault family

The VLE 400 fault family, an eastern splay of the well-known Icotea fault, and it is located between the Oca fault and the Bocono fault in Lake Maracaibo . The origin and displacement history of the VLE 400 fault family are controversial because of the structural complexities caused by the multiple tectonic events of the Maracaibo basin evolution. Very few studies have examined the VLE 400 fault family, especially from the view point of hydrocarbon exploration. The fault family, a key structural element, divides the field into eastern and western

blocks. Hydrocarbons accumulated to the east of the fault family but not to the west.

Faults generally in sedimentary basins can act as migration paths or as barriers to hydrocarbon flow, or both and contribute significant hydrocarbon potential for exploration and development (Smith, 1980; Watts, 1987). The VLE 400 fault family may be important in hydrocarbon migration and accumulation in the field.

1.3.3. Petroleum system of the Maracaibo basin

Table 1. Recovery efficiency of the Maracaibo basin comparison with North Sea

	Basin	Source			Hydrocarbon		
	Area (sq.km)	Thickness (m)	T.O.C. wt%	S.P.I tHC/sq.m	Generated (B.Bbl)	In-Place (B.Bbl)	Recovery Efficiency
NorthSea	260,000	300	6	15	54,000	125	0.23 %
Maracaibo	50,000	65	5.6	10	1,850	261	14 %
Ratio	0.19	0.67	0.93	0.67	0.034	2.1	61

Data sources:Talukdar and Marcano, 1994; Kelmme, 1994; Demaison and Huizinga, 1994

Petroleum system recovery efficiency is “the percent of ultimately conventionally recoverable BOE to the amount of BOE that could have been generated from a pod of active source rock if the source rock was completely spent” (Klemme, 1994). Klemme (1994) found that the highest petroleum system recovery efficiency was less than 1% in fourteen Jurassic source rocks.

The recovery efficiency is related to the migration from source to the charged reservoir rocks and to the leakage of the trapped hydrocarbons. The efficiency of migration, trapping and preservation in the Maracaibo basin is excellent in comparison with the North Sea. It is worthwhile to study what makes the high efficiency.

Usually, source rocks are the first consideration for prolific basins, but source rocks are not directly related with efficiency. Because efficiency is the percent of the trapped hydrocarbon to that generated from source rock, petroleum systems with poor source rocks can have high efficiency. The lithology of the Maracaibo basin that covers source rocks is mainly marine shale. It is believed that the migration path from the source rocks to the reservoir rocks is controlled by faults. Faults might act as the control method that concentrated hydrocarbon to the reservoir rock. Petroleum system recovery efficiency has to be considered including timing of hydrocarbon generation; therefore, it is four-dimensional (4-D) analysis.

1.3.4 Tectonic evolution

1) Rifting (Jurassic)

The Jurassic basin was created by rifting (Kulke, 1995). The basin began to subside below sea level in the early stages of Cretaceous deposition (Burke, 1988; Lugo, 1991). Jurassic rifting was caused by separation of the North and South American continents. The northnortheast structural trend influenced tectonic features during the subsequent Cretaceous and Cenozoic tectonic episodes (Ostos, 1990). Synrift clastic sediments were deposited in a continental setting locally sourced by volcanic activities.

2) Passive Margin (Early- to Late- Cretaceous)

A stable passive margin subsided through the Early- to Late- Cretaceous (Burke, 1988; Lugo, 1991). A marine transgression, which is correlated to the eustatic changes, occurred at the beginning of the Cretaceous. During the period of passive margin development, the basal trangressive clastics of the Rio Negro Formation were characterized by fluvial and alluvial fan facies (Audemard, 1992; Lugo and Mann, 1995). This deposit is restricted to the area west of the Icotea fault in the Maracaibo basin. A stable, shallow-water carbonate platform overlies the clastic deposits. During the Late Cretaceous highstand of sea level, the La Luna Formation, the basin source rock, was deposited in an anoxic environment in more than 150 m water depth (Talukdar and Marcano, 1993).

3) Active Margin Transition (Paleocene – Oligocene)

Tectonic convergence, characterized by a series of collisions and suturing of Caribbean-derived terranes against the previously passive continental margin occured from Paleocene to Oligocene (Audemard, 1992; Lugo and Mann, 1995). Flexural subsidence converted the stable platform into a series of foreland basins (Maguregui, 1990; Ambrose et al., 1995).

4) Foreland Basin (Eocene)

A Paleocene – Eocene foreland basin developed in the Lake Maracaibo area. The thickness of the Misoa Formation is up to 7,000 m and subdivided into the "B" and "C" sandstones according to sea level change (Maguregui, 1990; Ambrose et al., 1995). The "C" sands appear to be transgressive sediments with a mixed fluvial/tidal aggradational delta system in the lower section and tidal progradational delta system in the upper part of the section (Maguregui, 1990; Ambrose et. al., 1995). Above a regional flooding surface, progradational "B"sands and shale of the Pauji formation overlap the regional flooding surface.

5) Transpression (Late Eocene – Pliocene)

A transpressive tectonic episode which provided structural traps in the basin occurred in three stages: (1) middle late Eocene, the main movement; (2) late Eocene- early Miocene, relative quiescence with a sea-level fall; and (3) middle to late Miocene, rejuvenation (Lugo and Mann, 1995). During the middle

Miocene, large-scale compressional tectonism began (Burke, 1988; Audemard, 1992) which culminated during the Plio-Pleistocene. A marine environment persisted in the basin, but gradually changed to fresh water as the seas retreated toward the north (Audemard, 1992; Lugo and Mann, 1995).

1.3.5. Foreland basin models of the Maracaibo basin

The Eocene sediments in the Maracaibo basin were deposited in the foreland basin, according to the deposit of wedge shape geomorphology and orogenic belts. DeCelles and Giles (1996) suggested a new term of a foreland basin system and defined them as "an elongate region of potential sediment accommodation that forms on continental crust between a contractional orogenic belt and the adjacent craton, mainly in response to geodynamic processes related to subduction and resulting peripheral or retroarc fold-thrust belt." This definition implies an accommodation of three types of tectonic loads, such as; 1) orogenic load by continent-continent collision (e.g., Himalaya); 2) subduction load by continental and oceanic collision (Apennine fold – thrust belt; Royden, 1993); and 3) dynamic subducted slabs by continental and oceanic collision (Sunda shelf region northeast of Java and Sumatra; Gurnis, 1992).

The flexural subsidence response which generates accommodation space for sediments deposition is related to collision between continental-continental or continental-oceanic lithospheres. Shortening caused by any type

of collision provides tectonic loads and generates flexural response. Therefore, tectonic loads are a necessary condition to generate a foreland basin.

A few types of tectonic loads have been suggested for the flexural subsidence of the Maracaibo basin including the oblique collision between the Caribbean and South American plates (Lugo, 1991; Lugo and Mann, 1995), but the causes of the load are not well-known. It is usually attributed to the complicated tectonic evolution around the Caribbean area. A peripheral setting of the foreland basin with tectonic loads by terrane accretion may fit for the basin with some modification (Figure 1-2). For several reasons, the existing peripheral setting cannot be directly used for the basin. First, subduction loading is not expected in the basin. The motion of the Caribbean plate around the basin has been complicated. It has two opposite directions; when it meets the South American plate it dips east, but it dips west with the Proto-Caribbean plate. Second, strike-slip movement is evident between the Caribbean plate and the South American plate, but the cause of orogenic belts is not well-explained by this model. The transgression and regression cycle of the Misoa Formation during the Eocene may have been controlled by mainly orogenic load and unload, which is usually observed during evolution of a peripheral foreland basin (Cant and Stockmal, 1989).

1.5. Petroleum geology

Comparing the size of the reserves and the production history of the basin, a detailed petroleum geology needs further studies based on individual fields. Source and reservoir rocks were well-described by previous studies, whereas seal, migrate path and trapping mechanisms were barely documented, because of the complicated tectonic evolution.

1.5.1. Source rock : La Luna Formation

There are three source rocks in the basin. 1) The La Luna carbonate source rock, classified as a marine type II kerogen, is the principal contributor to the oil accumulation (Blaser and White, 1984; Talukdar and Marcano, 1994). 2) The Paleocene Orocue Formation is coaly source rock containing terrestrial type III keorgen. The Orocue source rock, coeval with the Guasare Formation in the study area, covers the southwestern part of the basin (Talukdar and Marcano, 1994). 3) Tertiary source rocks are mainly composed of terrestrial materials and restricted to western and southern parts of the basin (Blaser and White, 1984). Some of the discovered hydrocarbons in the basin contain mixtures of oils from marine and terrestrial source rocks. However, the total contribution of the hydrocarbon reserves from the Orocue, Tertiary and mixed sources is thought to be negligible (Talukdar and Marcano, 1994). Source-rock analysis suggests two peak oil-generation times: the first during the middle-late Eocene and the

second during the late Miocene-Holocene. The second phase provided the main oil migration (Talukdar and Marcano, 1994).

1.5.2. Reservoir rock: Misoa Formation

During the Eocene, sediments were supplied to the Maracaibo basin from the Santander massif region to northeast (Maguregui and Tyler, 1991). These fluvial-deltaic tide-dominated depositional systems covered most of the basin (Figure1-3).

The Misoa Formation provides a good example of subsurface reservoir rocks affected by tidal influence during sea level rise and fall in the foreland setting. The Misoa Formation can be divided into two stratigraphic units. The first is informally referred to as “C sandstones,” deposited during the transgressive phase, and the second is informally named “B sandstones,” deposited during a regressive phase (Maguregui and Tyler, 1991).

1.5.3. Seal: Pauji Formation (?)

A marine high gamma ray shale covers the Misoa Formation and acts as a top seal in the field. The VLE 400 family penetrates the shale and mostly terminates before or at the Eocene unconformity. Few faults develop above the unconformity, and these faults are considered to be non-migration paths because of their minor offsets. Vertically, the fault acts as a migration path and cannot be evaluated as a sealing fault because of several reactivations by

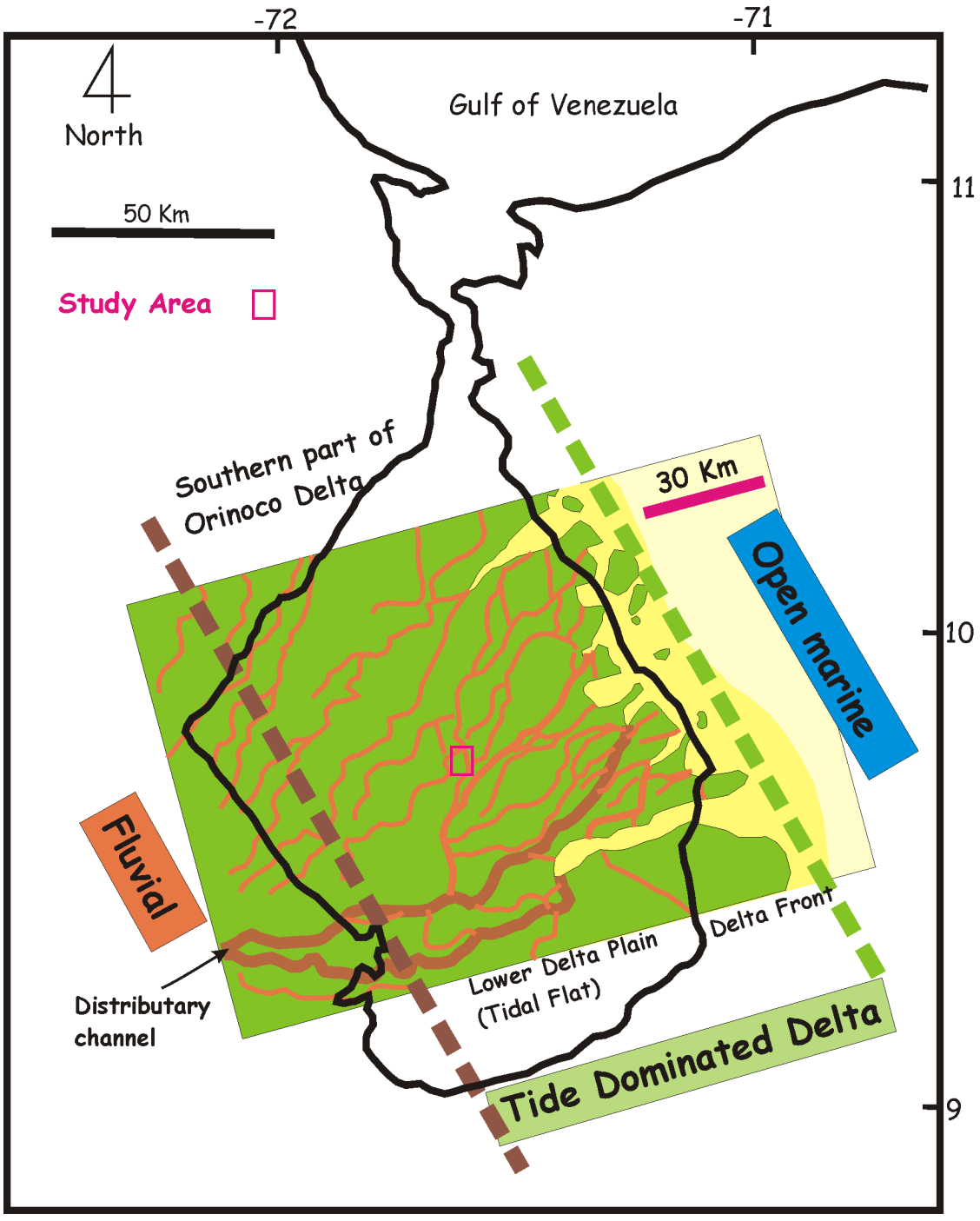

Figure 1-3. Depositional model of the Maracaibo basin for the Misoa Formation.

tectonic movements. Unnamed sediments deposited in the western block of the VLE 400 fault family act as lateral seals for the Misoa Formation of the eastern block. Ductile shale from the high gamma ray top seal shale and/or the thick Guasare Formation might create a shale-rich smear gouge zone along the VLE 400 fault family as an impermeable barrier (Watkins et al., 2004).

1.5.4. Migration path: VLE 400 fault family

The VLE 400 fault family is a possible migration path from the primary source rock La Luna Formation through the thick marine shale Guasare Formation to the main reservoir rock Misoa Formation. The thick shale of the Guasare Formation serves as a barrier from the source rock to the reservoir rock, and therefore, direct hydrocarbon migration by carrier beds cannot be expected. According to the complicated tectonic history of the basin, the VLE400 fault family moved several times, developed from the source rock to the reservoir rock, and therefore, is assumed to have a favorable condition for the vertical migration path. Another possible migration path is the family of en echelon faults in the eastern block. They developed during the shearing episode that created the VLE 400 fault family during the Miocene, and they are partly connected from the main source to the reservoir rocks.

1.5.5. Trapping: Strike-slip movements

The field has complicated structural features caused by the multi-tectonic evolution of the basin. The trapping structures are believed to be formed by several tectonic movements. Tectonic movements affected the VLE400 fault family deformation and are closely related to the structural development of the field. The most prominent and important structure for hydrocarbon was caused by compression during the Eocene and then modified by later strike-slip movements.

2. CHARACTERISTICS OF THE VLE 196 - LAMAR FIELD

The VLE 196-Lamar field, located in the central portion of Lake Maracaibo (Figure 2-1), was discovered in 1958. It has produced about 200 MMBbl from the 50 wells completed in the Eocene C-4 and C-5 members of the Misoa Formation (Holditch & Associates, 1997). Ages of reservoir rocks increase toward the northwest. Most fields are associated with northeast-southwest trending thrust and strike-slip faults. Few unfaulted fields have been discovered. Figure 2-1 shows the distribution of oil fields in the Lake Maracaibo basin. The Lamar field is a prolific Maracaibo basin field and gives a clear view of the petroleum system in which reservoirs are directly connected to source rocks by the VLE 400 fault family (Figure 2-2).

The generalized stratigraphic column for the field shows a simplified habit of hydrocarbon, depositional environment and tectonic evolution (Figure 2-3). Hydrocarbon expelled from the La Luna Formation is trapped in the Misoa Formation with a faulted anticline created by compression and shear stress during the Eocene and Miocene (Talukdar and Marcano, 1994). The Cretaceous La Luna Formation consists of carbonates deposited in shallow and deep water, whereas the Eocene Misoa Formation is composed of shallow marine deltaic clastic sediments (Parnaund et al., 1995). In total, four main tectonic regimes influenced the structural features of the field, beginning with rifting in the Jurassic, followed by a passive margin regime during the

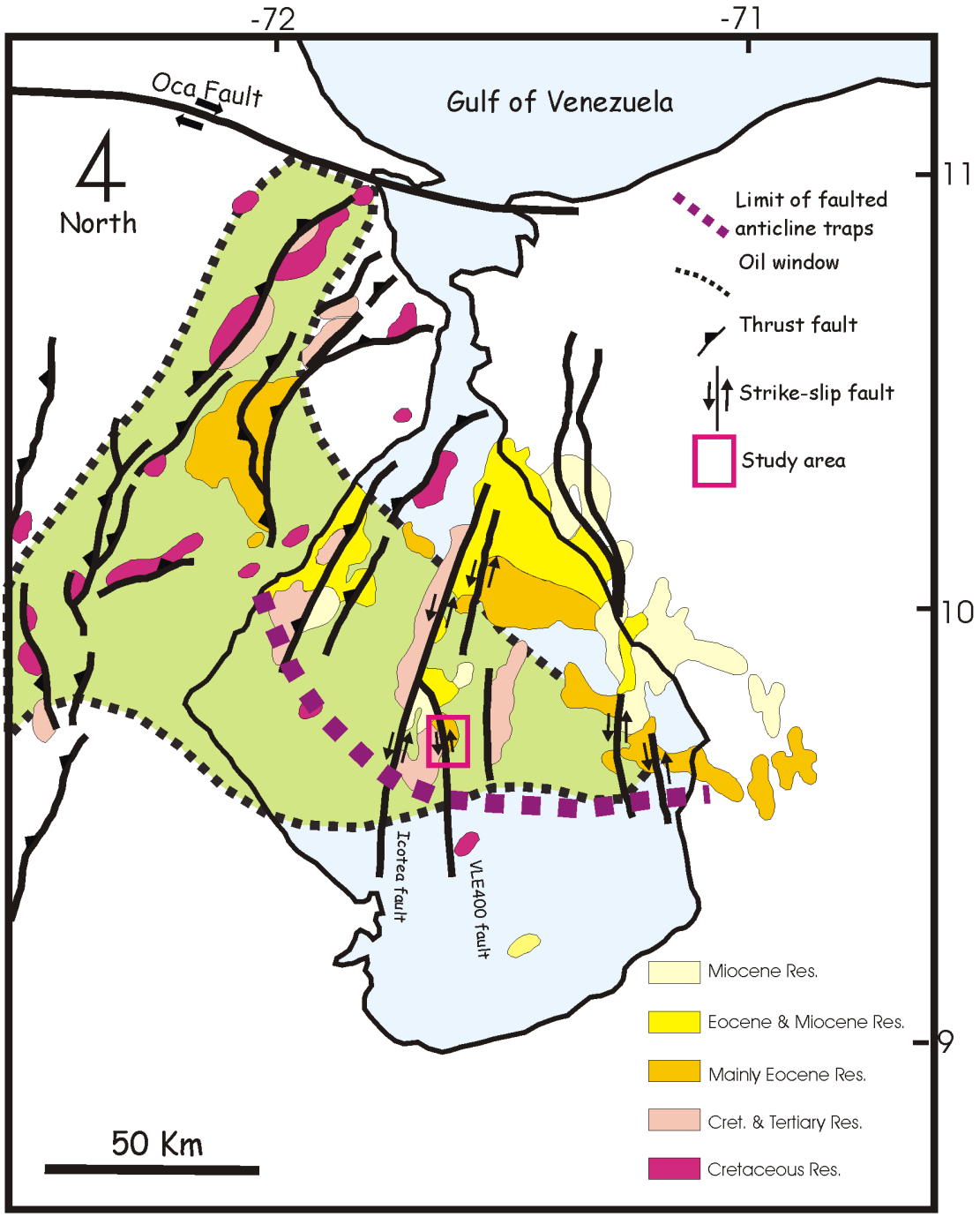

Figure 2-1. Distribution of oilfields in the Maracaibo basin (from Talukdar and Marcano, 1994) and the limitation of faulted anticline traps.

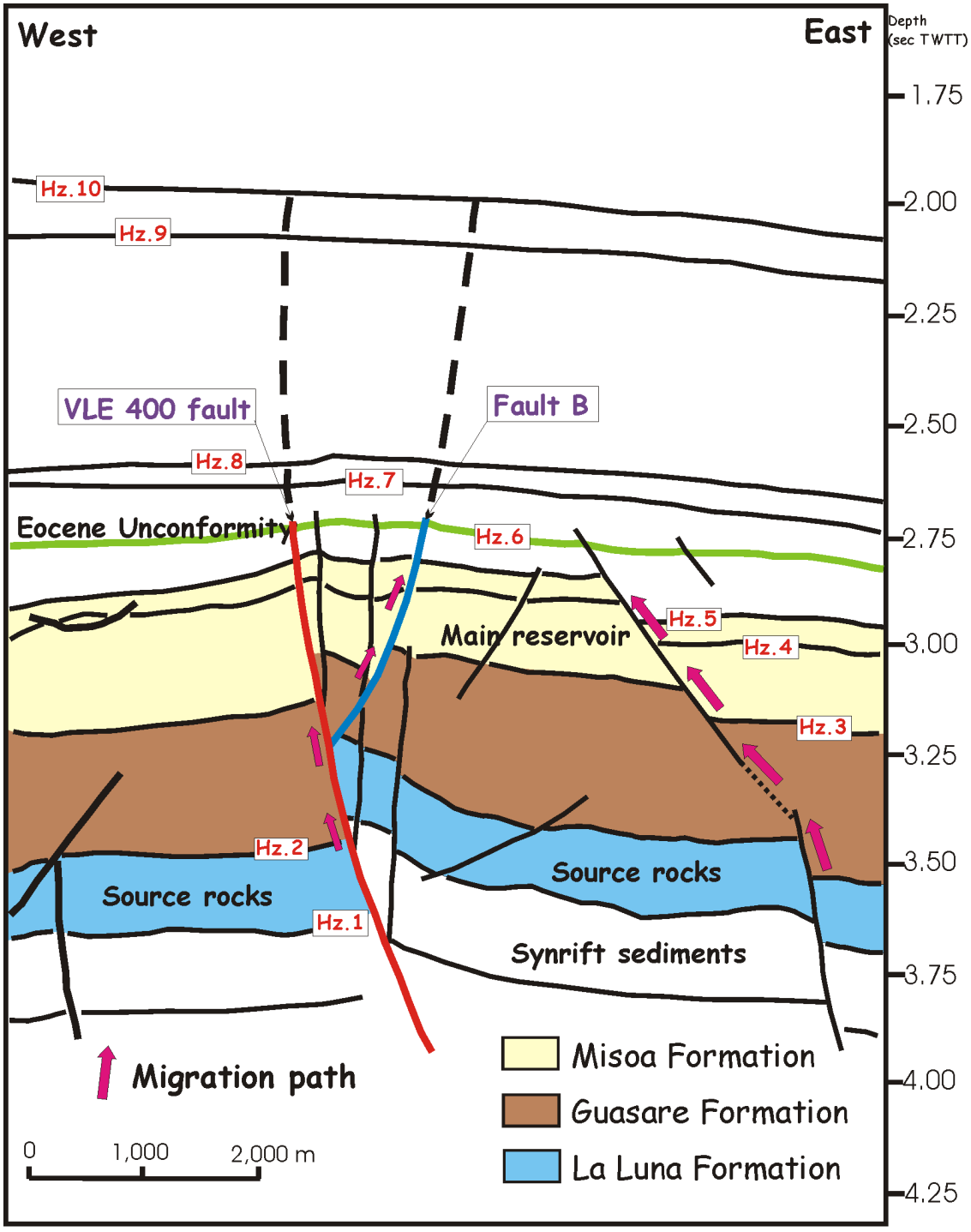

Figure 2-2. Geoseismic section of inline 640 showing the Misoa Formation (main reservoir rock), the Guasare Formation and the La Luna Formation (main source rock). See Figure 3-24 for the location.

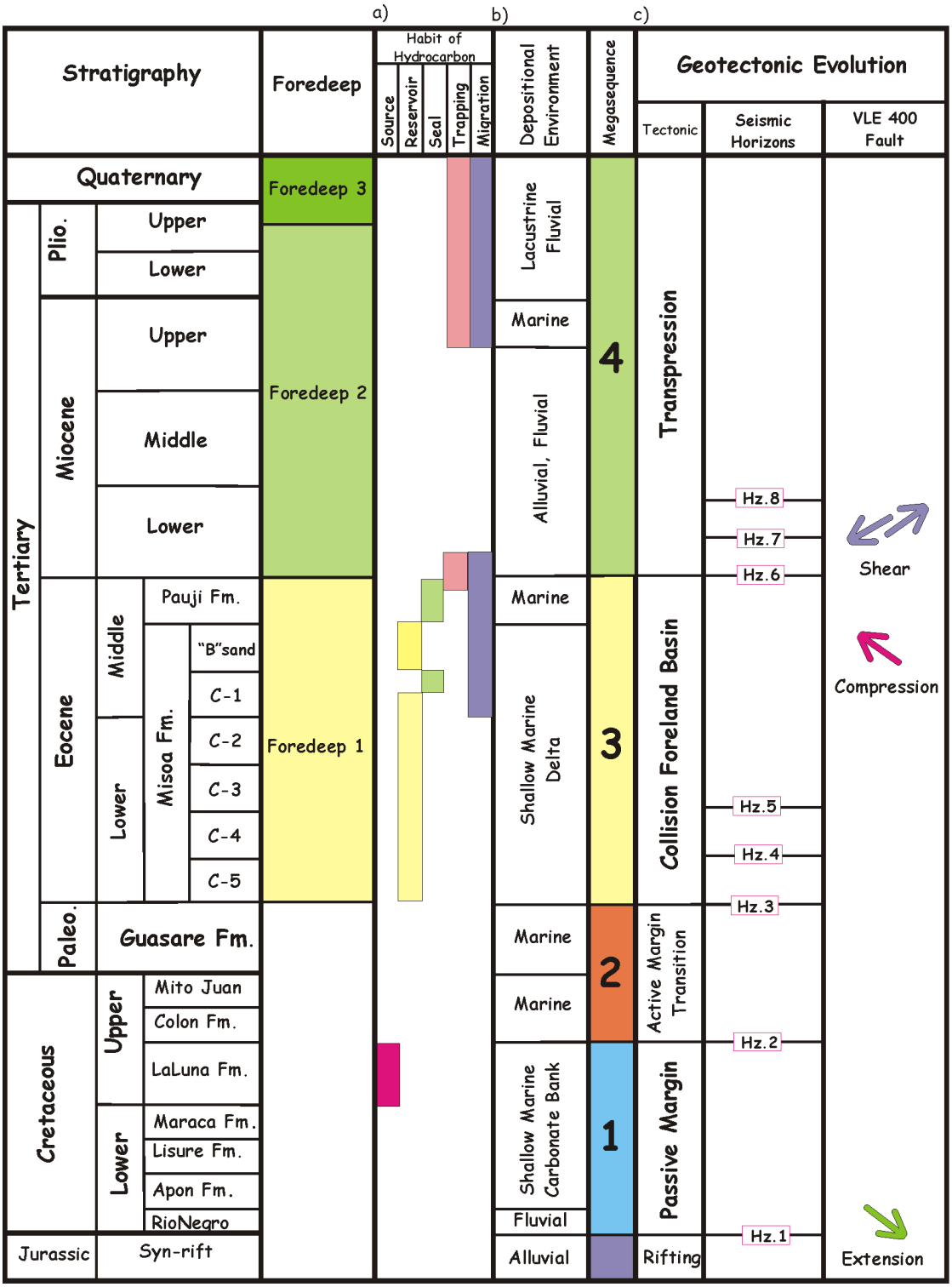

Figure 2-3. Generalized stratigraphy column. a) Habit of Hydrocaron(from Talukdar and Marcano, 1994); b) Depositional environment (from Parnaud et al., 1995); c) Geotectonic evolution (from Lugo and Mann, 1995).

Cretaceous, then Eocene collision-generated foredeep deposition that changed into transpression from Miocene time.

The main trap is a structural closure associated with the north-south striking VLE 400 fault family. The fault family subdivides the field into two main structural blocks: an eastern block that produces hydrocarbons from the Misoa Formation and a western block deposition that has not yet been determined (Figure 2-4). The uppermost pre-Eocene unconformity sediments in the western block consist of sediments belonging to either the Misoa or Pauji Formation or both. The role and origin of the Misoa-Pauji sediments is an objective of this research.

2.1. Seismic stratigraphic megasequences

Mainly on the basis of the seismic reflection configuration and facies of the sedimentary units, five megasequences were identified for the study. Additionally, six seismic horizons within the megasequences were interpreted for detailed evaluation of reservoir rocks and subtle movements during the Miocene (Figure 2-2). All megasequence boundaries are believed to be unconformities because of the regional geology and the abrupt change of seismic facies. They are not confirmed by well-log data because of the limited data (Figures 2-5, 2-6).

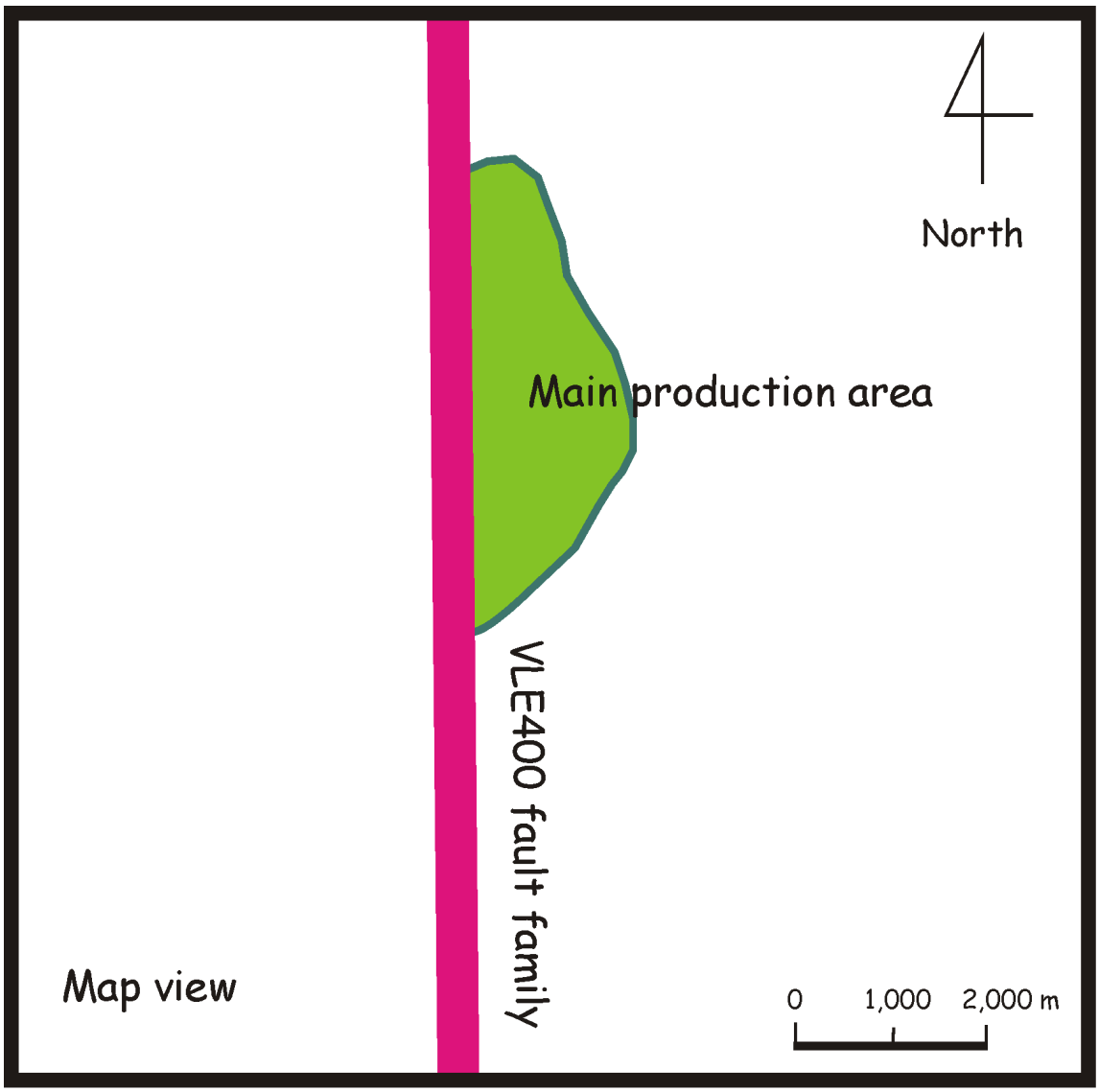

Figure 2-4. Simplified main features of the VLE 196 field. The main production area is in the east of the VLE 400 fault family.

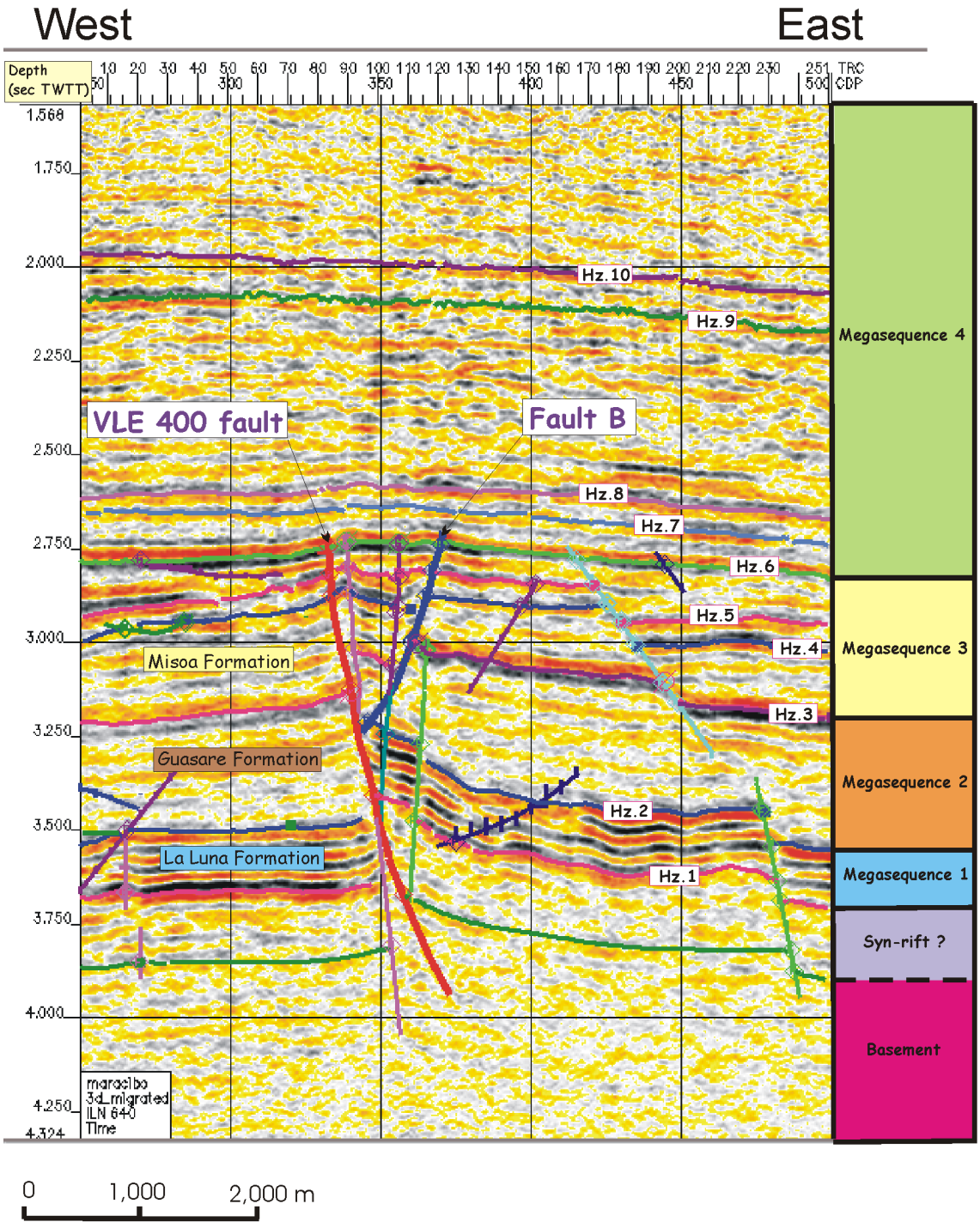

Figure 2-5. Seismic inline 640 showing interpreted seismic horizons and megasequences. See Figure 3-24 for the location.

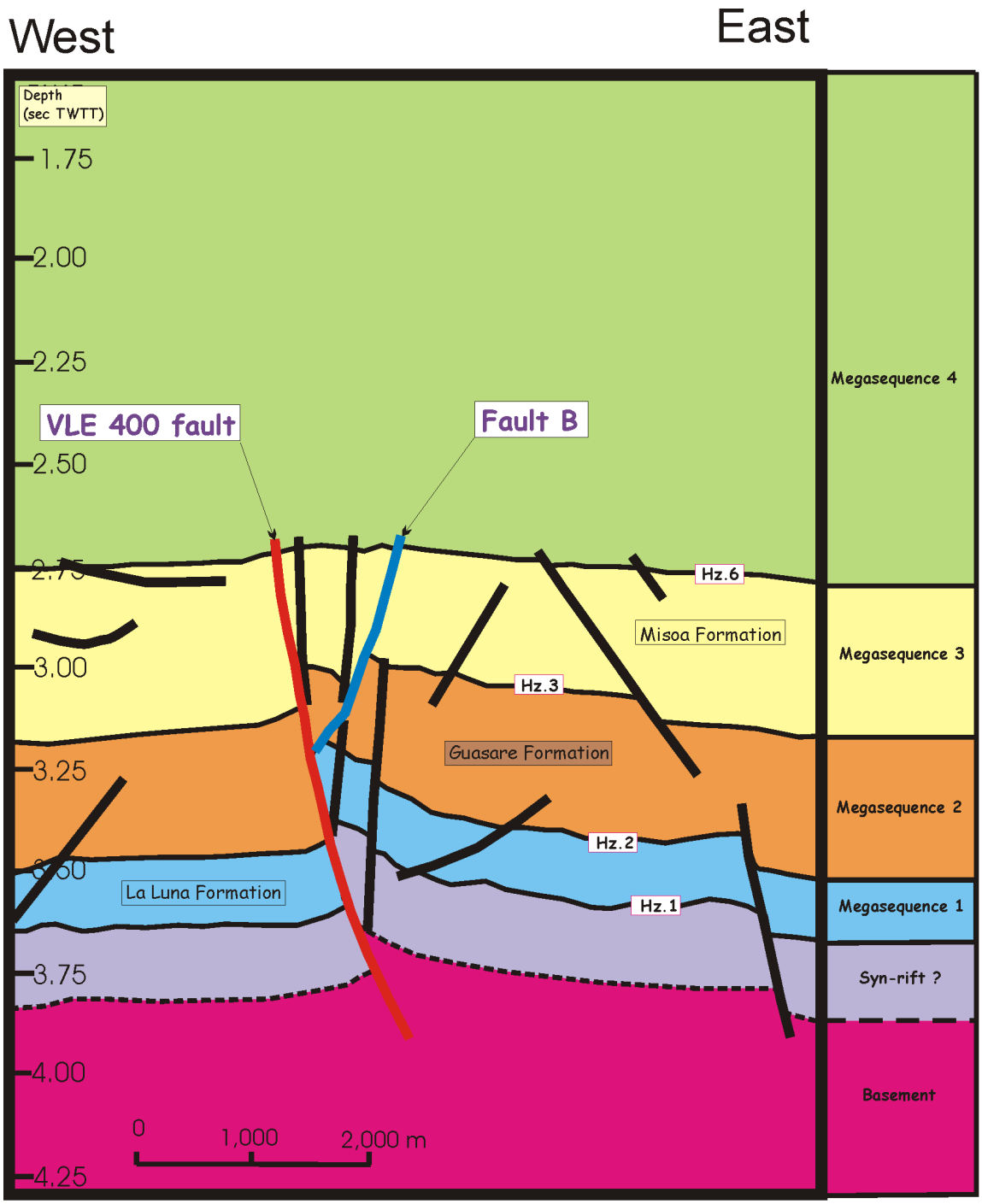

Figure 2-6. Geoseismic inline 640. See Figure 3-24 for the location.

2.1.1. Synrift sediments

Synrift sediments are mainly composed of Jurassic fluvial and alluvial sediments. From the seismic data of the study area, the top of the synrift sediments is distinguished by strong and continuous seismic reflectors, whereas the bottom of the synrift sediments is not clear.

Seismic reflection characters of the synrift sediments are low to medium amplitude, subparallel and semicontinuous. The top of this unit is bounded by high amplitude reflectors caused by the impedance contrast between the clastic synrift sediments and the overlying Cretaceous limestone. This unit is more or less continuous with the same thickness within the study area. The characteristics of the unit may be affected by the thick, strong-amplitude seismic package on top of the unit, which interferes with penetration of seismic energy. Seismic reflection characteristics suggest that the synrift strata are clastic sediments. Jurassic synrift sediments are not well-defined by previous studies and the synrift unit of this study is identified by seismic data only.

2.1.2. Megasequence 1

Megasequence 1 consists of high amplitude, parallel and continuous reflections, and is defined by the top of synrift sediments at the base and the top of the La Luna Formation at the top. Seismic characteristics and regional geology data indicate that the unit mainly consists of alternation of limestones and shales deposited in a platform environment. The unit may be composed of

Lower Cretaceous and Upper Cretaceous carbonate formations, but it is not possible to identify the detailed classification from this 3-D seismic data. Data from elsewhere in the basin (Blaser and White, 1984) indicate that this megasequence is the source rock La Luna Formation.

Three or sometimes four distinct strong reflector pairs comprise the megasequence. Each seismic reflector probably represents a different unit. The megasequence shows compressional features of the VLE 400 fault clearly. The eastern block is a reverse fault hanging-wall uplifted toward the western block. Maximum throw is 38 millisecond two-way travel time (ms twtt) measuring at the top of Megasequence 1. Reverse faulting is clearly observed in the VLE 400 fault family, and normal faulting is also recorded apart from the VLE 400 fault family within the megasequence. Gently wavying seismic reflectors (Figure 2-5) are easily observed within the megasequence, which implies ductile movement of carbonate rocks. The strong seismic amplitudes of the megasequence are partially weakened, especially in some areas on top of local fault planes.

2.1.3. Megasequence 2

Megasequence 2 consists of low-amplitude, parallel to sub-parallel and continuous to semicontinous reflectors. This megasequence extends from the top of the La Luna Formation to the top of the Guasare Formation above. This megasequence is composed mainly of shale with minor sandstones deposited

while the tectonic setting changed from passive margin into active margin. This megasequence consists mainly of marine shale deposited during the transition from passive marine to collision foreland basin, before sediments were supplied by the mature drainage system from thrust belts and peripheral bulges. Increasing thickness of the megasequence is observed near the VLE 400 fault family. This is presumably a result of shale mobilization through the weakened fault fracture zone during compression and transpression at Eocene and Miocene times.

2.1.4. Megasequence 3

Megasequence 3 lies between the top of the Guasare Formation and the Eocene-Miocene unconformity. In the study area, this megasequence consists mainly of the Misoa Formation, which has been informally named the “C sandstones” (from now on “C members”). The two main reservoir sandstones, “C-4” and “C-5” are interpreted within this megasequence for the detailed study of the reservoir sandstones. The unnamed sediment unit, correlated to the Misoa-Pauji sediments, is identified on the western block of the VLE 400 fault family within this megasequence. Megasequence 3 consists of strong to moderate amplitude, parallel to subparallel, and continuous to semicontinuous seismic reflectors. Within this megasequence, the Misoa-Pauji sediments are developed in the western block of the field. The thickness of the western block of this megasequence increases toward the north, especially from the middle of

the field, because of the Misoa-Pauji sediments. Among the five megasequences, this megasequence is the most highly faulted.

2.1.5. Megasequence 4

Megasequence 4 lies between the Eocene-Miocene unconformity and the base of the Quaternary sediments. The upper boundary of the top is not clearly defined by seismic. Four seismic reflectors are interpreted within this megasequence for analysis of the VLE 400 fault family movement including lateral changes of seismic characteristics.

2.2. Structure

Evolution of the VLE 400 fault family is closely related with the tectonic movement of the basin. The VLE 400 fault family was created by tensional stress when the basin opened during rifting of Jurrasic age (Kulke, 1995). It was reactivated by compression in the middle Eocene (Lugo and Mann, 1995) which created inversion structures through the VLE 400 fault family. Finally, the VLE 400 fault family was modified by shear stress and superimposed over the previous structures (Castillo, 2001).

During basin opening, normal faults were created by rifting and synrift sediments were deposited. A break-up unconformity divides synrift sediments and the overlying La Luna, Guasare and Misoa Formations. The VLE 400 fault

family was created by rifting and rejuvenated by compression during the Eocene. From the Oligocene to Miocene, compression changed to shear. It was probably not an abrupt change, but instead, it occurred gradually with the changing collision direction of tectonic plates. It provided strike-slip movement of the fault and generated its associated structures, such as positive flower structures, en echelon folds, and normal and reverse faults. The VLE 400 fault family can be considered as a series of more or less parallel strike-slip faults developed between two major strike-slip faults trending east-west.

2.3. Depositional environment of reservoir rocks

Gamma-ray logs were used to infer sand/shale distribution and depositional environments in the reservoir sands (Figure 2-7). Electronic facies, geometry of sedimentary bodies and characteristics of internal contacts of sedimentary bodies were used for well-to-well correlation.

2.3.1. Well-to-well correlation

Three Misoa sub-units are identified from well 1063 for well-to-well correlation (Figure 2-8). The 770 ft C-5 member consists of three subunits, each about 250 ft thick. The C-5 member shows dominant fining-upward and minor coarsening-upward features. The C-4 member also contains three units. Overall thickness is about 300 ft and unit average is about 100 ft. Logs indicate

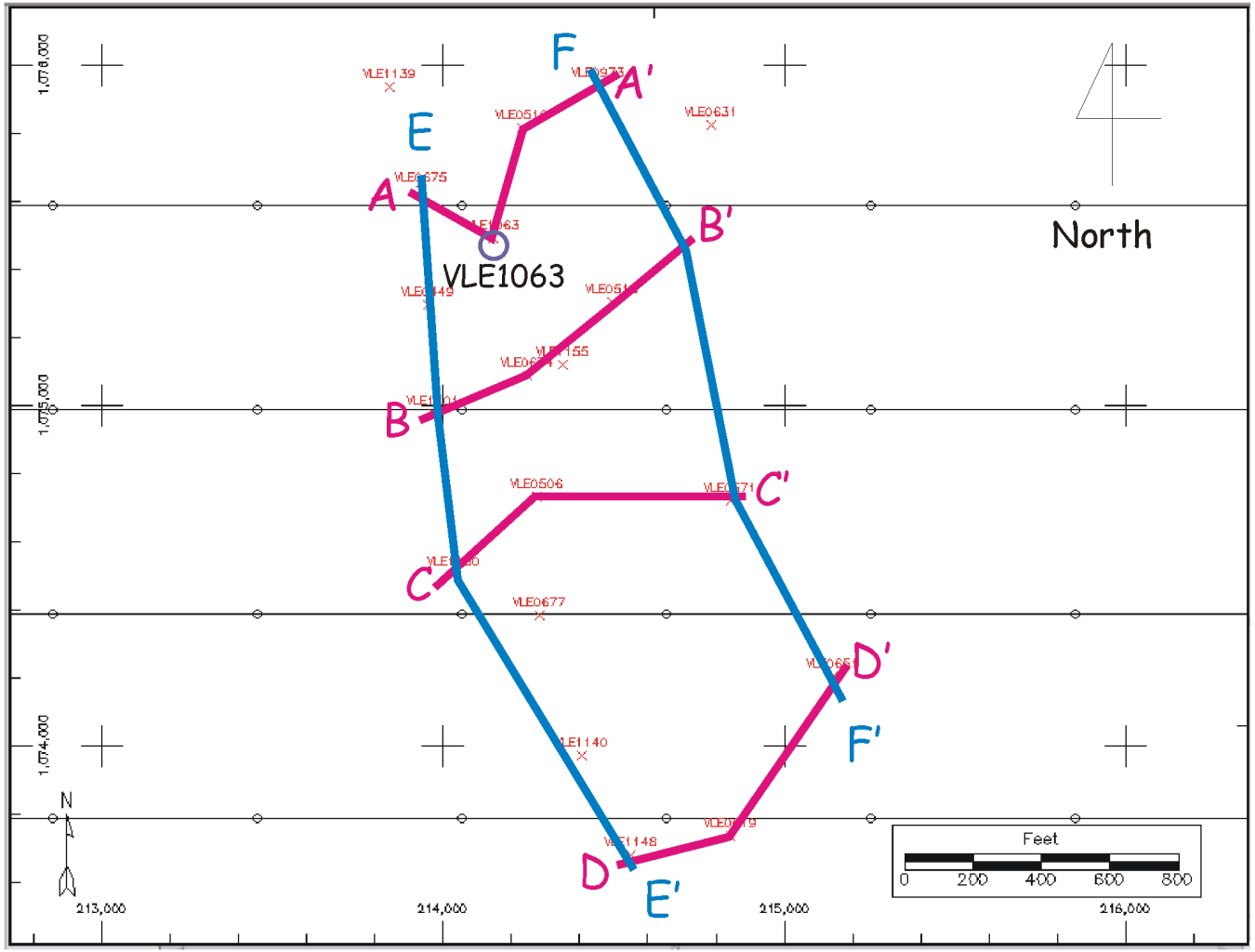

Figure 2-7. Location of well VLE 1063, well-to-well correlation of A-A', B-B', C-C', D-D', E-E' and F-F'.

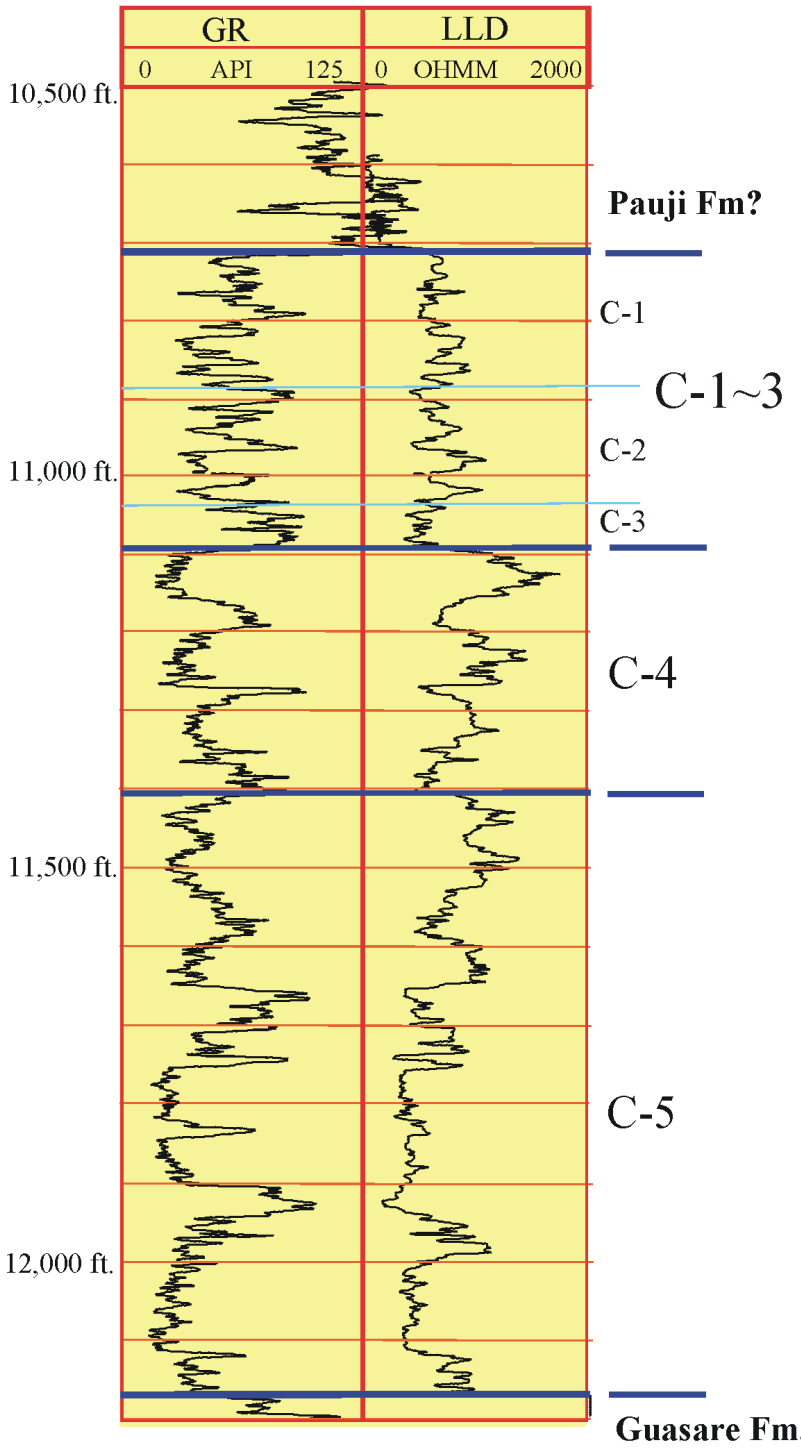

Figure 2-8. Well log facies of C-5, C-4 and C-1~3 members from well VLE 1063 (modified from Holditch & Associates, 1997). See Figure 2-7 for the location.

mainly fine upward with partly interbedded coarsening-upward features. The C-1~3 member is consisted of C-1, C-2 and C-3 bedsets. Overall thickness of the C1~3 member is about 400 ft. The thickness of individual bedsets ranges from about 20 to 80 ft. Logs show coarsening-upward dominating this interval.

Lithology changes abruptly from sandstones to mudstones above the top of C-4 member. It is easily recognized from its gamma-ray response. The log response of the top of the C-5 member generally is similar to the top of the C-4 member, although a few wells encountered sandstone-to-sandstone contacts. The top of the C-1~3 member is distinguished because of regional mudstone deposits. However, the top of the C-1~3 member is not correlated because of the limitation of the available data set.

1) Well-to-well correlation of A-A' line

The A-A' line is on the west-east cross-section of the field, consisting of wells VLE0675, 1063, 0510 and 0973 from west to east (Figure 2-9). The top of the C-4 member was picked as a reference level and then well-to-well correlation was followed.

The C-4 member is approximately 350 ft thick and is more or less uniform. Sandstone dominated bedsets with interbedded fines and thin mudstones in the VLE0675 well change eastward into variable thickness mudstones and interbedded sandstones in the VLE0973 well. Fining-upward beds predominate, but the base of the C-4 member commonly shows

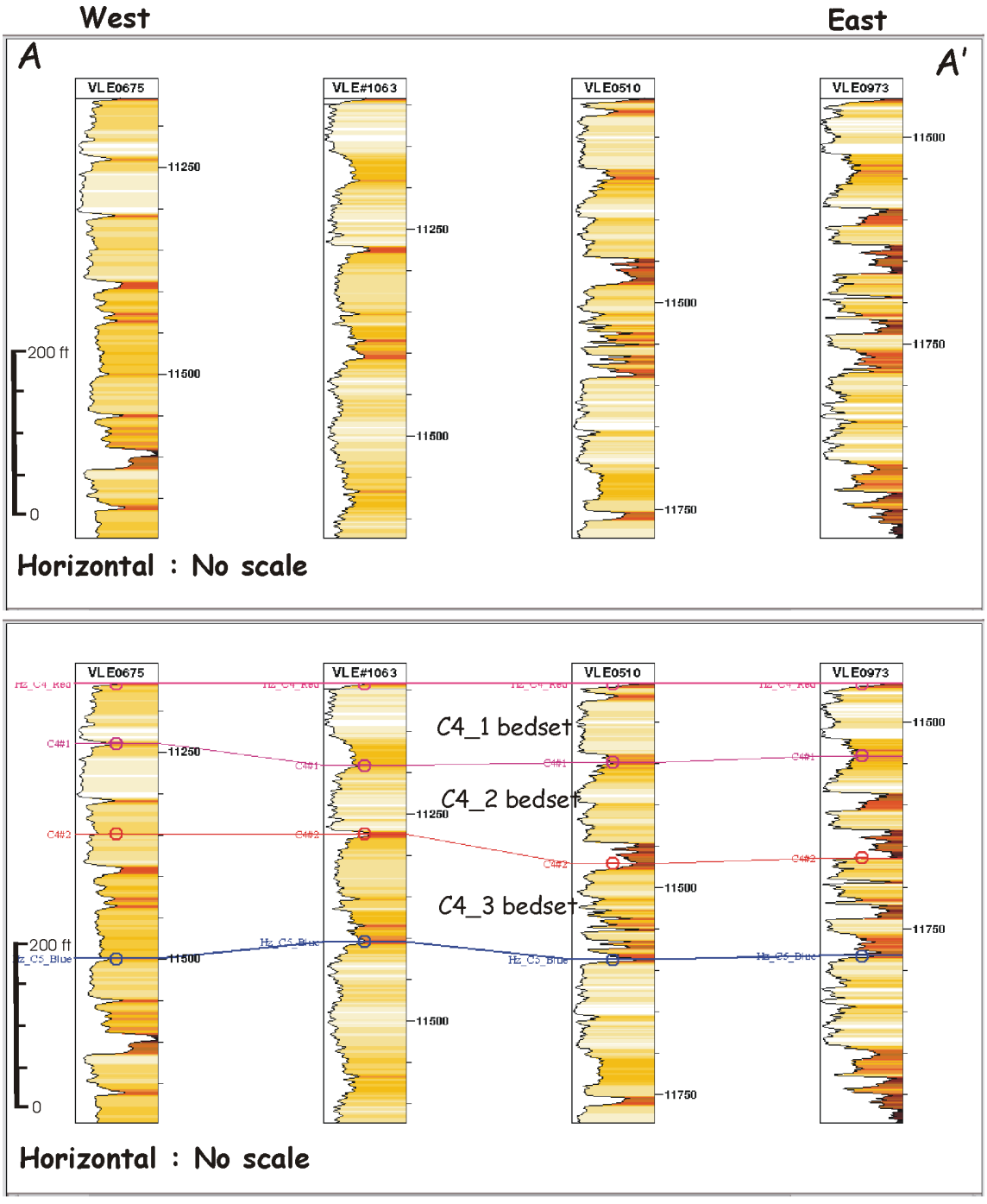

Figure 2-9. Well-to-well correlation of A-A' consists of wells VLE 0675, 1063, 0510 and 0973. See Figure 2-7 for the location.

coarsening-upward characteristics. Electronic facies of bedsets between wells change sharply even though the distance between wells is only a few hundred meters.

The C-4-3 bedset has a sharp contact at its base except in the VLE0675 well, which has a sandstone-to-sandstone contact. The bedset consists of a few coarsening-upward and fining-upward beds and is about 150 ft thick. Compaction might reduce the thickness of the bedset in high percentage mudstone wells. More frequent thin layers of mudstones are recorded toward the west of the line.

The C-4-2 bedset has a sharp basal contact except for the sandstone-to-sandstone contact of the VLE0675 well. It has two or three beds and increases to several beds in the VLE0973 well with high mudstone percentage. The average thickness of the bedset is about 100 ft.

The C-4-1 bedset gradually changes lithology from mudstone to sandstone toward its base. It consists of one or two beds here but increases in number eastward.

2) Well-to-well correlation of B-B' line

The B-B' line shows a southwest-northeast cross-section of the field as illustrated in Figure 2-10. It consists of the VLE1101, 0674, 0516 and 1004 wells from west to east. The top of the C-4 member is the reference level. The average thickness of the C-4 member along the B-B' line is about 300 ft. Even

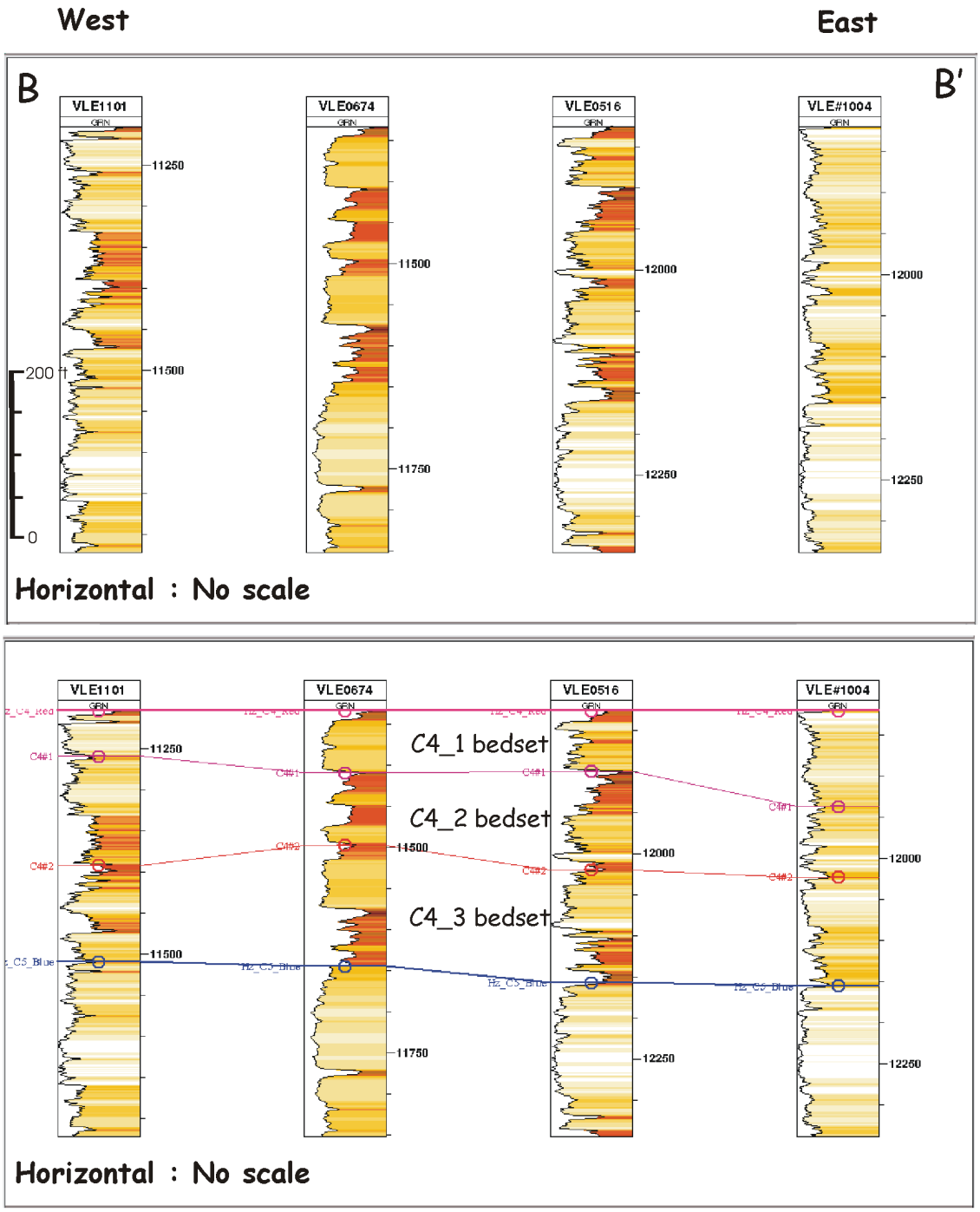

Figure 2-10. Well-to-well correlation of B-B' consists of wells VLE 1101, 0624, 0516 and 1004. See Figure 2-7 for the location.

though the overall thickness of the C-4 member is constant between wells of the line, thickness of each bedset within the C-4 member changes from well to well.

C-4-1 thickness increases toward the east whereas the C-4-2 and C-4-3 thicknesses change randomly. Thickness variations of C-4 bedsets are random.

Around 20- to 30-ft thick shales and thin shales are recorded in the C-4-2 bedset from the VLE0674 and 0516 wells. Blocky sandstones dominate the C-4-2 bedset in the VLE0674, 0516 and 1004 wells. The lithology of the C-4-2 member in the VLE1101 and 0674 wells changes abruptly, different from the gradual lithology changes in the VLE0516 and 1004 wells. C-4-3 lithology changes abruptly similar to the cut and fill in VLE1101. The shale has high gamma ray values in the VLE0674 and 0516 wells.

3) Well-to-well correlation of C-C' line

The line crosses represent three wells; VLE1130 in the west, VLE0506 in the middle and VLE0571 in the east (Figure 2-11). The C-4 member thins eastward, mainly with the thinning of the C-4-1 bedset. The C-4-1 bedset in the VLE0571 well has the same gamma ray log characteristics as the VLE1130 and 0506 wells. Basal contact with the top of the C-4-2 bedset is very sharp from thin but high gamma ray to blocky sandstone in the VLE1130 well. It shows the same trend in the VLE0506 but displays almost sandstone-to-sandstone contact in the VLE0571 well.

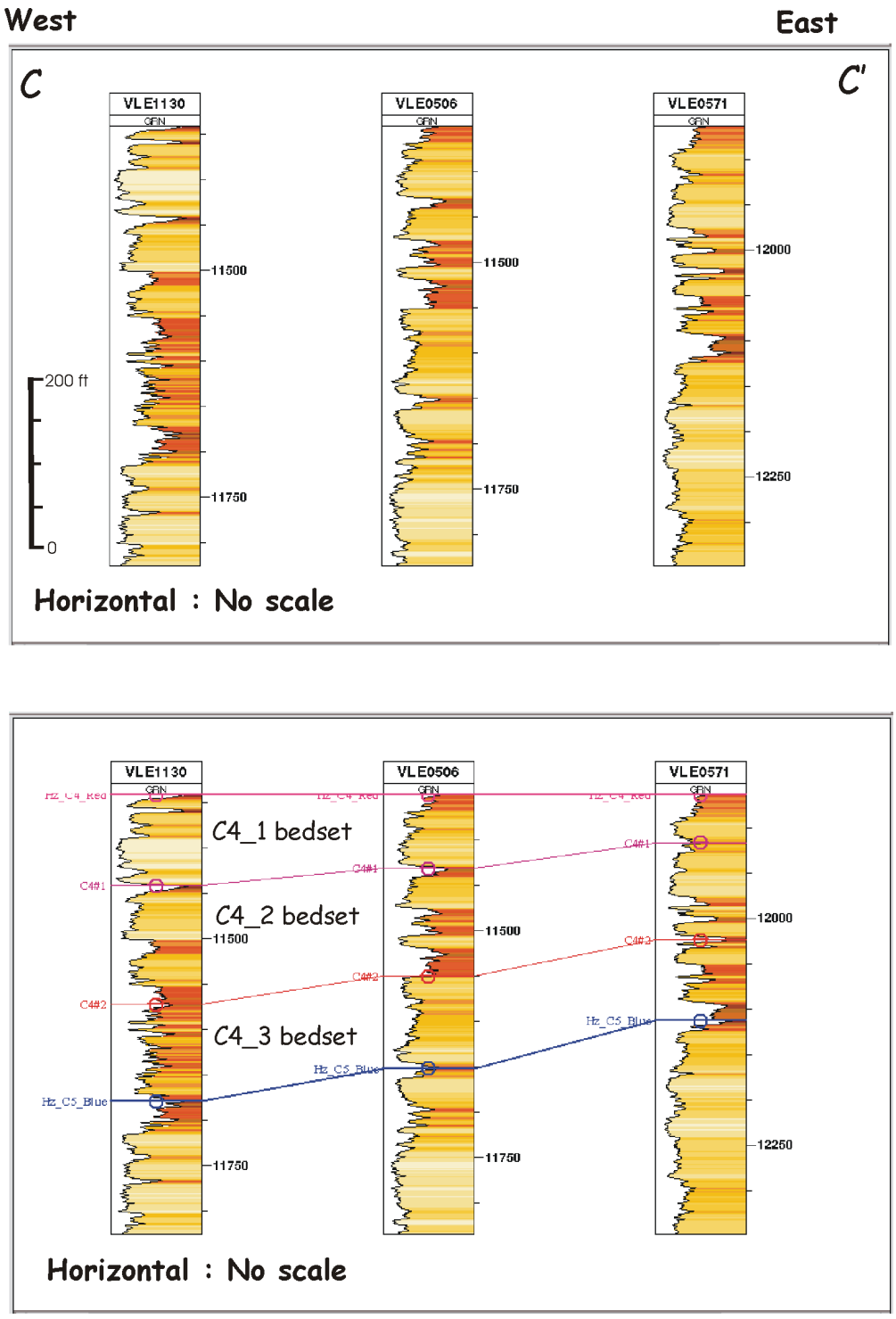

Figure 2-11. Well-to-well correlation of C-C' consists of wells VLE 1130, 0506 and 051. See Figure 2-7 for the location.

The C-4-2 bedset has three distinct fining-upward beds, but one fining-upward unit is missed in the VLE1130 well. Thickness of individual beds varies and shale percentage is greater in the VLE0506 well.

Lithology of C-4-3 bedset is extremely variable. Thin sandstones and thin shales are interbedded in VLE1130 well, fining and coarsening sandstones are in VLE0506 well and three distinct subunits appear in the VLE0571 well.

4) Well-to-well correlation of D-D' line

The D-D' line crosses the VLE1148, 0619 and 0651 wells (Figure 2-12). The thickness of the C-4 member varies from 250 ft in VLE0619 to 350 ft in VLE1148 mainly reflecting differences in the C-4-3 bedset.

The C-4-1 bedset can be subdivided into two subunits: a lower coarsening-upward sandstone unit and an upper fining-upward sandstone unit. Although the C-4-1 bedset thins in the VLE0619 well, log characteristics are similar among the three wells.

The C-4-2 bedset consists of two subunits in the VLE1148 and VLE0651 wells, and three subunits in the VLE0619 well. Total thickness of the C-4-1 and C-4-2 is similar between wells because the thickness variation of the members compensate each other. The most significant thickness change is in the C-4-3 bedset, especially in the VLE0619 well. The C-4-3 bedset can be subdivided into two units: a lower coarsening-upward with thin high gamma ray shale

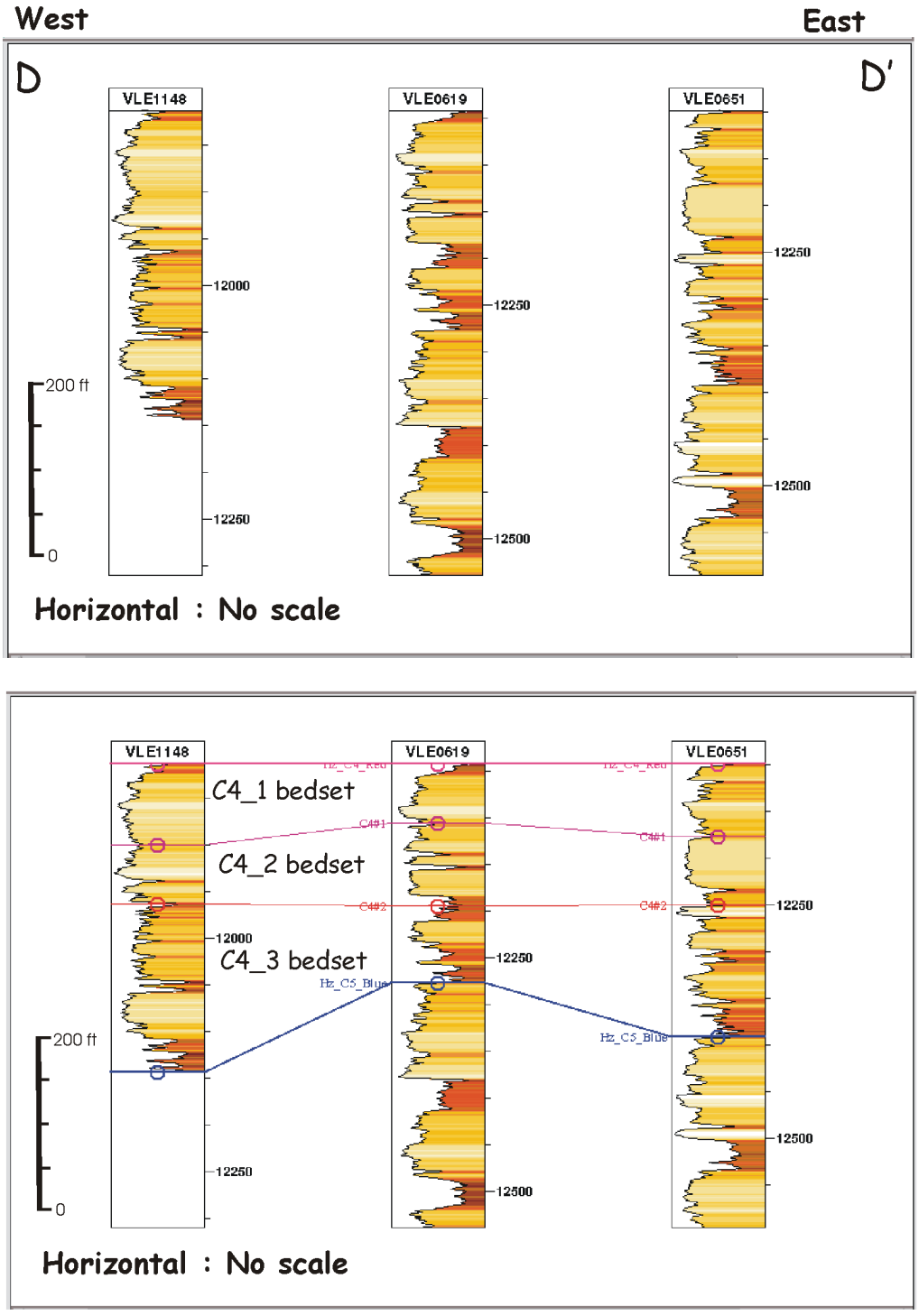

Figure 2-12. Well-to-well correlation of D-D' consists of wells VLE 1148, 0619 and 0651. See Figure 2-7 for the location.

interbeded and an upper sandstone with very thin interbedded shale. The VLE0619 well has about a 20-ft-thick shale instead of the sandstones.

5) Well-to-well correlation of E-E' and F-F' lines

Lines E-E' and F-F' are north-south cross-sections (Figures 2-13, 2-14). These display greater thickness variation in bedsets than in the west-east lines. There are no thickness change trends, and gamma ray log characteristics are vary significantly from well to well. Thickness of the C-4 member is similar along the line except in the VLE0571 well, which is about 70 to 80 ft thinner than around wells. Generally, lithology, thickness and log characteristics of bedsets in this direction display more significant differences than do west-east lines.

Changes of log patterns between wells and well-to-well correlations suggest lithology variations vertically and horizontally. Integrated interpretation of well logs and 3-D seismic data suggest a tide-dominated delta (Ambrose et al., 1995; Castillo, 2001). The southern part of the Orinoco delta appears to be a good analogue.

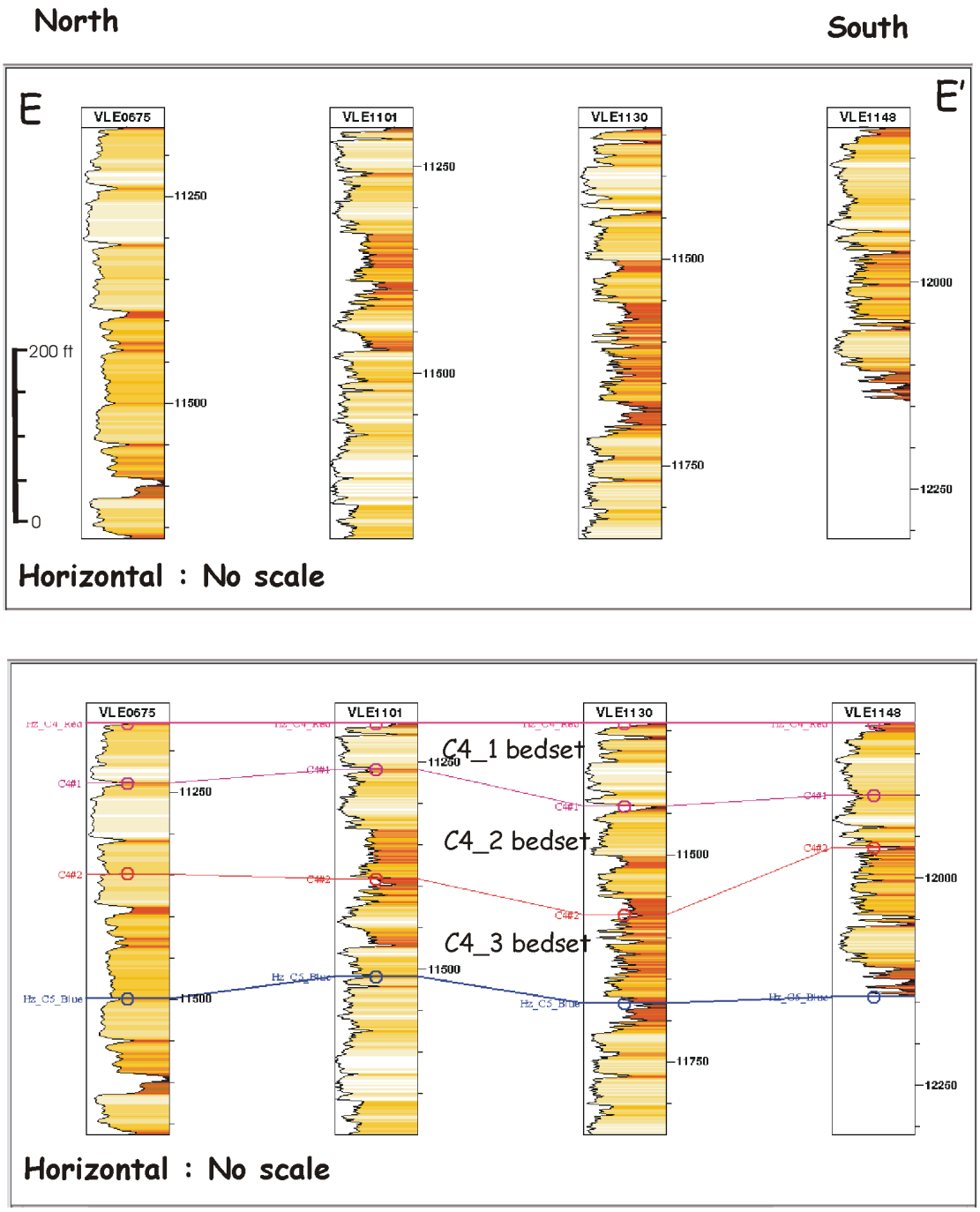

Figure 2-13. Well-to-well correlation of E-E' consists of wells VLE 0675, 1101, 1130 and 1148. See Figure 2-7 for the location.

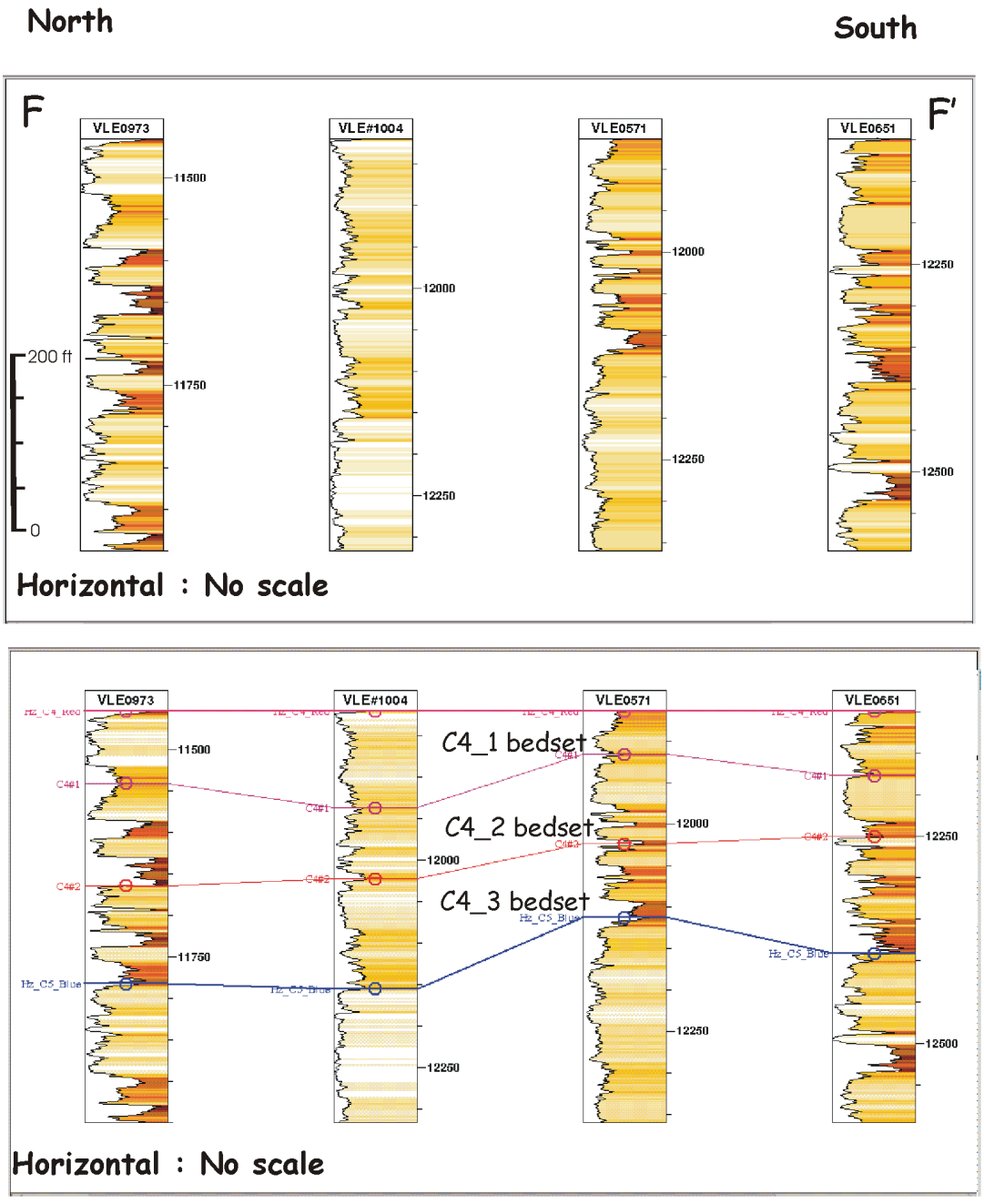

Figure 2-14. Well-to-well correlation of F-F' consists of wells VLE 0973, 1004, 0571 and 0651. See Figure 2-7 for the location.

2.4. Sealing mechanism of the VLE 400 fault family

Faults in sedimentary basins can act as migration paths or barriers to hydrocarbon flow and contribute significant hydrocarbon potential for exploration and development (Watts, 1987). Fault closure requires an impermeable material over the trap area and lateral juxtaposition of the entire hydrocarbon-bearing reservoir against a sealing lithology along or within the fault plane. Faults can be classified into four types according to the sealing capacity, hydrocarbon migration and time range, principally concerning leaking across and not along faults: 1) Sealing faults, 2) Juxtaposition faults, 3) Temporary sealing faults, 4) Non-sealing faults (Skerlec, 1999). Juxtaposition, clay smearing, clay injection, cataclasis and diagenesis are the main sealing mechanisms that increase the capillary-entry pressure.

2.4.1. Sealing faults

If the seal is considered to be a homogeneous membrane, the sealing mechanism is then related to the capillary entry pressure required for hydrocarbons to enter the largest interconnected pore throat of the seal (Berg, 1975; Smith, 1980; Watts, 1987). A membrane seal will trap a hydrocarbon column until differential pressure across the membrane exceeds the capillary displacement pressure of the seal. Clay smearing, clay injection, cataclasis and

diagenesis provide membranes. These reduce the diameter of the pore throats in the fault plane raising the capillary displacement (Berg, 1975).

2.4.2. Juxtaposition faults

Juxtaposition faults form a trapping element to an isolated hydrocarbon accumulation and sealing occurs from juxtaposition of the reservoir section against a sealing lithology (Watts, 1987; Knott, 1993). Juxtaposition fault seals do not consider the vertical fluid flow but a lateral, impermeable barrier. The vertical sealing capability of a fault is determined by the capillary entry pressure of the top seal bed at the fault (Harding and Tuminas, 1989). The sealing capacity of juxtaposition faults mainly depends on the lithology of the section against the reservoir. A high sand percentage of the section decreases the chance of juxtaposition faults sealing. Juxtaposition faults are usually combined with characteristic changes of the fault zone such as clay smearing.

2.4.3. Temporary sealing faults

The fault can act as a hydrocarbon migration path over geologic time and as a pressure barrier to subsurface fluids during the production period. Even though temporary sealing faults do not provide migration barriers during geologic time, they are pressure barriers in field production. Therefore, an understanding of the probability of a fault acting as a pressure barrier is critical

for field development where fault-bounded compartments may not be in pressure communication because of temporary sealing faults (Knott, 1993).

2.4.4. Non-sealing faults

Non-sealing faults do not act as barriers to fluid flow over geological time or during production. When faults are active, they can be more permeable and act as hydrocarbon migration paths (Knott, 1993). Therefore, when faults are analyzed for sealing, time has to be considered.

2.4.5. Vertical migration and across seal

Fault-parallel permeability is the main migration possibility from the underlying source rock that is separated by thick shale from the reservoir. The VLE 400 fault was rejuvenated from the normal faults, which might be related to the initial basin forming rift faults. Therefore, the faults have been reactivated through geologic time and received various stresses that generated a wide range of fracture zones along the fault planes, even though clay smearing, clay injection, catalasis and diagenesis increased capillary entry pressure across the fault plane. The sealing capacity of juxtaposition faults is controlled by the lithologic difference across the fault plane; therefore, the sandstone percentage of the reservoir is a main concern for this type. The reservoir sandstone of the Misoa Formation has high a percentage of net-to-gross ratio and the sandstone percentage of the VLE1063 well has been recorded as high as 80%. Therefore,

the juxtaposition fault seal of the field depended on the lithology of the upper formation of the reservoir and vertical throw of the fault. In this regard, the Misoa-Pauji sediments in the production interval of the Misoa Formation should serve an important role for the juxtaposition sealing because of the characteristics of the VLE 400 fault family and high sandstone percentage of the reservoir rock.

3. DEPOSITIONAL RESPONSE TO TECTONIC MOVEMENT

Megasequence 3 consists of Eocene foredeep sediments. It is reviewed from the viewpoint of tectonic movements because these are growth sediments that were deposited during active tectonic movements, whereas Megasequences 1 and 2 were deposited in a more or less inactive tectonic setting. Creation and destruction of accommodation space are controlled by tectonic subsidence/uplift and eustasy, and both result in relative sea level changes. However, the two factors do not always have equal influence on accommodation space. Sometimes one factor prevails, especially if the active tectonics setting is favorable for tectonic movements to control the sediment basin with minor effects of eustasy. Depositional features of the megasequence show predominant aspects of tectonic influences, such as syn-tectonic sediments or “growth strata” and tectonically controlled transgressive deposits. Tectonic movements in the Maracaibo basin are complicated, especially the Eocene sediments that are highly deformed by various tectonic activities. Therefore, it is not easy to establish a suitable tectonic evolution model by structural analysis.

Three methods have been used to analyze the depositional response caused by tectonic movement: 1) The growth strata concept evaluated by isochron maps proved to be a useful method to detect subtle tectonic movements; 2) Conventional analysis of structure maps with fault polygons

provides fundamental information of tectonic movements; 3) Interpretation of well logs is essential for understanding depositional responses, especially when integrated with seismic data.

To evaluate tectonic movements using the growth strata concept the VLE400 fault and Fault B (Figure 2-5) were reviewed by isochrons of mappable units in seismic above and below the Eocene unconformity where the faults terminate. The isochron was expected to have an even thickness across the fault zone if the faults were inactive and the thicknesses of each block of the fault zone were expected to be different if the faults have extensional or compressional movements. Therefore, the isochron of the mappable unit could be used for analysis of structural movements. There were two assumptions for this analysis: The first was that the mappable units had to be bounded by comformities; the second was that the lithology variation was not significant across the fault zone. Sometimes different lithologies provide different compaction, which generates different thickness above the comformity units. The mappable units have to be distinguished by continuous seismic reflectors so that subtle thickness differences across the fault zone can be identified through the careful seismic interpretation.

After interpretation of 11 horizons, 10 isochron maps were generated between each horizon. The isochron maps are simply calculated from time differences between two horizons; therefore, they are not true thickness where the reflectors have dips or faults. Sometimes, non-structural features, such as

sinkholes, can cause thickness variation locally. Reviewing the general trend of the isochron reduces the errors caused by dips, faults or sinkholes so they are not so significant as to make analysis difficult.

A total of 11 time structure maps with fault polygons were generated after interpretation of 11 seismic horizons with careful fault correlations. Trends of fault traces and polygons of each seismic horizon were carefully reviewed from the view point of tectonic movements.

Interpretation of well logs is mainly based on gamma ray logs which reflect vertical lithology changes. Well-to-well correlations of six different well combinations in the north-south and east-west directions were used. Detailed correlations are described in Chapter 2.

3.1. Structural development

A total of 11 seismic horizons including the top of a possible basement were interpreted for structural evaluation of the field. The time structure map of the basement shows a distinct closure in the eastern block against the north-south trending VLE 400 fault (Figure 3-1). The top of the basement in the western block deepens northward. The north-south trending VLE 400 fault bands north-west near the northern boundary of the study area. The VLE 400 fault has a single plane in this seismic horizon depth. East-west trending

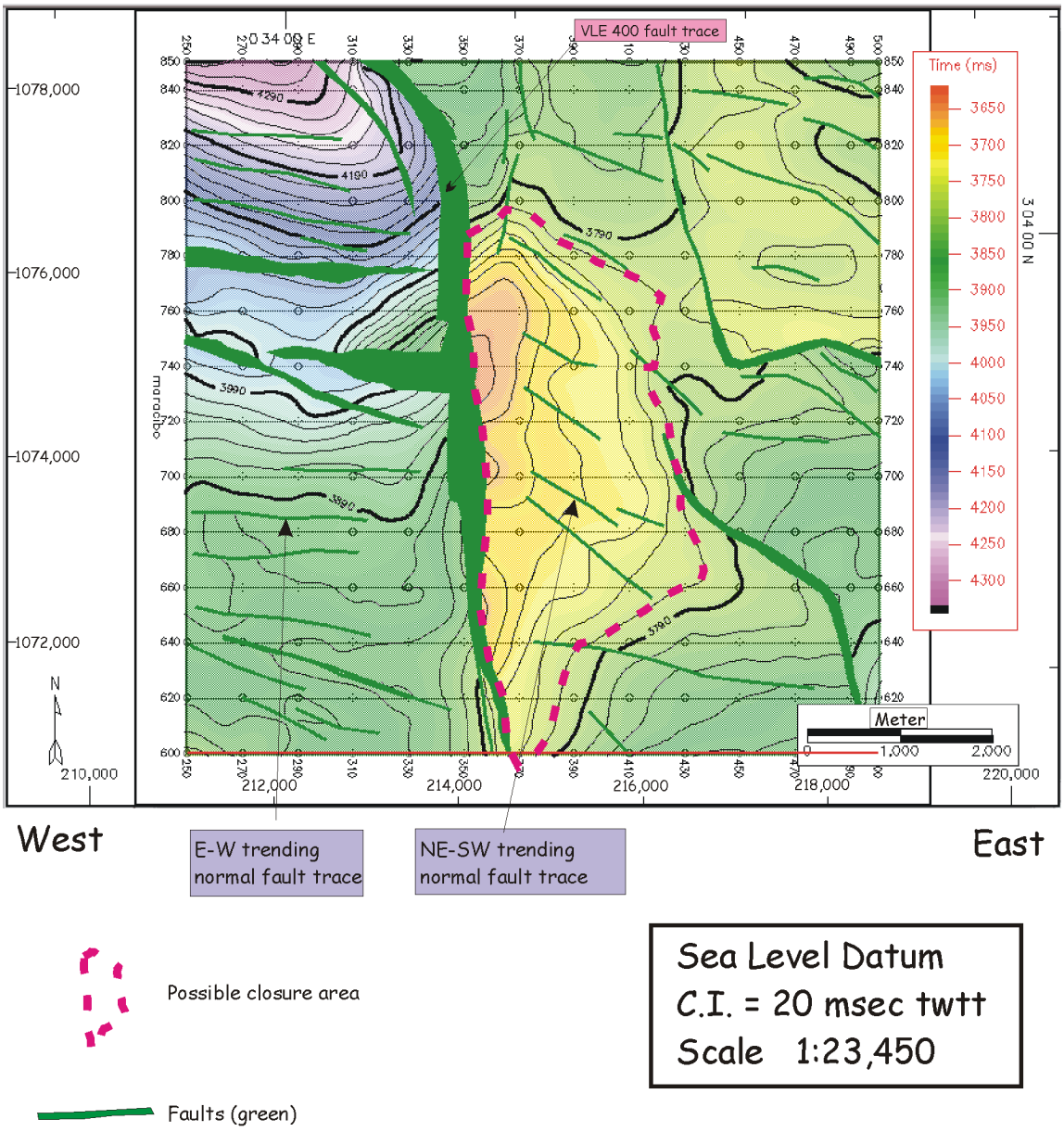

Figure 3-1. Time structure of the acoustic basement. A closure was developed with the VLE400 fault in the eastern block of the fault.

normal faults are well-developed in the western block and northeast-southwest trending normal faults prevail in the eastern block. The east-west trending normal faults in the western block may be related with sub-block rotation by the VLE 400 fault and the northeast-southwest trending normal faults in the eastern block might be created as en echelon faults during strike-slip movements of the VLE 400 fault. The amplitude display of possible basement shows dispersed features with trends influenced by faults (Figure 3-2). Amplitude anomalies are not observed within the closure area. Amplitude of the seismic horizon may not be influenced by depositional features or hydrocarbons but strongly disturbed by faults.

The time structure map of Hz.1 (top of synrift sediments) shows closures against the VLE 400 fault in the eastern block (Figure 3-3). The VLE 400 fault shows the same trend as that of the possible basement, and Fault B is developed as a continuous straight line trending north-south and diverting into two faults toward the north. No strong amplitude anomaly is observed within the closure, but one does appear in the southern part in the western block (Figure 3-4).

The time structure map of Hz.2 (the top of the La Luna Formation) shows a closure with Fault B in the eastern block (Figure 3-5). Faults trending westnorthwest-eastsoutheast are prevalent, with a few east-west faults in both blocks. A few more faults developed in the VLE 400 fault family. Strong amplitude anomalies are observed between the VLE 400 and Fault B within the

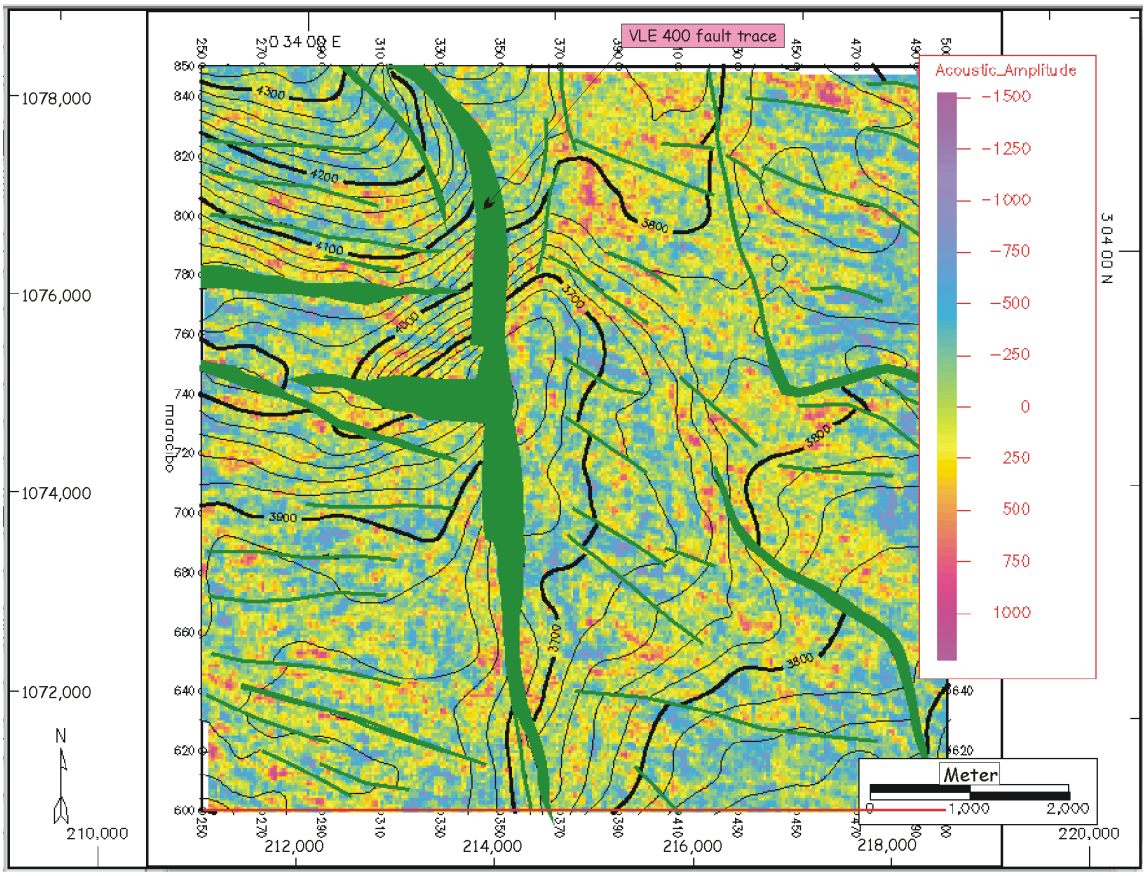

Figure 3-2. Amplitude display (arbitrary scale) of the acoustic basement with time structure contours. Strong amplitude anomaly is identified in the southern area of western block of the VLE 400 fault. Trends of amplitude are influenced by faults.

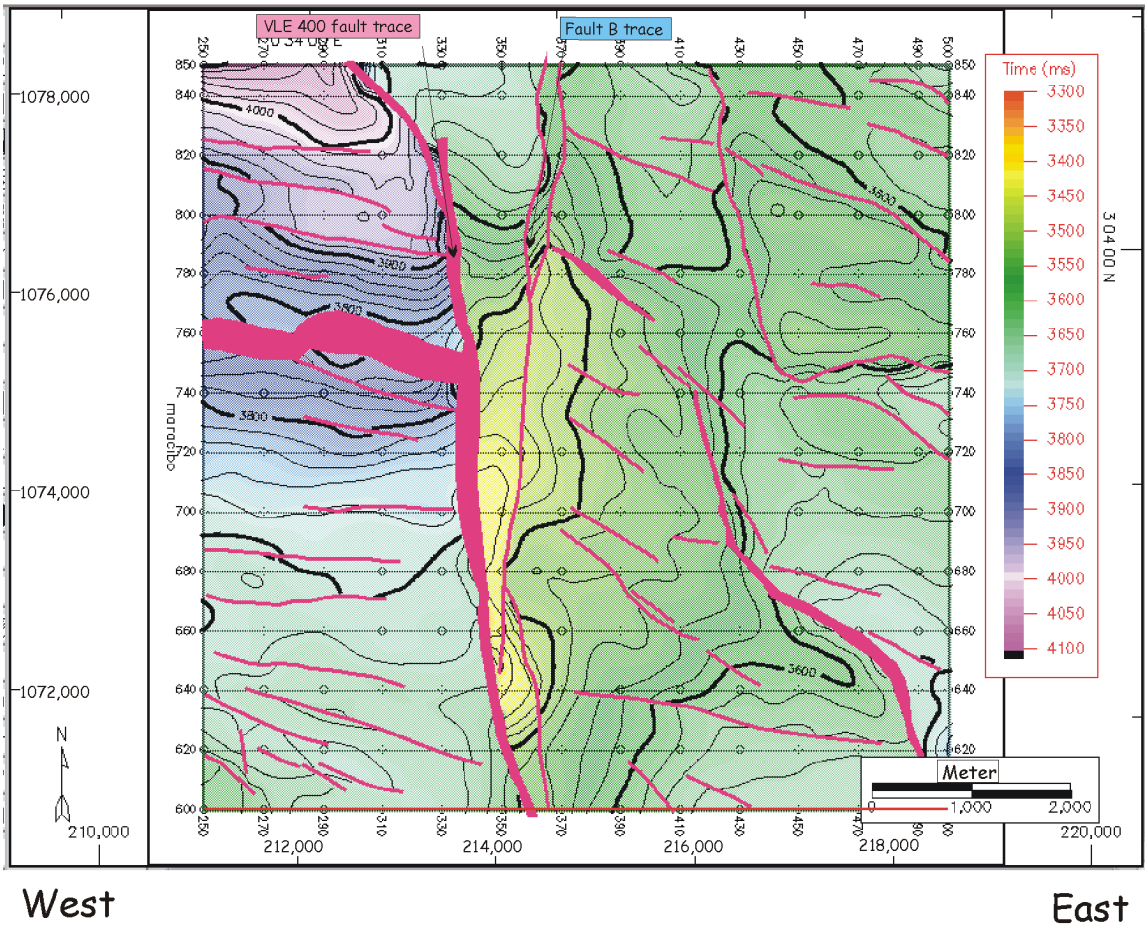

Figure 3-3. Time structure of Hz.1. A closure was developed with the VLE400 fault in the eastern block.

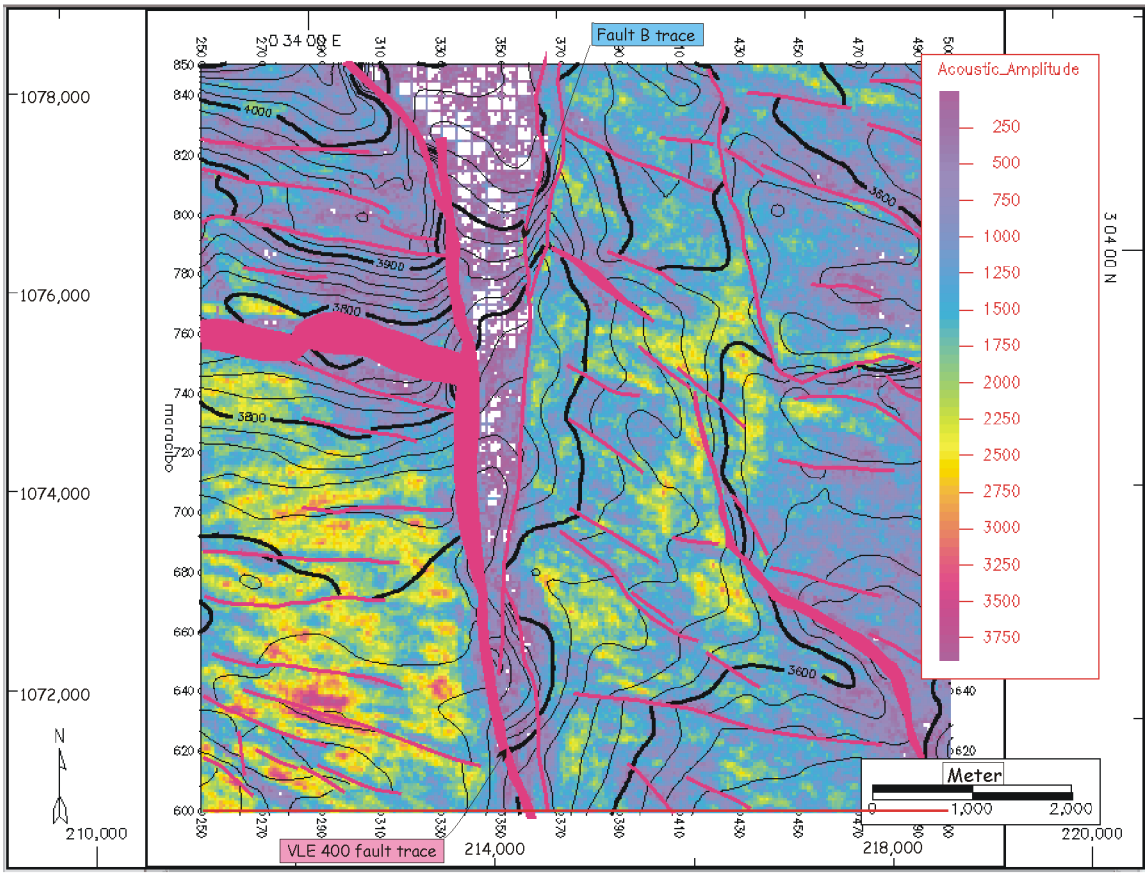

West

East

Faults (red)

Sea Level Datum
C.I. = 20 ms twtt
Scale 1:75,760

Figure 3-4. Amplitude display (arbitrary scale) of Hz.1 with time structure contours. Strong amplitude anomaly is identified in the southern area of western block of the VLE 400 fault. Eastsoutheast-westsouthwest trending normal faults are dominant in the western block and northwest-southeast trending normal faults prevail in the eastern block of the VLE 400 fault.

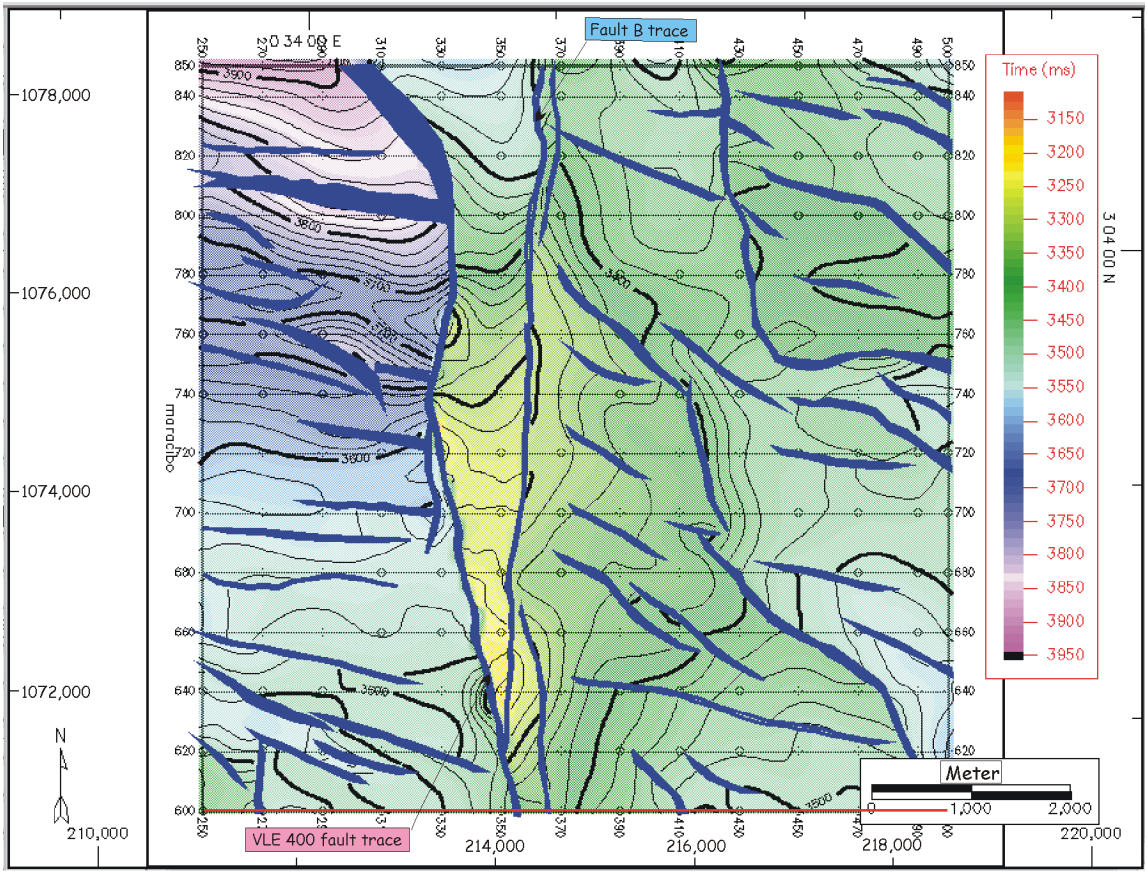

Figure 3-5. Time structure of Hz.2 (top of the La Luna Formation). A closure was developed with Fault B in the eastern block. Another closure appears between the VLE 400 fault and Fault B.

possible closure by the two faults, whereas the closure in the eastern block has no amplitude anomalies (Figure 3-6). The time structure map of Hz.3 (the top of the Guasare Formation) shows a closure including the VLE 400 fault in the eastern block with strong amplitude anomalies (Figures 3-7, 3-8). Northwest-southeast trending normal faults are well-developed in this seismic horizon.

The time structure map of Hz.4 (top of the C-5 member) shows a complicated feature in the VLE 400 fault family (Figure 3-9). The VLE 400 and Fault B are well-developed in north-south trending with northwest-southeast trending normal faults and northnortheast-southsouthwest trending reverse faults. A closure is developed including Fault B in the eastern block with amplitude anomalies (Figure 3-10). Even though amplitudes are disturbed by faults, especially northwest-southeast trending normal faults, they show a northeast-southeast trend. The amplitude anomalies may be influenced by hydrocarbon, especially within the closure; at the same time, they display depositional features.

The time structure map of Hz.5 (top of the C-4 member) shows a closure including Fault B with well-matched amplitude anomalies in the closure (Figure 3-11, 3-12). Compared to the structural features of seismic horizons of Hz.3 and below getting deeper toward north in the western block from the VLE 400 fault, Hz.4 and Hz.5 show an extended boundary starting from Fault B. Amplitudes of the seismic horizon display northeast-southwest trending with

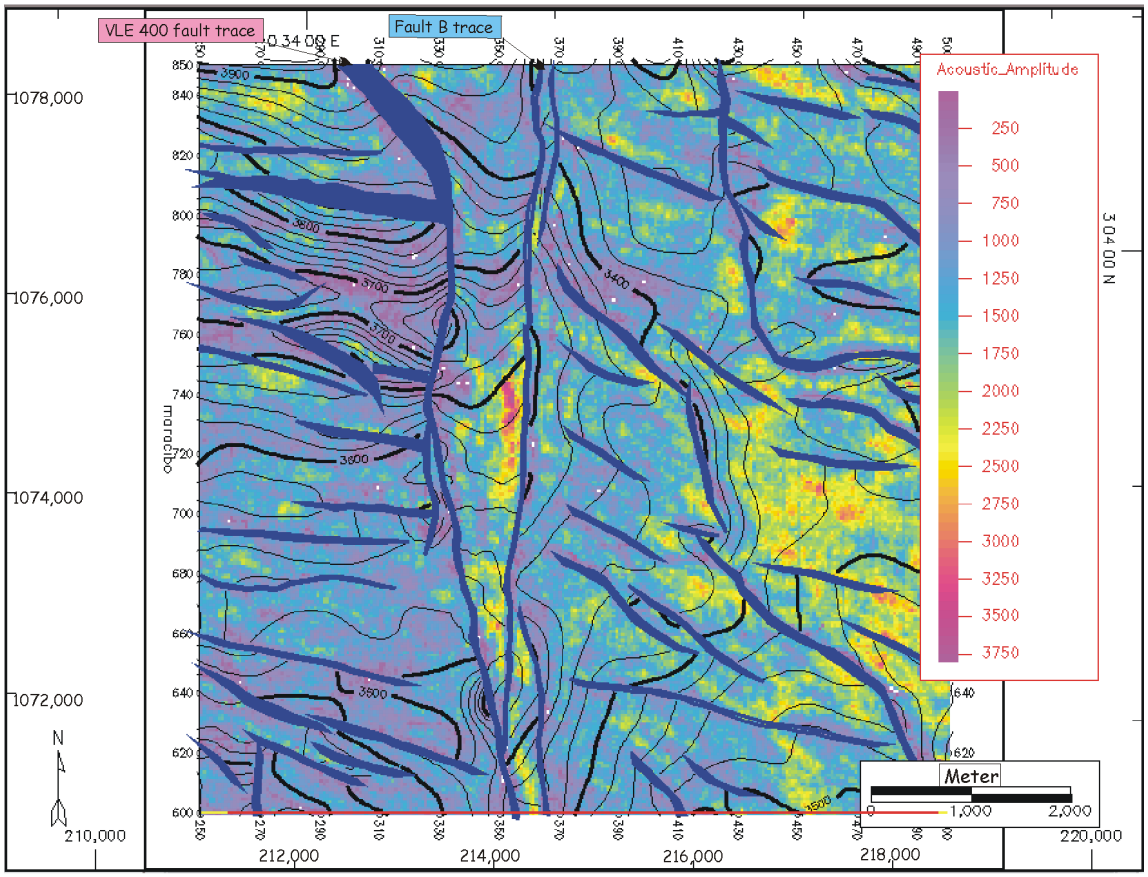

West

East

Faults (blue)

Sea Level Datum
C.I. = 20 ms twtt
Scale 1:75,760

Figure 3-6. Amplitude display (arbitrary scale) of Hz.2 with time structure contours. Eastnortheast-westsouthwest trending normal faults are in the western and northwest-southeast trending normal faults with few east-west trending faults are in the eastern block. Strong amplitude anomalies are identified between the VLE400 and Fault B.

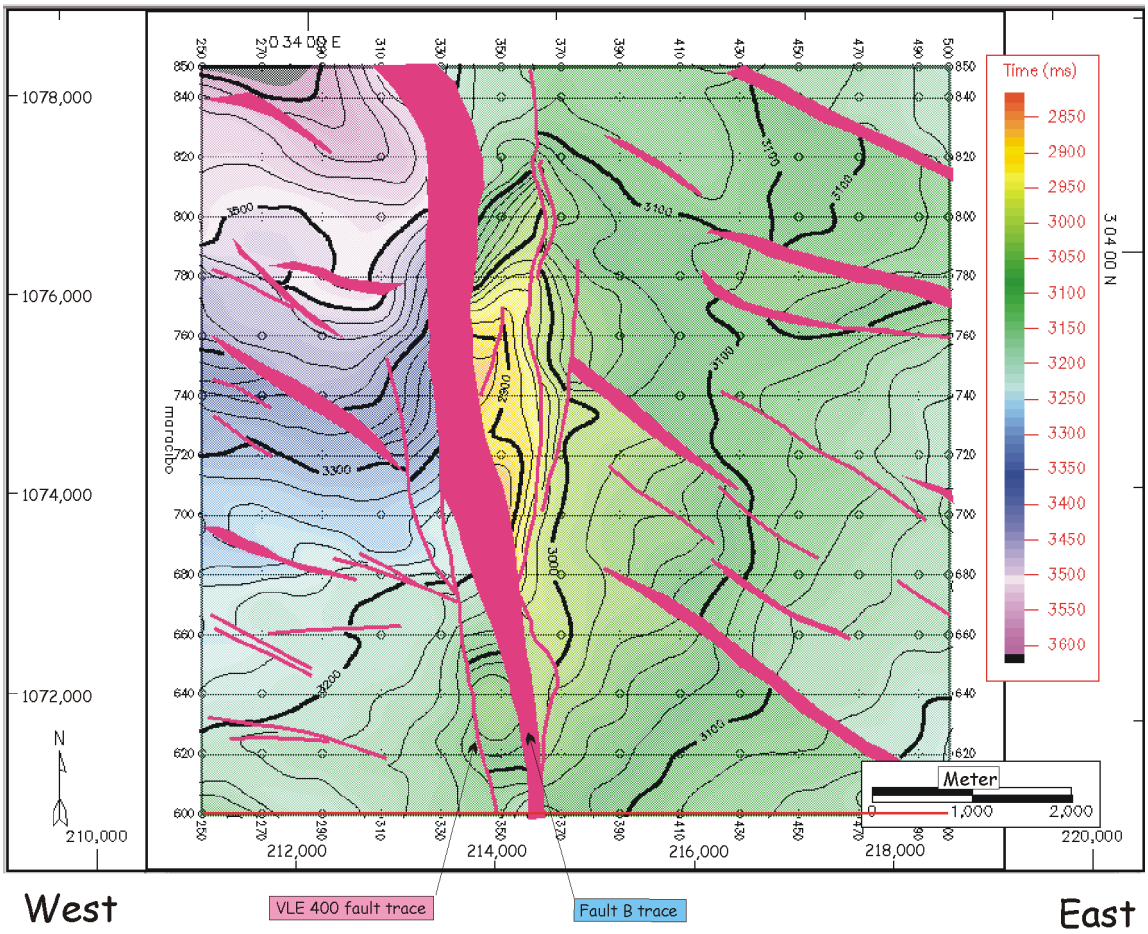

*No detailed interpretation was possible because of the poor seismic image between the VLE 400 fault and Fault B, which caused the wide fault polygon.

Sea Level Datum
C.I. = 20 ms twtt
Scale 1:75,760

Faults (red)

Figure 3-7. Time structure of Hz.3 (top of the Guasare Formation). A closure developed in the eastern block of the VLE 400 fault.

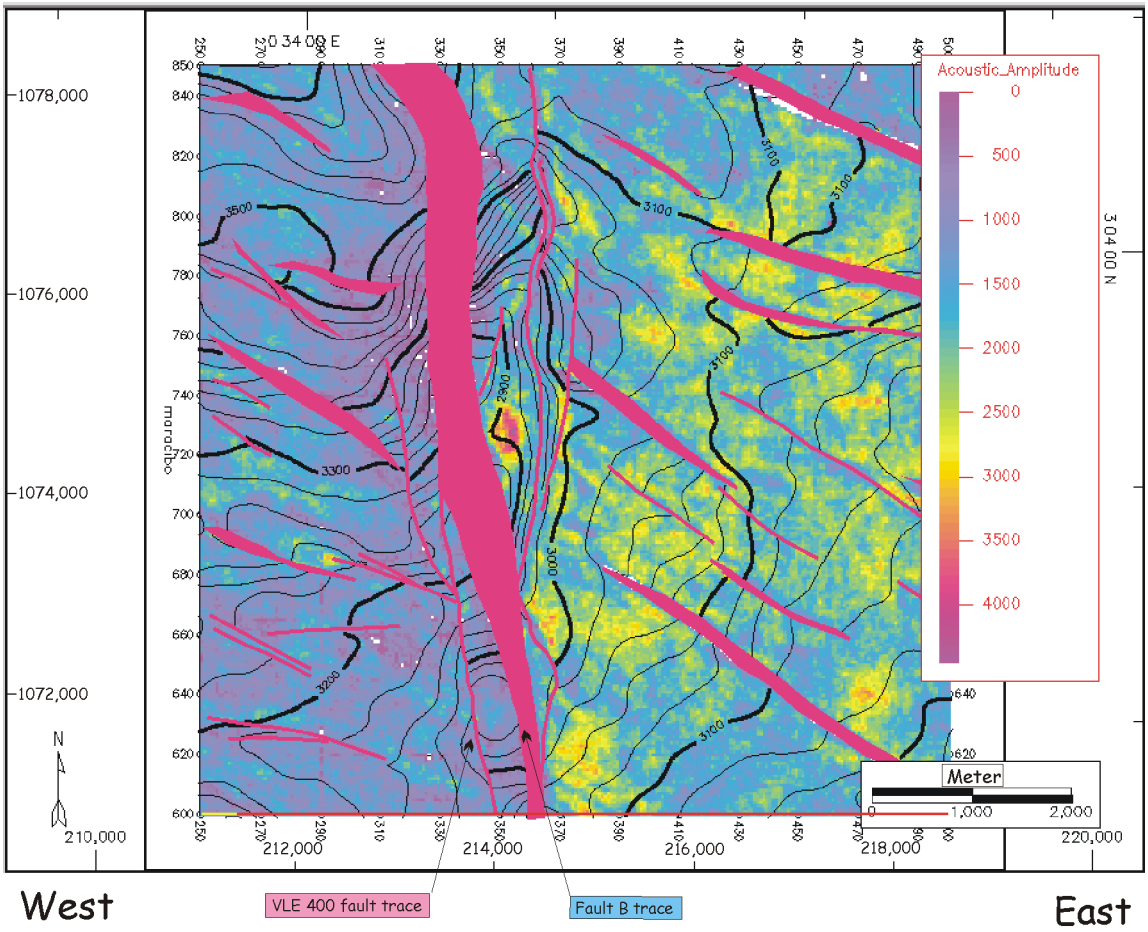

*No detailed interpretation was possible because of the poor seismic image between the VLE 400 fault and Fault B, which caused the wide fault polygon.

Sea Level Datum
C.I. = 20 ms twtt
Scale 1:75,760

Faults (red)

Figure 3-8. Amplitude display (arbitrary scale) of Hz.3 with time structure contours. The throw of VLE 400 is increased within the seismic horizon. East-west trending normal faults are very few and northwest-southeast trending normal faults are developed on both sides of the VLE 400 fault. Strong amplitude anomalies occurred between the VLE 400 and Fault B.

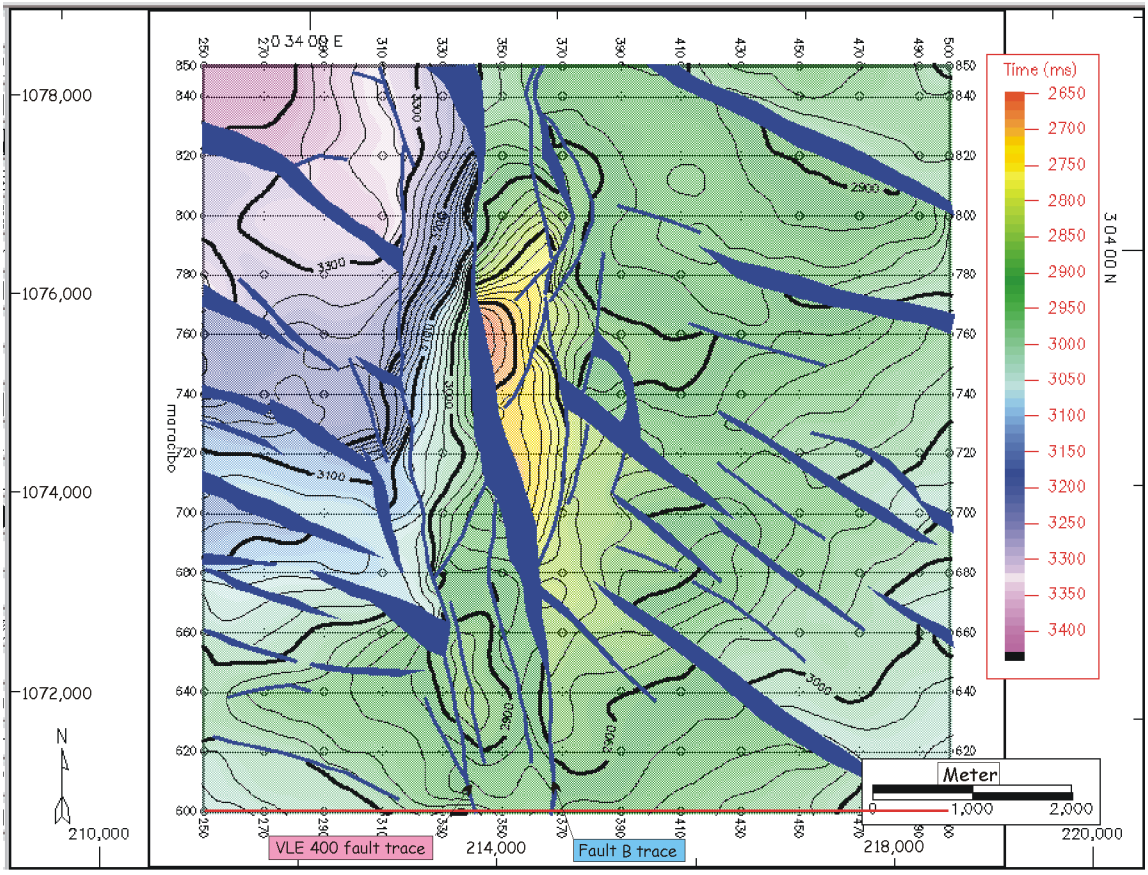

Faults (blue)

Sea Level Datum
C.I. = 20 ms twtt
Scale 1:75,760

Figure 3-9. Time structure of Hz.4 (top of the C-5 member). A closure developed with Fault B in the eastern block.

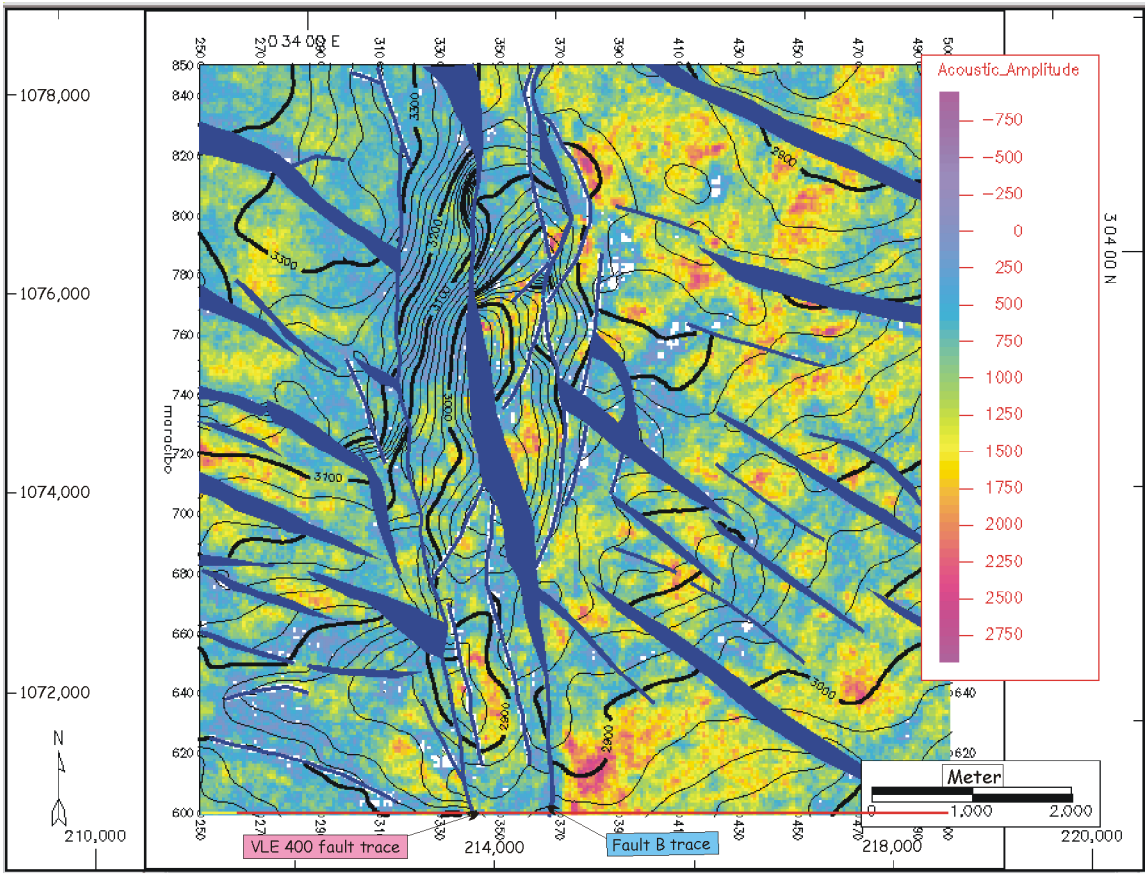

Figure 3-10. Amplitude display (arbitrary scale) of Hz.4 (top of the C-5 member) with time structure contours. Eastnortheast-westsouthwest trending normal faults are very few. Northwest-southeast trending normal faults developed in both blocks of the VLE 400 fault. Strong amplitude anomalies are identified between the VLE 400 and Fault B. Closures developed in the eastern block of only Fault B.

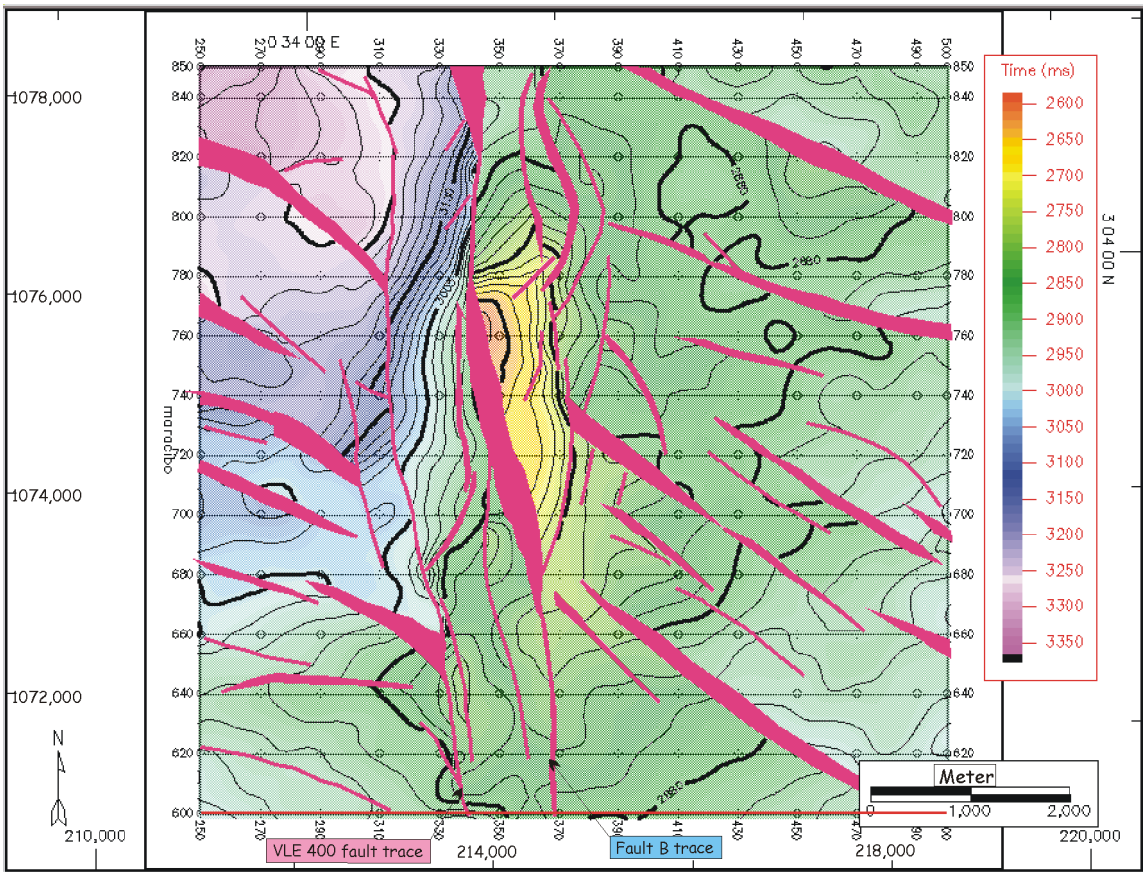

Figure 3-11. Time structure of Hz.5 (top of the C-4 member).
A closures developed with Fault B in the eastern block .

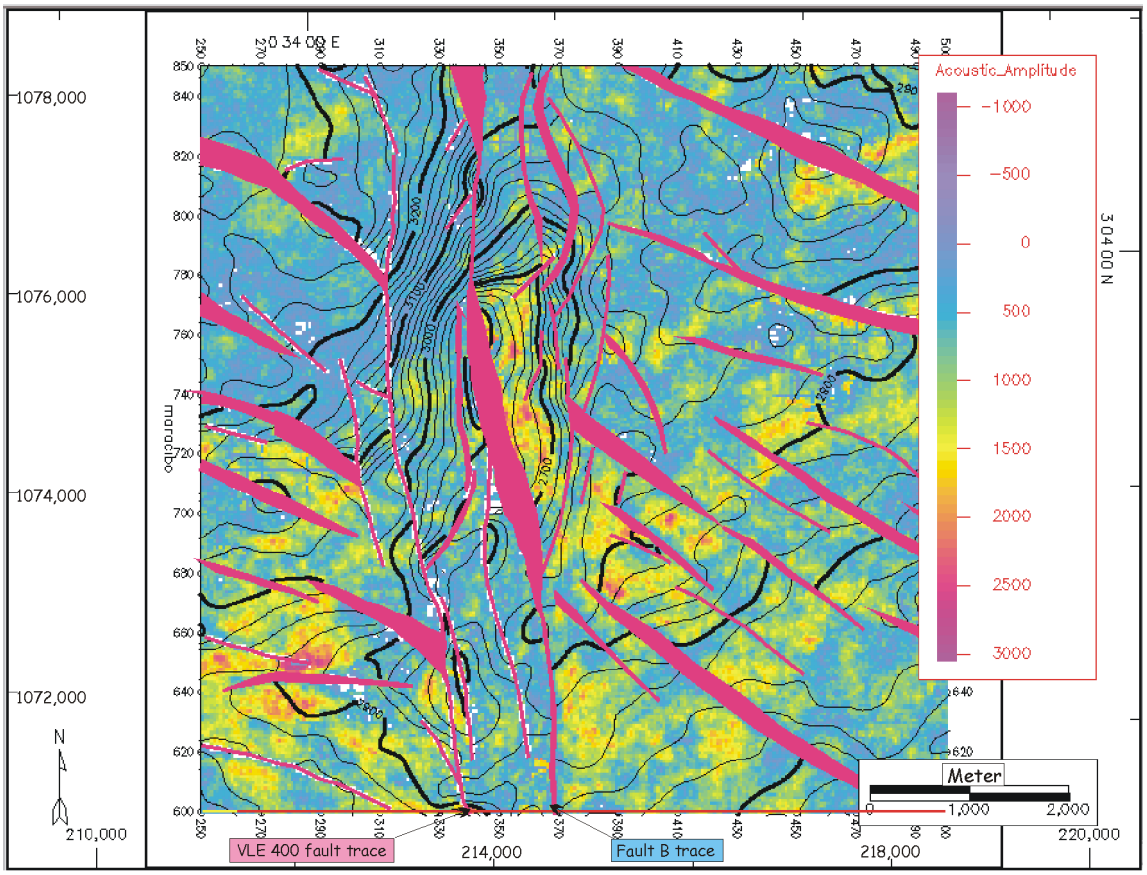

Figure 3-12. Amplitude display (arbitrary scale) of Hz. 5 (top of the C-4 member) with time structure contours. Eastnortheast-westsouthwest trending normal faults are very few. Northwest-southeast trending normal faults developed in both blocks of the VLE 400 fault. Strong amplitude anomalies are identified between the VLE 400 and Fault B. Closures developed only in the eastern block of only Fault B. Amplitude displays have northeast-southwest trends, even though they are disturbed by northwest-southeast trending normal faults. Strong amplitude anomalies within the closure of the eastern block of the VLE 400 fault are caused by trapped hydrocarbon.

disturbances by northwest-southeast trending normal faults. The amplitude anomalies within the closure are believed to be effects of hydrocarbons and the amplitudes' northeast-southwest trending is influenced by depositional features of the C-4 member.

The time-structure maps of Hz.6 (the Eocene unconformity) shows a pop-up structure (Figure 3-13). This seismic horizon has a distinct closure within the VLE 400 fault family, but hydrocarbons have not been discovered from this interval. Some strong amplitude anomalies discovered from this interval developed out of the closure area along the faults (Figure 3-14). Some of them may have been caused by hydrocarbon leakage along the faults from reservoir rocks below the horizon, and some may result from depositional features. One of the dominant structural features observed in the horizon is dipping toward the southeast. The trend is gentle but obviously observed from this seismic horizon.

The time structure map of Hz. 7 is influenced by the structural feature of Hz. 6 (the Eocene unconformity) and has a closure on the same area as that of Hz. 6 without any amplitude anomalies (Figure 3-15). A northwest-southeast trending, curved, normal fault developed within the closure. The dipping toward southeast becomes predominant in this seismic horizon. A time-structure map of Hz. 8 has the same structural features as that of the Hz. 7 with dispersed amplitude anomalies (Figure 3-16, 3-17). Time-structure maps of Hz. 9 and Hz. 10 show different features from those of Hz. 7 and Hz. 8. They display a

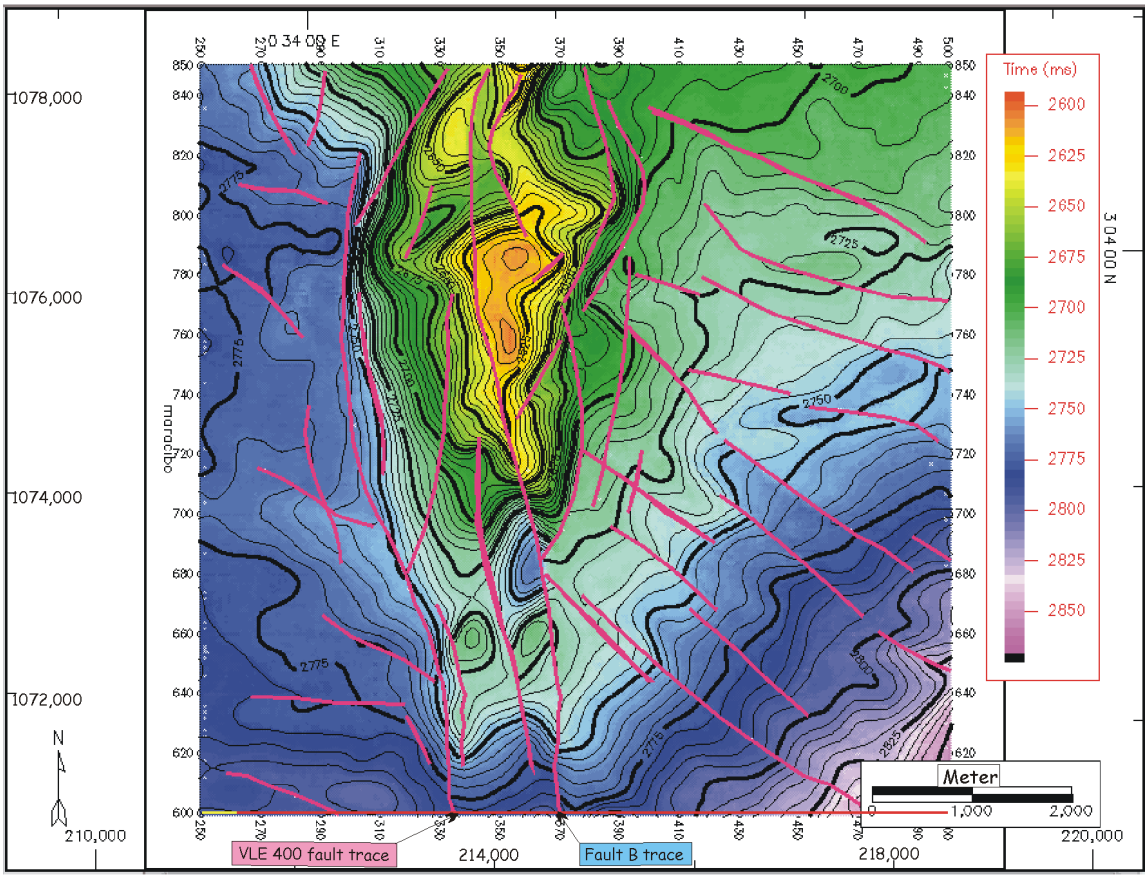

Figure 3-13. Time structure of Hz. 6 (Eocene unconformity).

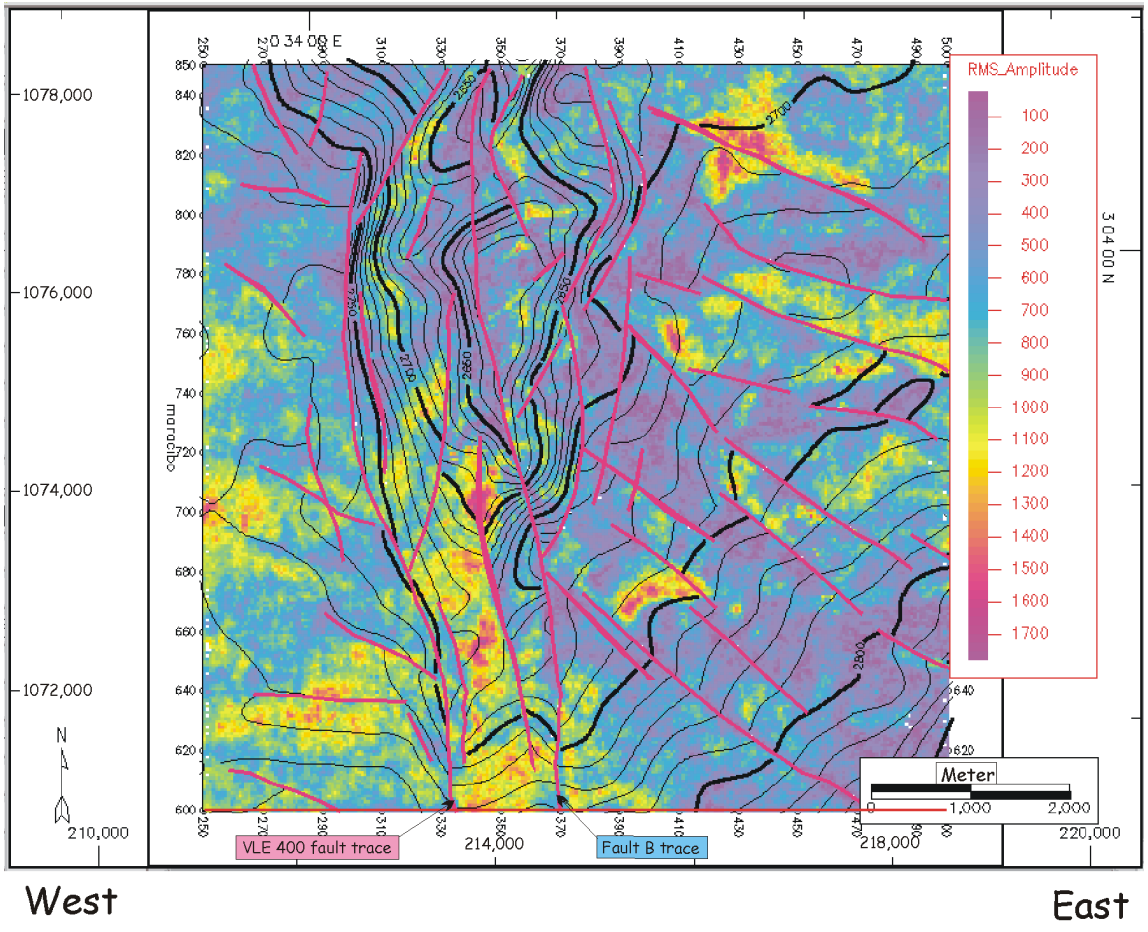

Figure 3-14. Amplitude display (arbitrary scale) of Hz.6 (Eocene unconformity) with time structure contours. The VLE 400 and Fault B are well recognized within the seismic horizon. Northwest-southeast trending normal faults and northnortheast-southsouthwest trending reverse faults were developed in both blocks of the VLE 400 fault. An anticline developed with the VLE 400 fault and Fault B.

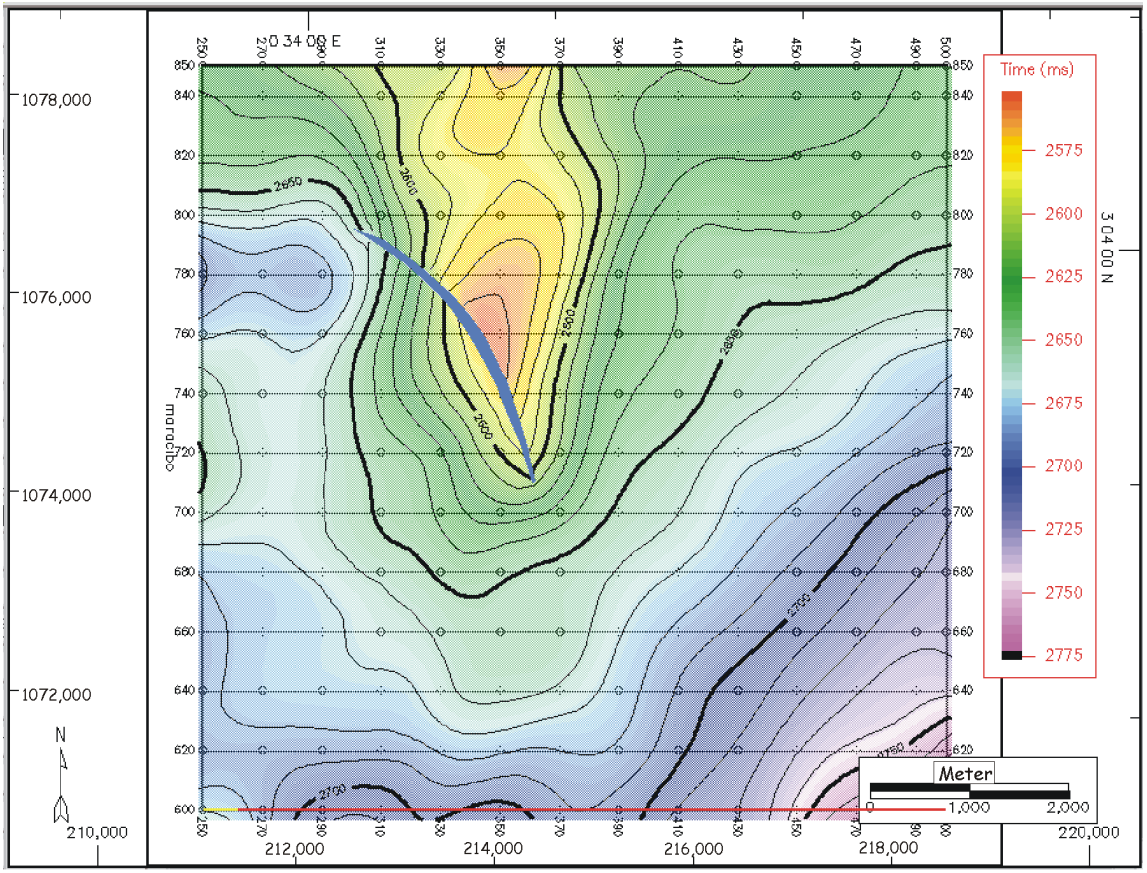

Figure 3-15. Time structure of Hz. 7. The structure had a closure with a northwest-southeast trending normal fault and dipping toward the southwest.

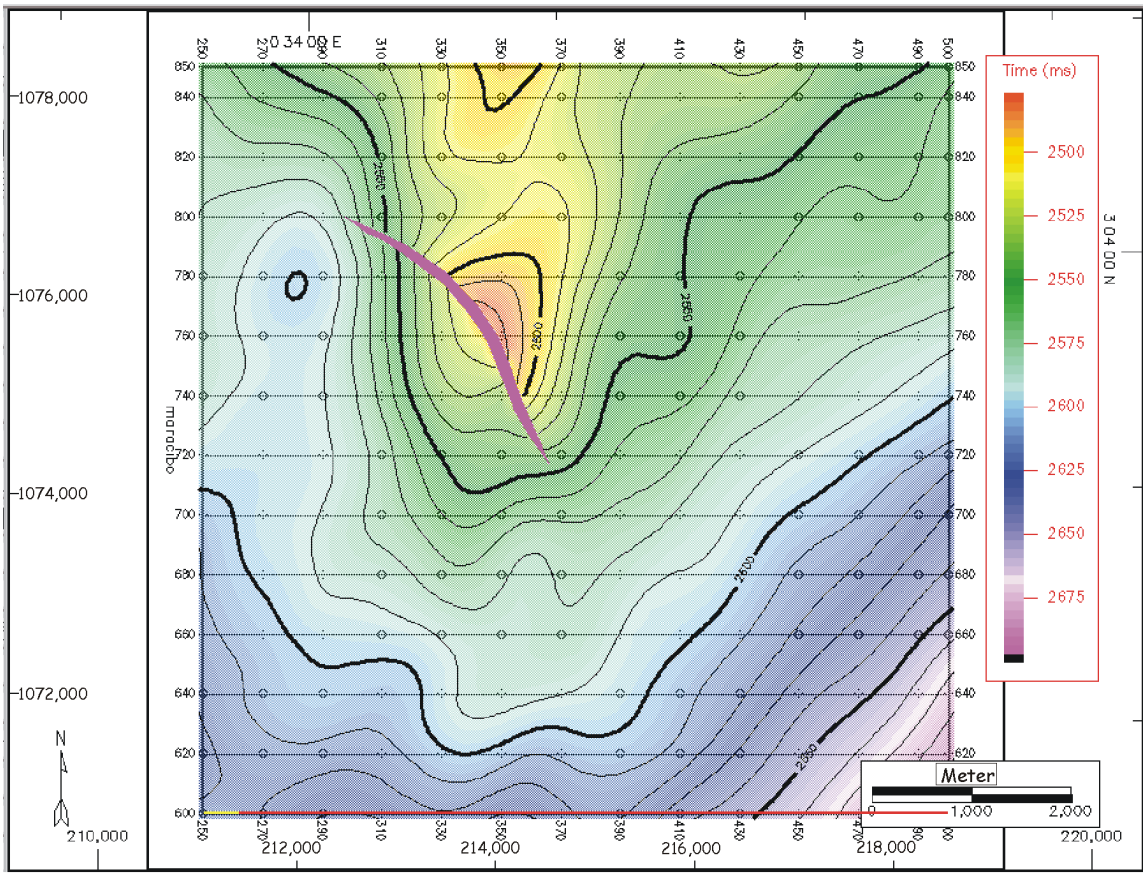

Figure 3-16. Time structure of Hz. 8. The structure had a closure with the northwest-southeast trending normal fault.

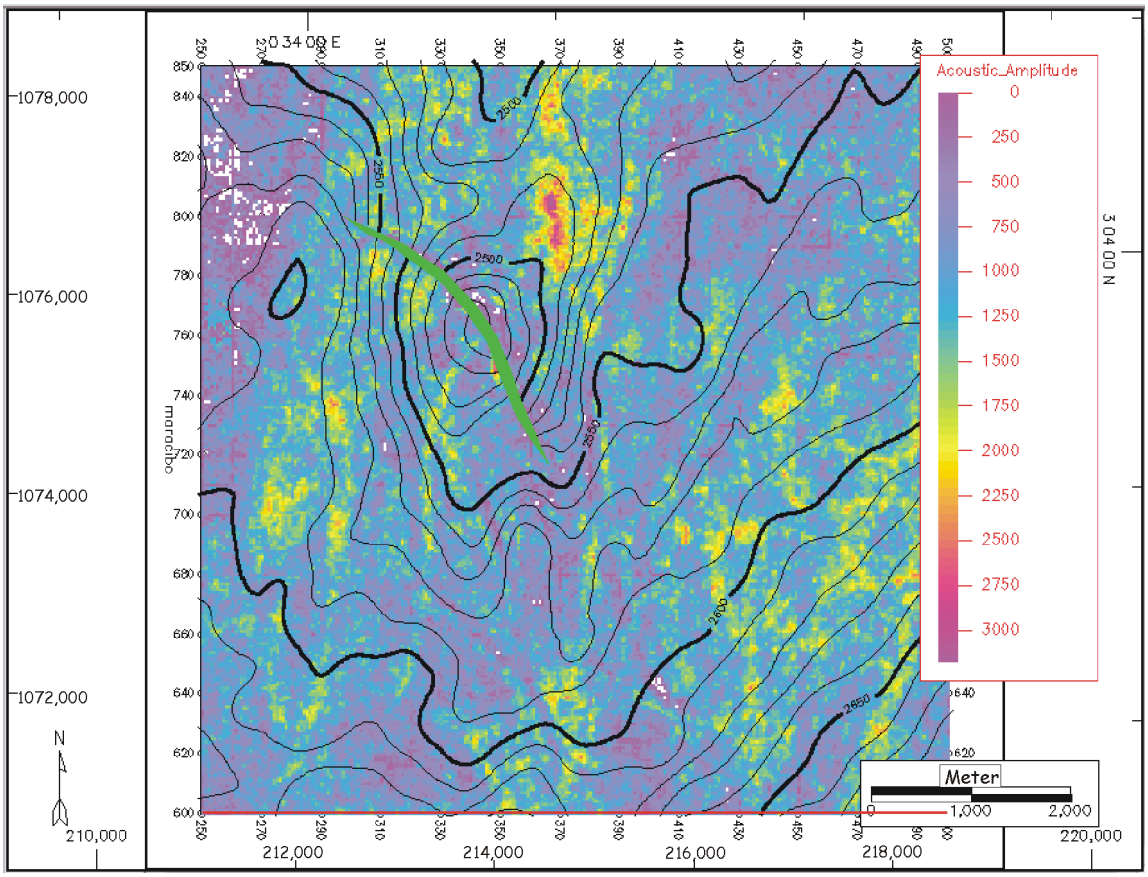

Figure 3-17. Amplitude display (arbitrary scale) of Hz.8 with time structure contours. A northwest-southeast trending normal fault developed from the VLE 400 fault. The structure pattern is similar to the Hz. 6 (Eocene unconformity) .

monocline structure slightly modified by the northwest-southeast trending, curved, normal fault (Figures 3-18, 3-19). Amplitude anomalies are dispersed through the study area and may be influenced by depositional processes (Figures 3-20, 3-21).

3.2. Depositional response and architecture

The main reservoir rock of the Misoa Formation is divided into C-5, C-4 and C-1~3 members from old to young, interpreted as depositions of a tide-dominated delta. The sandstones introduced as the C-1, C-2 and C-3 are considered here as the C-1~3 member because of their thickness and similar characteristics. Compared to river- and wave-dominated deltas, facies models for tide-dominated deltas are not well-established, because of their relatively complex spatial changes (Dalrymple, 1992). Analysis of geometry and bedding architecture is also important to understand internal heterogeneity of a complex reservoir. In this regard, geometry and bedding architecture of the formation have been studied on the basis of vertical log-pattern trends, log character and seismic attributes.

The total thickness of about 800 ft (244 m) of the C-5 member comprises 200- to 250-ft (60- to 76-m) thick bedsets of fluvial/distributary channel deposits arranged in an aggradational stacking pattern (Figure 3-22). After deposition

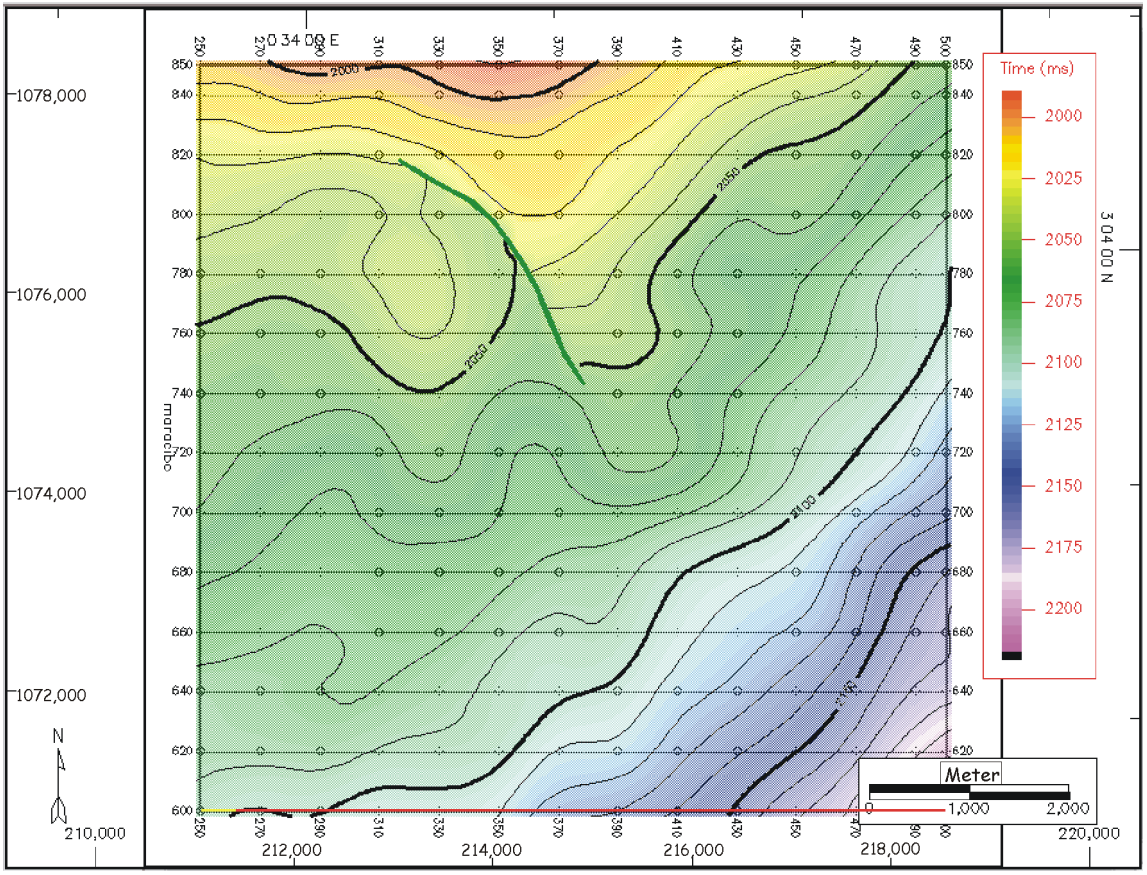

Figure 3-18. Time structure of Hz. 9. The structure was dipping toward southeast, which might have been caused by thrust loading from the southeastern part.

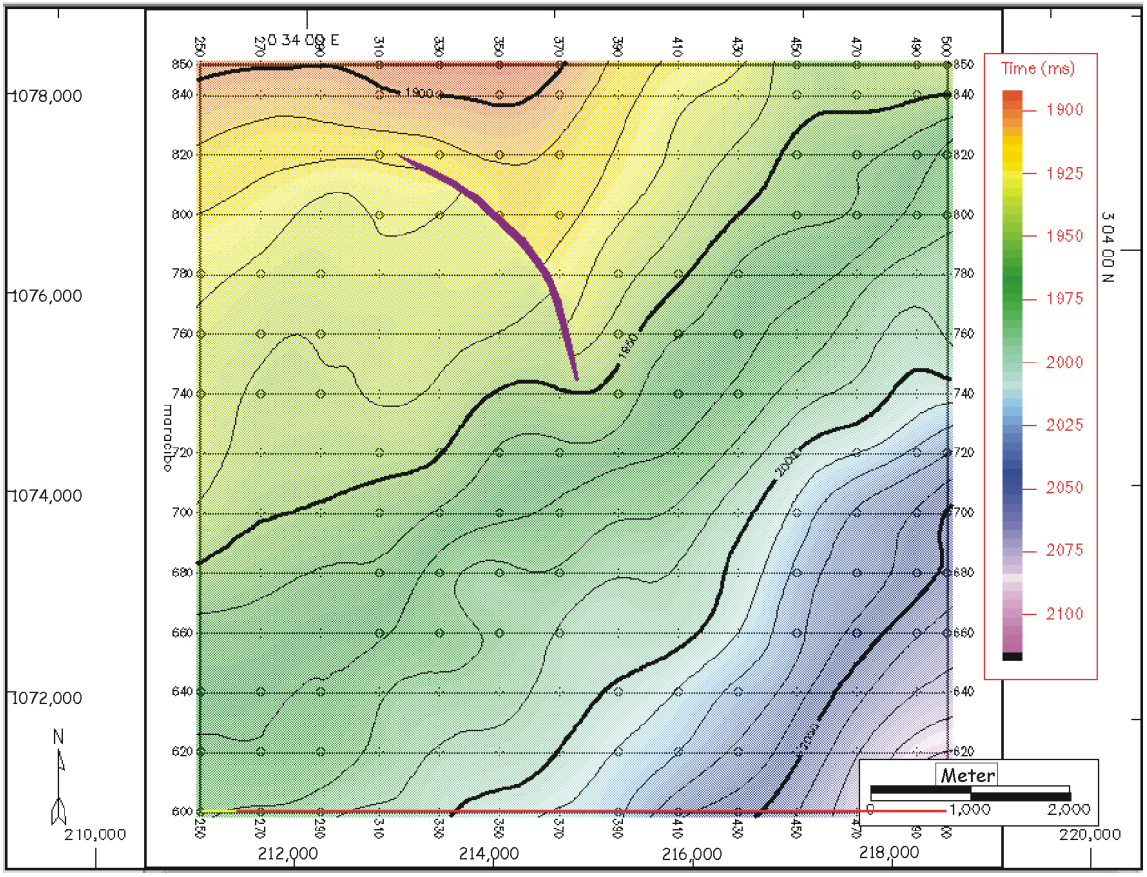

Figure 3-19. Time structure of Hz. 10. The structure was dipping toward southeast, which might have been caused by thrust loading from the southeastern part.

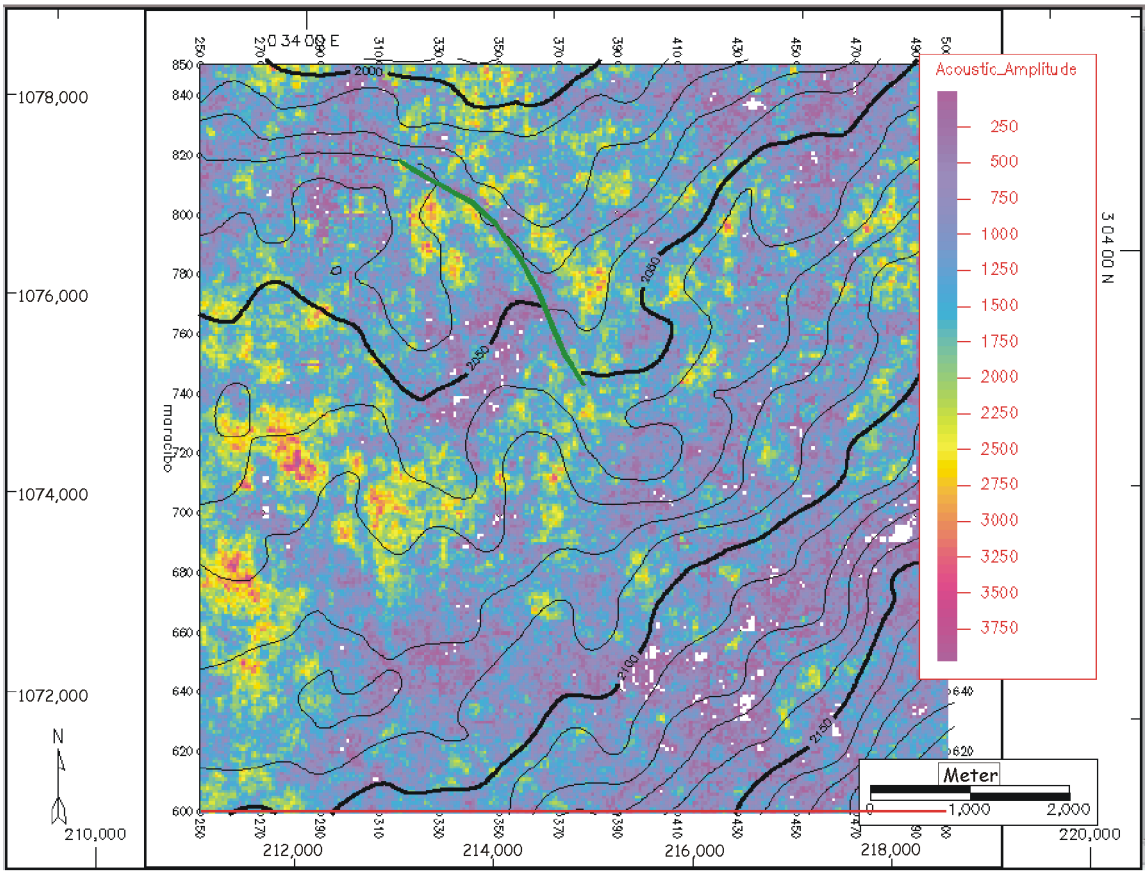

Figure 3-20. Amplitude display (arbitrary scale) of Hz.9 with time structure contours. The structure pattern is monoclinal, dipping southeast, which differs from Hz. 6 (Eocene unconformity) .

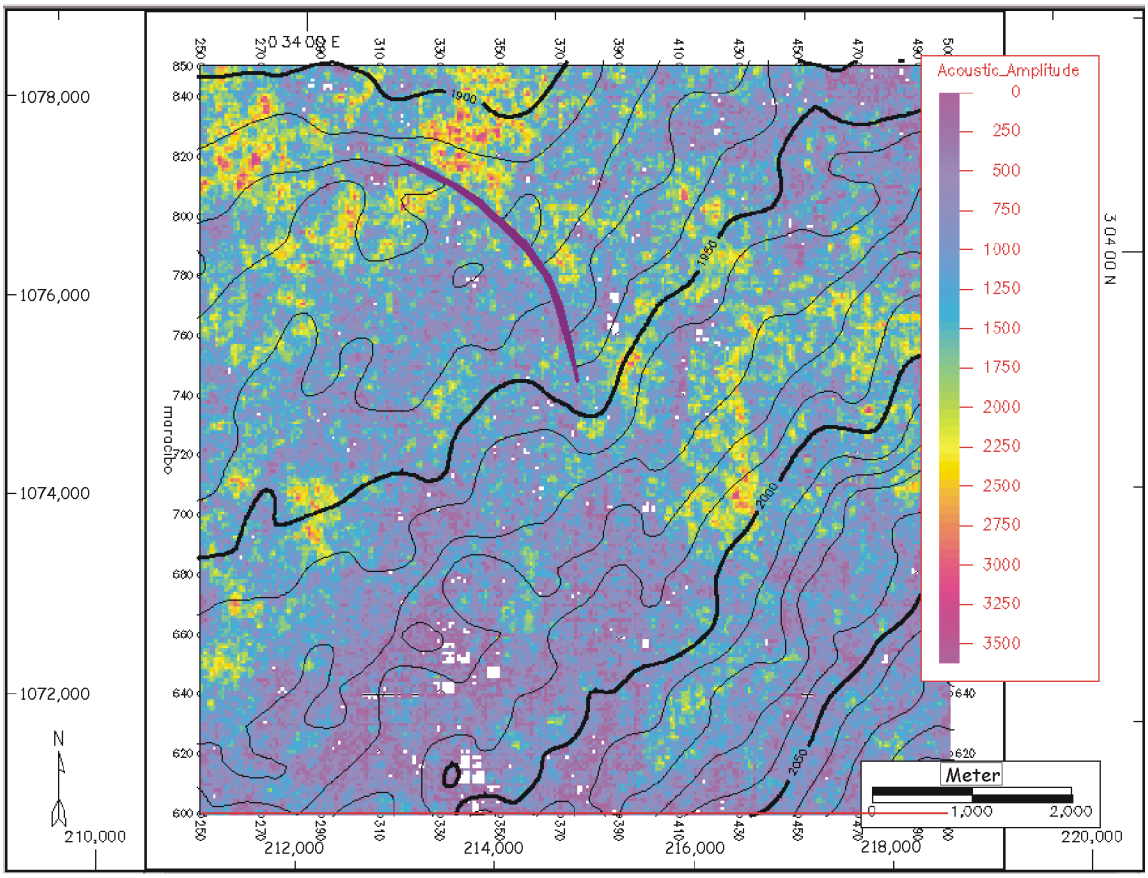

Figure 3-21. Amplitude display (arbitrary scale) of Hz.10 with time structure contours. A northwest-southeast trending normal fault, developed from the VLE 400 fault, is identified within the formation.

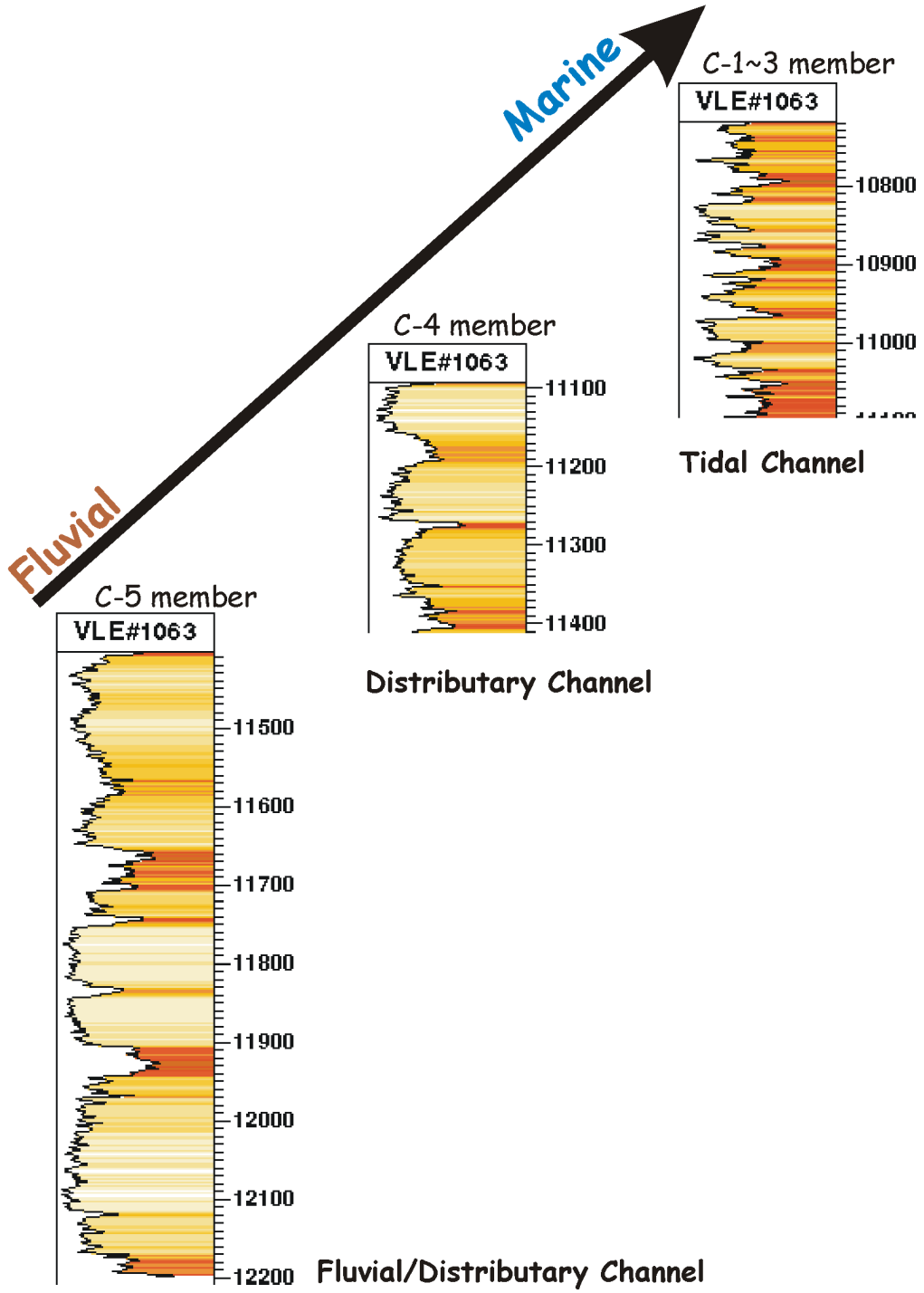

Figure 3-22. Depositional environment with wireline logging facies from the C-1~3 to the C-5 members.

of the C-5 member, trangression followed, and then the C-4 member was deposited with 80- to 120-ft (24- to 37-m) thick bedsets of distributary channel fills as a form of aggradation (Figure 3-22). A flooding surface that separates the C-4 member from the C-1~3 member consists of 20- to 50-ft (6- to15-m) delta-front sandstones developed by aggradation (Figure 3-22). There were transgression events between C-5 and C-4 members, and C-4 and C-1~3 members. Each member has aggradational deposition geometries and transgressional events between boundaries that generated overall retrogradational geometries in the basin. Usually, the few strata deposited during the transgression of the shoreline were preserved or shorelines too rapidly transgressed to deposit significant strata. The events may imply that significant tectonic movement influenced the rapid changes of sea level, which provided different environments to each of the members. Elongate tidal bars (sand ridges) are expected by interpretation of seismic attribute maps of the C-4 and C-5 members (Figures 3-10, 3-12).

3.2.1. C-5 member

These deposits comprise stacked upward-fining and blocky, 200- to 250-ft (60- to 76-m) thick sandstones interbedded with thin shales. The member can be subdivided into three bedsets with their sharp basal contacts. Blocky log patterns dominate, and many individual bedsets end with subtle fining-upward patterns. Thin, high gamma ray shales are frequently interbedded within

sandstone bedsets, and 10- to 20-ft (3- to 6-m) shales lie between sandstone bedsets.

The stacked, blocky, log patterns with subtle fining-upward and a few coarsening-upward trends can be interpreted as an aggradation geometry when sediment supply volume and new accommodation volume in the topset are approximately equal. The C-5 member is subdivided into three distinct bedsets. Individual bedsets do not have the same log patterns but vary between wells at distances from 50 to 200 m. Therefore, it was interpreted that the bedset log patterns are not controlled by relative sea level changes but by depositional processes. On top of that, no regional shale is recognized within the C-5 member, which may be interpreted as regional deposition by sea level change. Thickness of individual sandstone bedsets ranges from 250 to 300 ft (76 to 91 m), which implies that larger and deeper distributary channels developed near a fluvial environment. Total thickness of the C-5 member is controlled by depositional processes and can be subdivided by distributary and inter-distributary zones. Usually, thicker and higher net-to-gross ratios are expected from the distributary zone, and thinner and lower net-to-gross ratios are from interdistributary zones.

3.2.2. C-4 member

The C-4 member deposits comprise upward-fining, 80- to 120-ft (24- to 37-m) thick sandstones interbedded with thin shales. The C-4 member can be

subdivided into three bedsets with their sharp basal contacts and occasionally coarsening-upward vertical trends. The average total thickness is 220 ft (67 m) and ranges from 220 to 380 ft (67 to 116 m). Log trends within the C-4 member vary between wells. Three bedsets of the C-4 member have distinct upward-fining trends but change into coarsening-upward with denser, interbedded shale toward the south. The amplitude map of the C-4 member has a more or less northnortheast-southsouthwest protracted, high-amplitude trend. The amplitude has been affected by faults which developed in the northnortheast-southsouthwest and north-south directions.

The three stacked, fining-upward trending bedsets are interpreted as aggradation deposits. The boundary shales interbedded between the three bedsets can be well-correlated among wells. Therefore they are interpreted as regional deposits controlled by sea-level fracturation. Occasionally individual bedsets have sharp basal contact with the interbedded shales. These may be results of the distributary channel cut into flooding surfaces. The average thickness of the C-4 bedsets is greater than that of the estuarine distributary channel sandstones (around 30 ft, Maguregui and Tyler, 1991) studied using the Eocene reservoir in the same basin. There are two possibilities: The C-4 member may be subdivided into more than three bedsets, or the C-4 member might have been deposited by wider and deeper distributary channels near the fluvial environment. The log patterns of the C-4 member have a few distinct features. The member has subtle fining-upward trends observed in most of the

wells. Frequently, individual bedsets have sharp contacts at their bases. The total thickness of the C-4 member is constant, with some differences ranging to 20 or 40 ft (6 or 12 m) between wells. The differences do not have any trend, possibly because the study area is limited and the variation was not controlled by regional tectonic or sea-level change, but by depositional processes. The correlation of vertical wire-line logs facies trends of the C-4 members in the field suggests that the facies trend changes are not related to basin-wide episodes such as tectonic or sea-level change but depositional processes within the delta system connected from the fluvial to the open marine environment.

3.2.3. C-1~3 member

The C-1~3 member appeared in well VLE1063 and well VLE1004. The C-1~3 member should appear in other wells, but data are not available for the study. The C-1~3 member is 376 ft (115 m) in well VLE1063 and 853 ft (260 m) in well VLE1004. Thickness of individual bedsets ranges from 20 ft to 50 ft (6 to15 m) and coarsening-upward log facies trends are dominant with occasionally fining-upward trends. No thick shale intervals or high gamma ray shales are recorded in the two wells. The C-1~3 member log facies trends of well VLE1063 are similar to the bottom bedsets of well VLE1004. Coasening-upward log facies trends usually have sharp contacts at their base. This member comprises 20- to 50-ft (6- to 15-m) thick, mainly coarsening-upward and occasionally fining-upward vertical log facies trends.

3.3. Growth strata

The growth strata concept is useful to detect rejuvenated existing faults, especially subtle movements which are not recognized by conventional seismic interpretation. In total, five growth strata were evaluated by the isochron between two horizons interpreted from 3-D seismic data (Figure 3-23).

3.3.1. Growth strata 1

The growth strata between Hz.5 (the top of the C-4 member) and Hz.6 (the Eocene unconformity) are the most distinct growth strata among the five and have been identified as the Misoa-Pauji sediments (Figure 3-24). The growth strata might have been caused by collision between the South American and Caribbean plates. The collision created compression across the VLE 400 fault family located in the foredeep area within the foreland basin system. Compression created from the eastern side of the fault rejuvenated the existing geometry and uplifted the eastern block. Because of the uplifting of the eastern block, additional accommodation space was created and thicker sediments were deposited within the space. Growth strata 1 has different patterns than the others; the thickness difference between two blocks shows greater thickness across Fault B, growing thinner toward the south, and eventually disappearing.

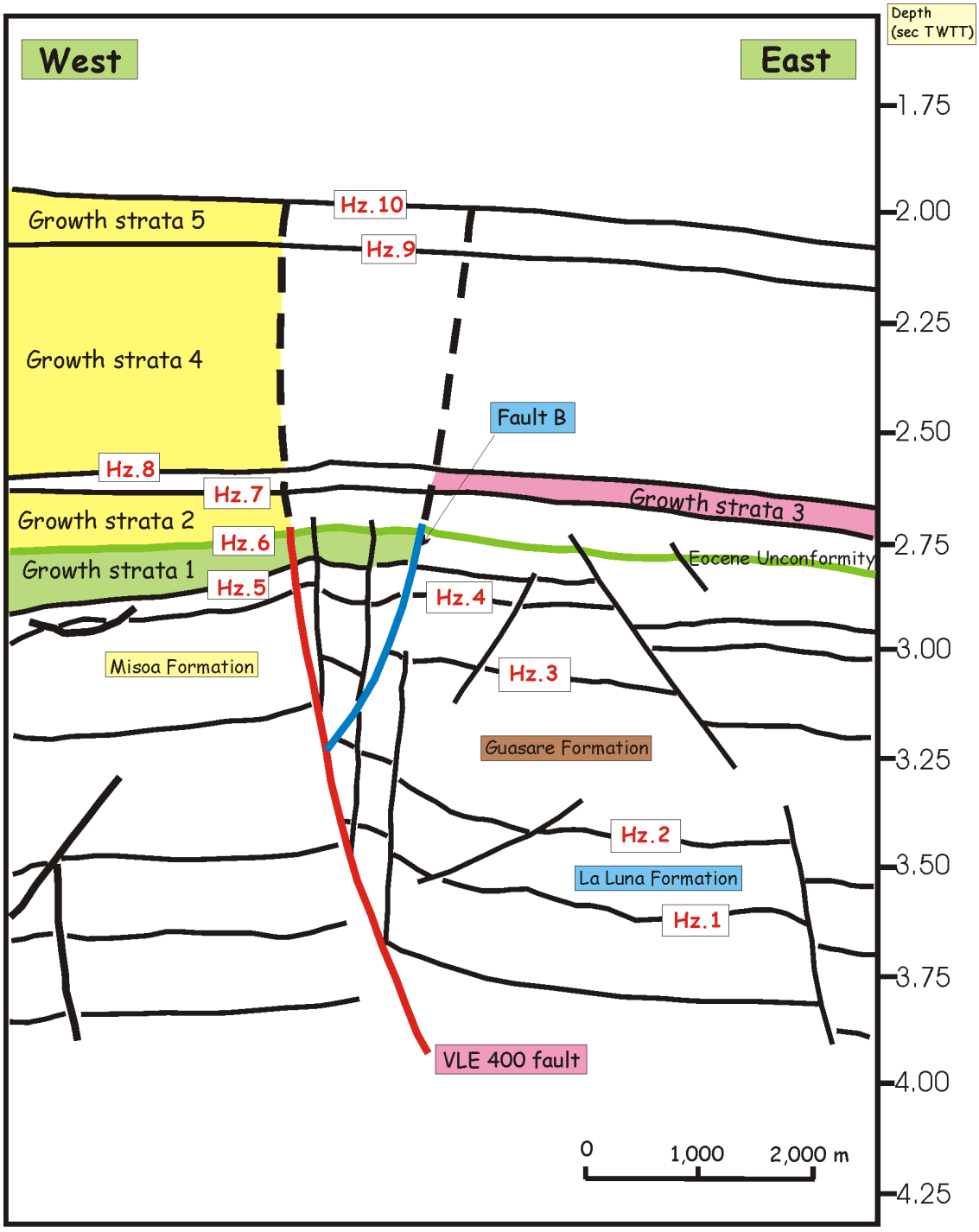

Figure 3-23. Geoseismic section of inline 640 showing the five growth strata. See Figure 24 for the location.

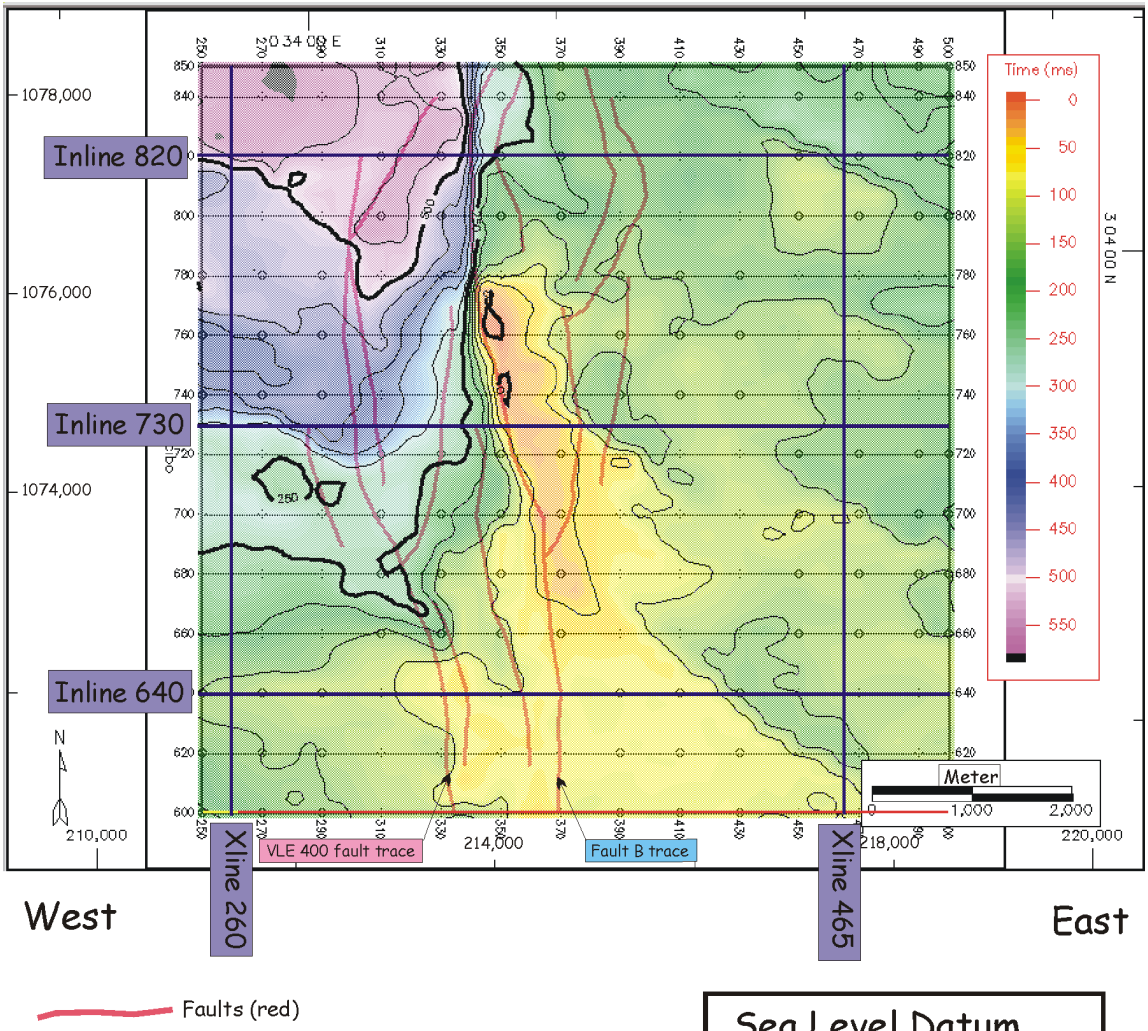

Figure 3-24. Isochron between Hz.6 (Eocene unconformity) and the C-4 member with the VLE 400 fault family traces (growth strata 1). The western block from Fault B is thicker than the eastern, and the western block gets thicker northward.

The thickness difference across Fault B generally follows the development of the VLE 400 fault; both faults show very little offset and simple linear geometry toward south but large offset and complicated geometry northward. This implies that growth strata 1 and the development of the VLE 400 fault family have a close relationship. Lithology of growth strata 1 is not directly available, but it acts as a lateral seal of the reservoir in the eastern block. Hydrocarbon is trapped within the eastern block of the fault family; therefore, either juxtaposition or the fault itself has to act as a lateral seal against the reservoir. The fault has moved several times, displaying normal faulting at the Jurassic, reverse faulting at the Tertiary and strike-slip faulting at the Miocene. Therefore, it is difficult to expect the fault itself to act as a seal. The ratio of sandstone in the reservoir is higher than 60 to 70%; therefore, it is unlikely to act as juxtaposition sealing of the reservoirs. So the most probable role of the growth strata 1 is the lateral sealing mechanism, which becomes thicker toward the north, where the thickness increases to 1,100 m (550 ms twtt).

3.3.2. Growth strata 2

Between Hz.6 (the Eocene unconformity) and Hz. 7, the western block of the growth stata shows thicker sediment deposition than the eastern block (Figure 3-25). The thickness difference between two blocks is about 40 m (20 ms twtt). There is no thickness variation within the western block except a slightly thinning part near the pop-up structure. Some dominant thinning parts

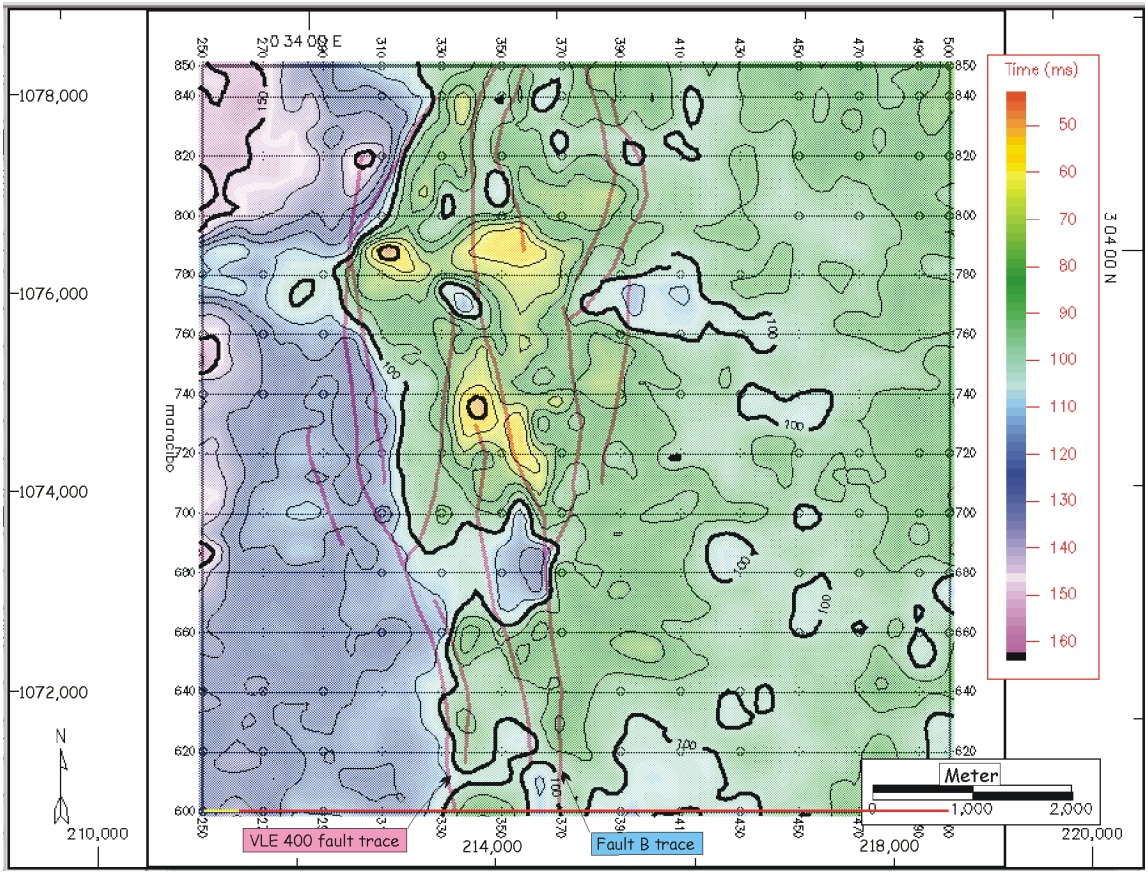

Figure 3-25. Isochron between Hz.7 and Hz.6 (Eocene unconformity) with the VLE 400 fault family traces (growth strata 2). The western block from the VLE 400 fault is thicker than the eastern block.

appear in the eastern block around the pop-up structure. According to the geomorphology of thicker sediments in the western block of the VLE 400 fault, it is obvious that the VLE 400 fault was rejuvenated by compression. Compaction effects from growth strata 1 (between the C-4 member and the Eocene unconformity) might provide additional accomodational space on the western block of the VLE 400 fault; however, the isochron pattern of growth strata 2 is different from isochron 2, so it is obvious that the effect of the VLE 400 fault is dominant. Some apparent thinning was caused by geomorphology of the Eocene unconformity.

3.3.3. Growth strata 3

The thickness between the Hz.7 and Hz.8 is different from the boundary of Fault B. The eastern block of Fault B is thicker than western block by about 40 to 60 m (20 to 30 ms twtt) (Figure 3-26). A thicker area is apparent in the western block through the east-west fault lines. The boundary between the thicker and thinner blocks is not a striking trend; however, the thickness difference is about 40 to 60 m (20 to 30 ms twtt) and shows generally different trends.

3.3.4. Growth strata 4 and 5

An isochron map between Hz.8 and Hz.9 (Growth strata 4) shows a depressed feature on the pop-up structure (Figure 3-27). This implies that the

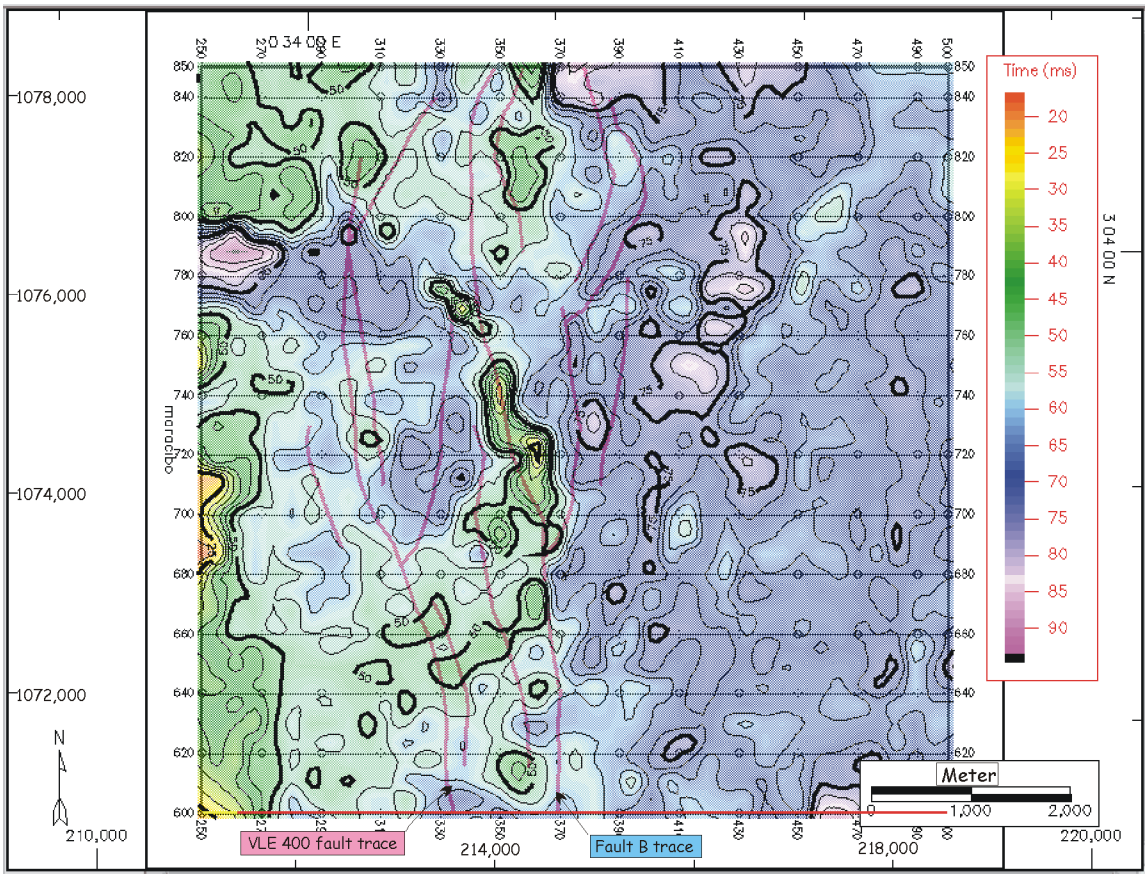

Figure 3-26. Isochron between Hz.8 and Hz.7 with the VLE 400 fault family traces (growth strata 3). The eastern block from Fault B is thicker than the western block.

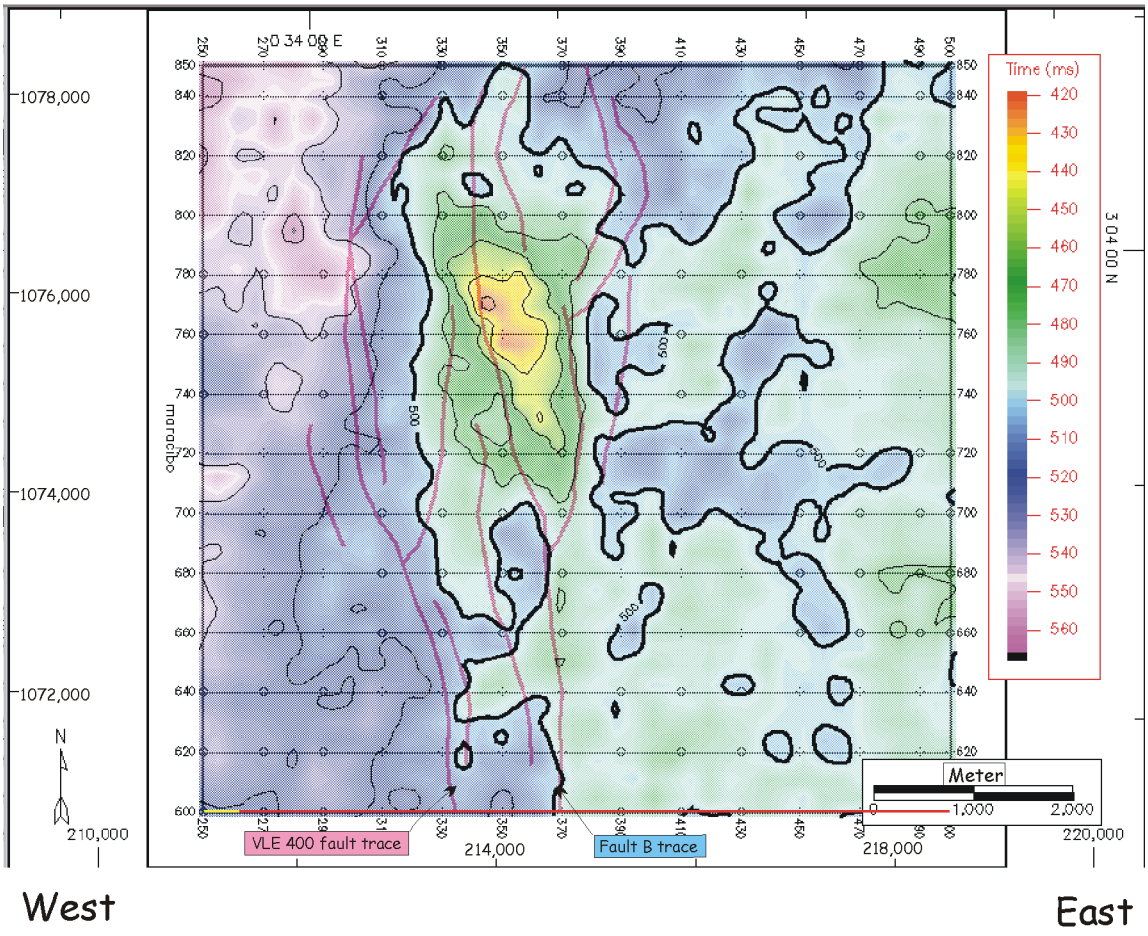

Figure 3-27. Isochron between Hz.9 and Hz.8 with the VLE 400 fault family traces (growth strata 4). The western block from the VLE 400 fault is thicker than the eastern block.

pop-up structure was active during deposition of growth strata 4. Sediments of the growth strata 4 in the western block from the VLE 400 fault are thicker than those in the eastern block. Growth strata 5 has the same thickness trend as growth strata 4 without a depression feature on the pop-up structure (Figure 3-28). Generation of the pop-up structure might have ceased before the growth strata 5 deposition. The thickness variation boundary in growth strata 5 is a little bit ambiguous; it might be the VLE 400 fault or Fault B.

3.3.5. Pre-growth strata

Formations below seismic horizon Hz. 5 (top of the C-4 member) can be considered as pre-growth strata as confirmed by their isochron maps (Figures 3-29, 3-30, 3-31, 3-32). Isochron maps of pre-growth strata show more or less constant thickness except thickness variation from fault geometry (Figures 3-29, 3-30). Some localized thickness variations are observed in isochron maps. Especially, the isochron maps between Hz.3 (top of the Guasare Formation) and Hz.4 (top of the C-5 member, Figure 3-31), and between Hz. 2 (top of the La Luna Formation) and Hz.3 (top of the Guasare Formation, Figure 3-30), display some thickness increase along the VLE 400 fault zone. This might be caused by ductile movements of shale in the Guasare Formation.

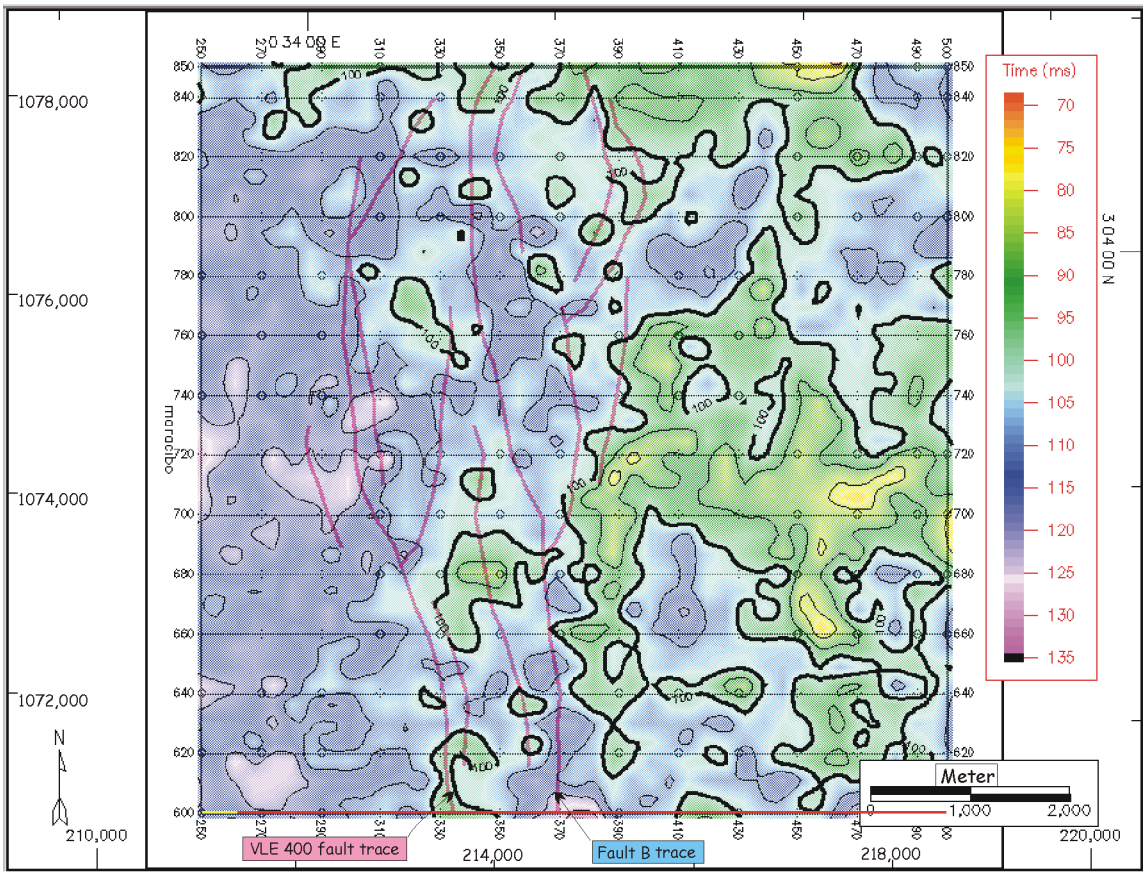

West

East

Faults (red)

Sea Level Datum
C.I. = 10 ms twtt
Scale 1:75,760

Figure 3-28. Isochron between Hz.10 and Hz.9 with the VLE 400 fault family traces (growth strata 5). The western block from the VLE 400 fault is thicker than the eastern block.

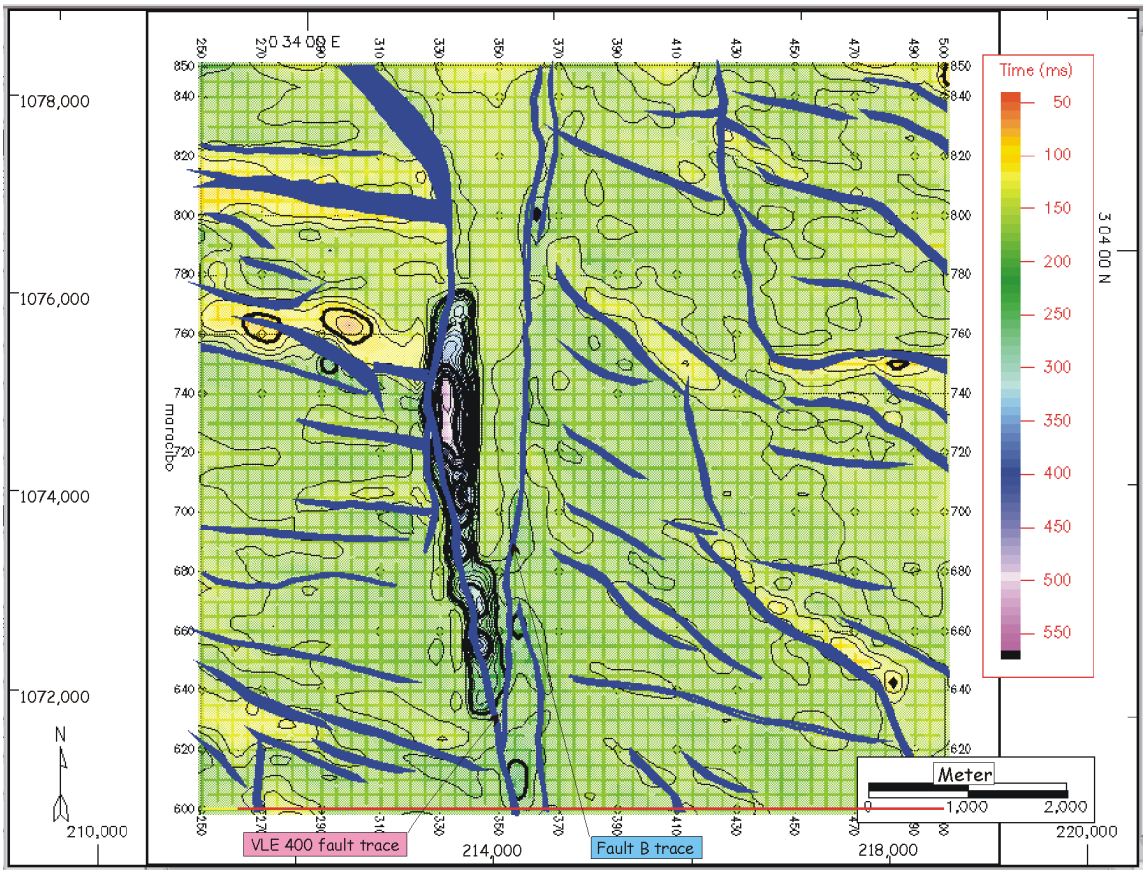

Figure 3-29. Isochron between Hz.2 (top of the La Luna Formation) and Hz.11 formation with the VLE 400 fault family traces. There is no thickness variation across the VLE 400 fault family except some caused by fault geometries.

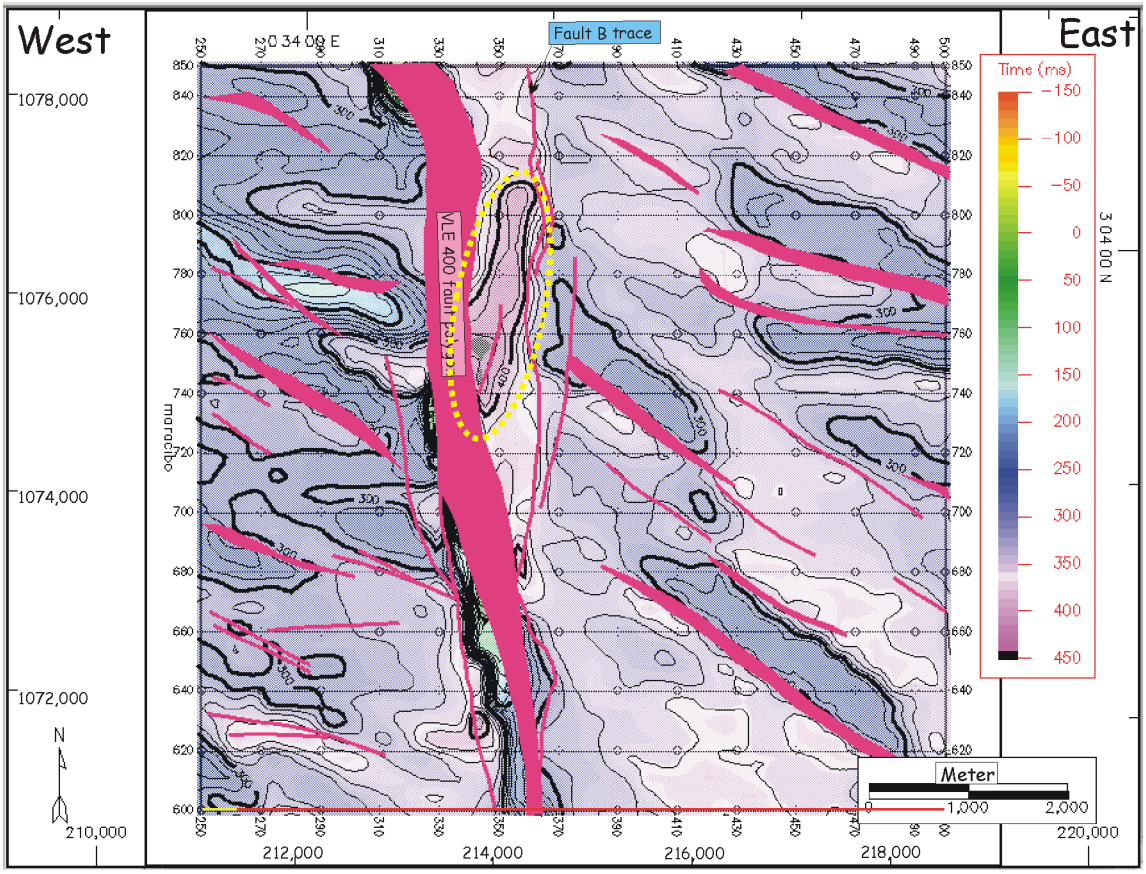

Thicker part

Faults (red)

*No detailed interpretation was possible because of the poor seismic image between the VLE 400 fault and Fault B, which caused the wide fault polygon.

Sea Level Datum
C.I. = 10 ms twtt
Scale 1:75,760

Figure 3-30. Isochron between Hz3 (top of the Guasare Formation) and Hz.2 (top of the La Luna Formation) with the VLE 400 fault family traces. There is no thickness variation across the VLE 400 fault family except some caused by fault geometries.

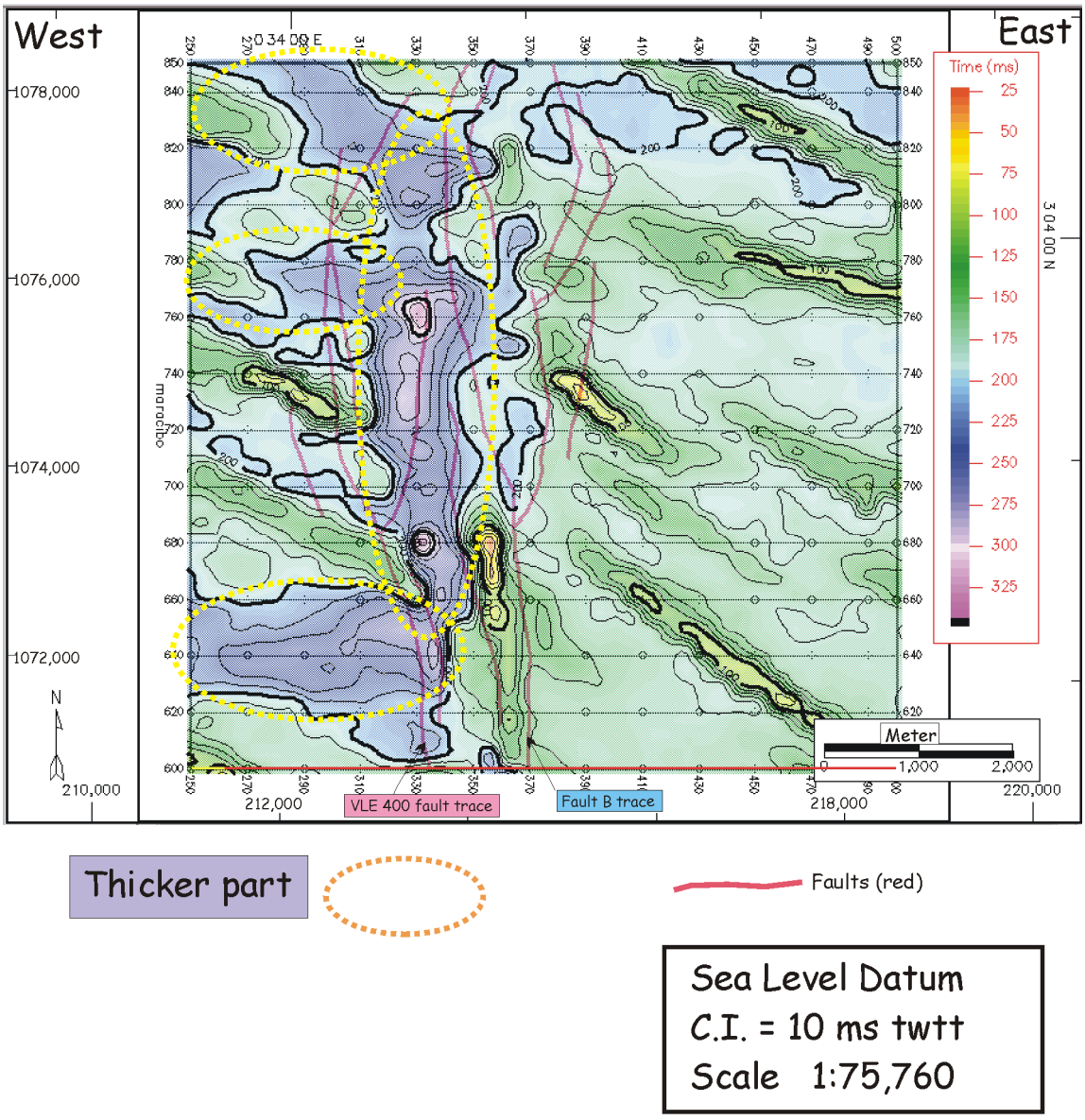

Figure 3-31. Isochron between Hz.4 (top of the C-5 member) and Hz.3 (top of the Guasare Formation) with the VLE 400 fault family traces. There is no thickness variation across the VLE 400 fault family except some caused by fault geometries.

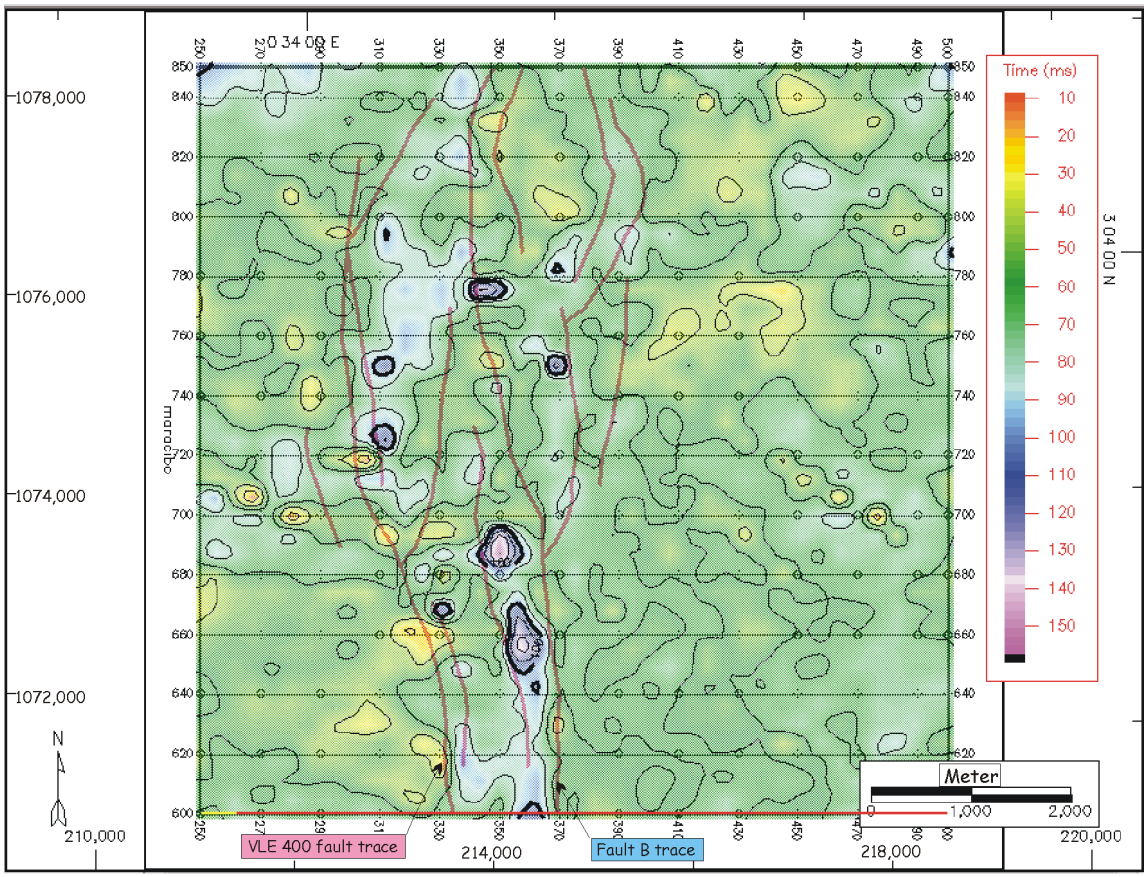

Figure 3-32. Isochron between Hz.4 (top of the C-5 member) and Hz.5 (top of the C-4 member) with the VLE 400 fault family traces (growth strata 1). No thickness variation across the VLE 400 fault family traces is observed.

3.4. Tectonically controlled transgressive deposits

Since seismic-sequence stratigraphy has been introduced by Exxon Prod. Res., eustatic sea-level change has been emphasized as a control of sedimentation. It has been widely accepted as one of the main controls in tectonically inactive basins such as a passive margin setting. However, tectonic movement combined with the eustatic sea level created relative sea-level changes, controls accomodational spaces, and may play a primary role for characteristics of deposition.

The lower Eocene, informally named the “C” sandstones, were deposited as a form of tide-dominated delta (Figure 1-4) during the regional transgression (Maguregui and Tyler, 1991). As these “C” sandstones were deposited as a form of tide-dominated delta in the central part of the basin, the fluvial paleo-deposition environment was developing toward the westsouthwest and an open marine environment was developing toward the eastnortheast (Figure 1-4). Vertically, the C-5 member mainly consisted of distributary channels near the fluvial environment; the C-4 member of distributary channels in a tide-dominated delta, and the C-1~3 member of tide channels near an open marine environment. Each member has aggradational geometry with thickness of individual bedsets thinning as illustrated in Figures 3-22 and 3-33. Each member is separated by sharp contacts caused by abrupt change of lithology and log response. Correlations between wells using log responses match well and with

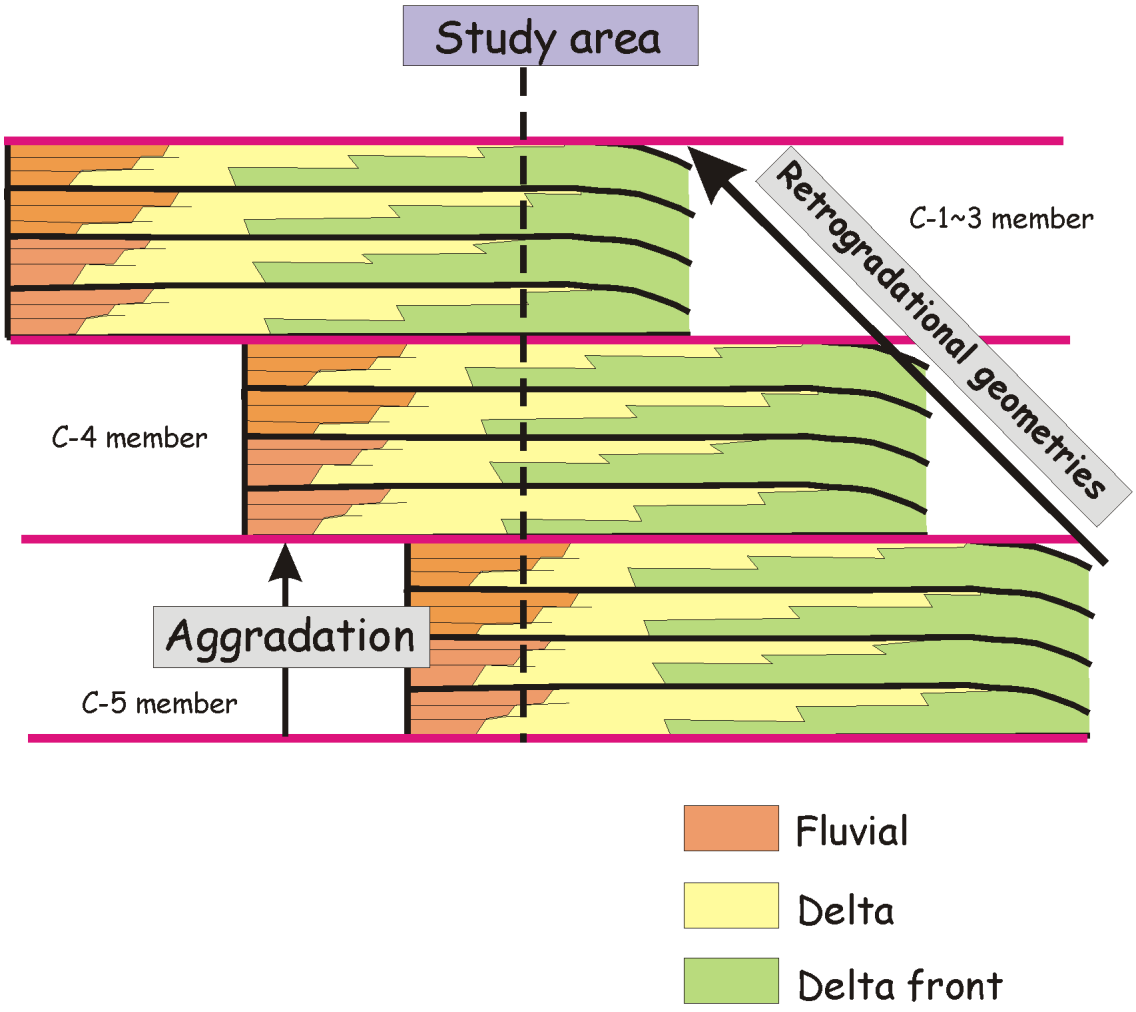

Figure 3-33. Aggradational parasequence set (modified from Van Wagoner et al., 1988)

confidence; therefore, characteristics of the members are results of basin-scale variation. Overall, stacking of the members provides a retrogradational geometry, as illustrated in Figure 3-34 and Figure 3-35. The near-fluvial depositional environment of the C-5 member is changed into delta in the C-4 member and then near-open marine in the C-1~3 member. Therefore, the boundary between the C-5 and C-4 members implies change of depositional environment from near-fluvial to delta. There are no gradual records of depositional environment from near-fluvial to delta and from delta to near-open marine, possibly because of an abrupt change of paleo water depth derived from tectonic movements. The boundaries between the members have sharp contacts, which shows abrupt change of depositional environment. There are no distinct erosional surfaces on the boundaries, so the change might not have been caused by the erosional process after gradual deposition between two different environments. Instead, the transgression during the Eocene may have been caused by the effect of flexural subsidence often observed in foreland basins. While tectonic loading is continuously increased, flexural subsidence follows and provides additional accommodation space in the top set area. Fluxural subsidence and eustatic sea-level rise provided the transgression during the early Eocene. Basin rebounds and orogenic unloading generated progradational deposits on top of transgressional sediments and then provided regional unconformity. This cannot be well-defined by the available data set; however, considering the thickness of the progradational deposit,

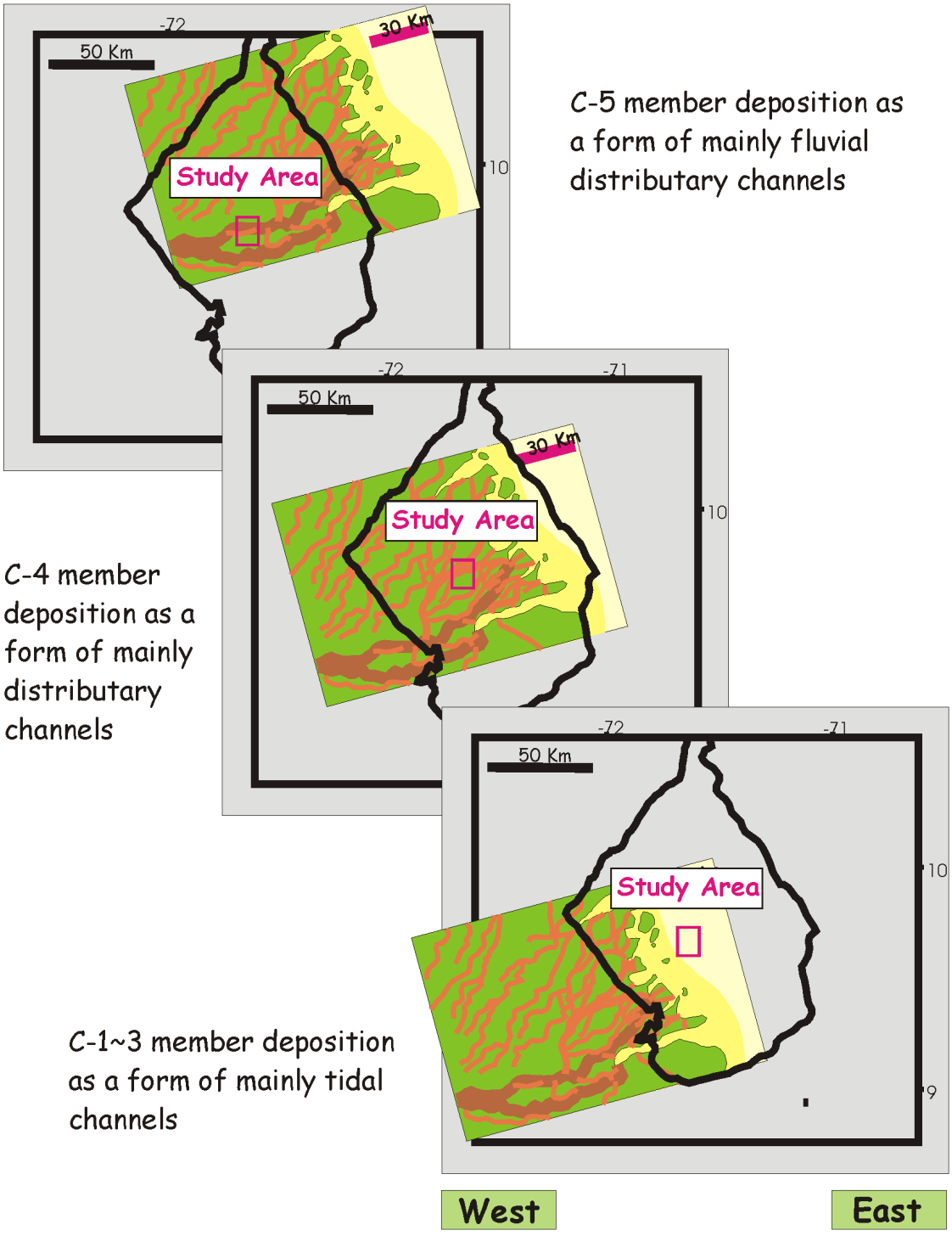

Figure 3-34. Study area and expected possible depositional environment from the C-1~3 to C-5 members.

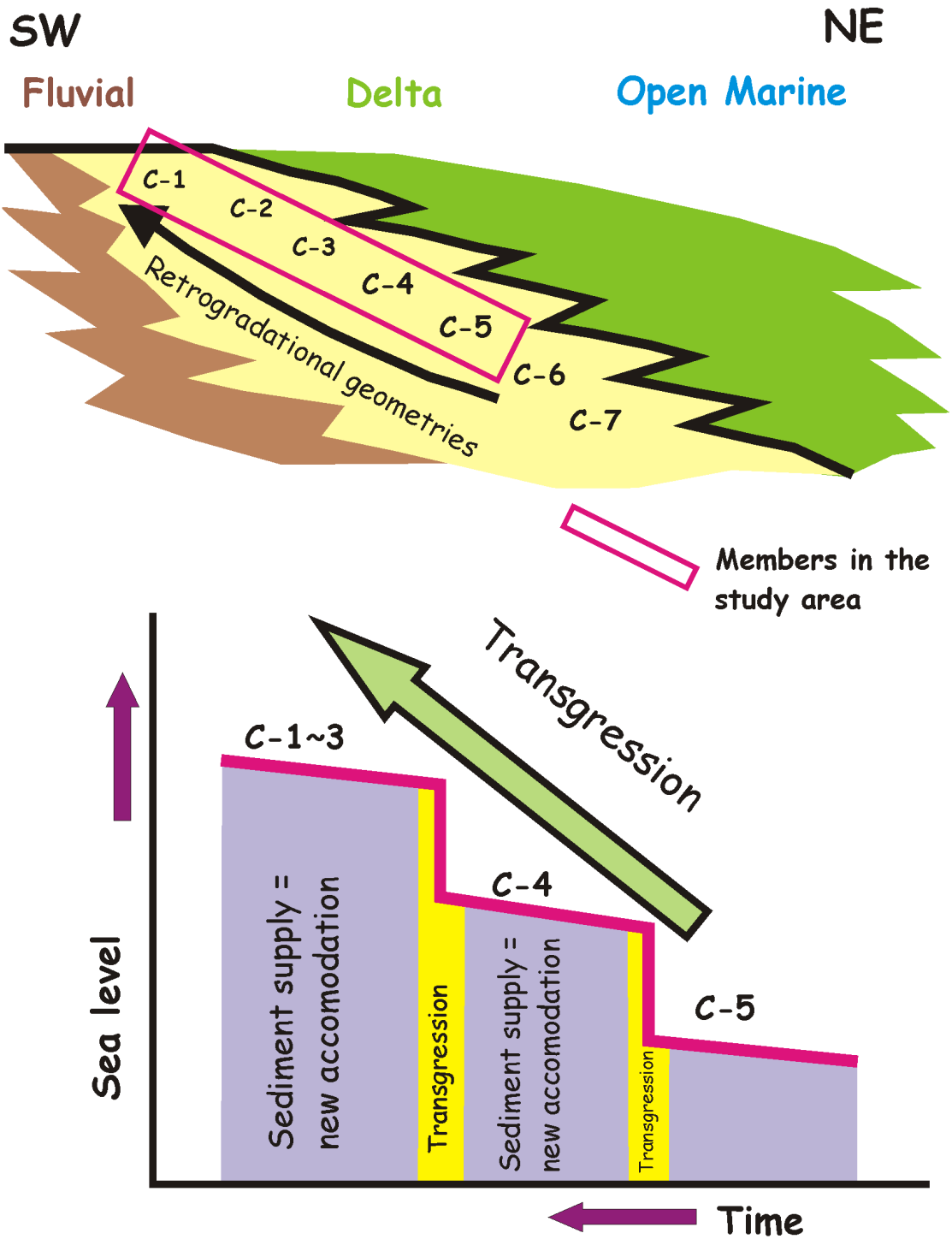

Figure 3-35. Conceptual cross-section showing stacked aggradational components display retrogradational geometries of the Misoa Formation consisting of C-1 through C-7 members.

informally named “B sandstones,” which are reported at more than 1,300 ft (Antonio, 1998), the study area was already lifted above the surface and might have acted as a sediments-source province for the “B sandstones” in the northeastern area. Tectonics controlled the distribution of the reservoir in the basin. Deltaic sandstones by transgression were deposited toward the southwest during flexural subsidence and deltaic sandstone by regression toward the northeast during orogenic unloading and basin rebounds. Therefore, oil fields in the central and eastern part have “C sandstones” reservoirs and western parts have “B sandstones” reservoirs. Sea level might control the architecture and distribution of the reservoir; however, the main control of the reservoir distribution is tectonic movements.

3.5. Misoa-Pauji sediments

The Misoa-Pauji sediments overly the main reservoir rock in the western block, and hydrocarbons are produced from the area east of the VLE 400 fault family. The sediments were deposited only to the west of the VLE 400 fault family (Figures 3-36, 3-37, 3-38, 3-39). The thickness of the sediments gradually increases toward the north, especially from the middle of the field (Figure 3-37). An isochron map between Hz.6 (the Eocene unconformity) and Hz.5 (top of the C-4 member) shows abrupt thickness increase across Fault B in the western block and gradually increases in thickness toward the north within the western

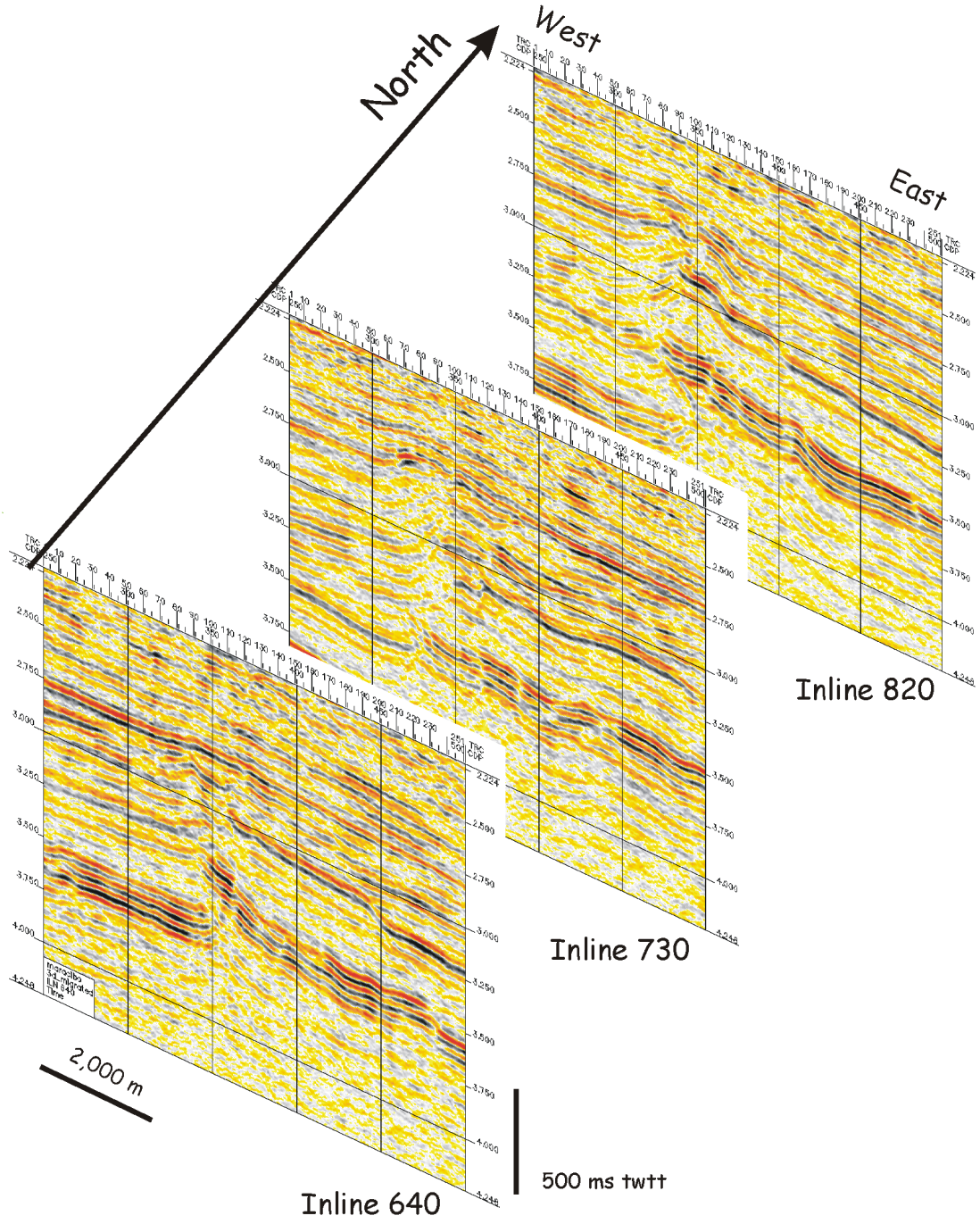

Figure 3-36a. Three seismic inlines of 640, 730 and 820 showing structural developments from south to north within the study area. See Figure 3-24 for the location.

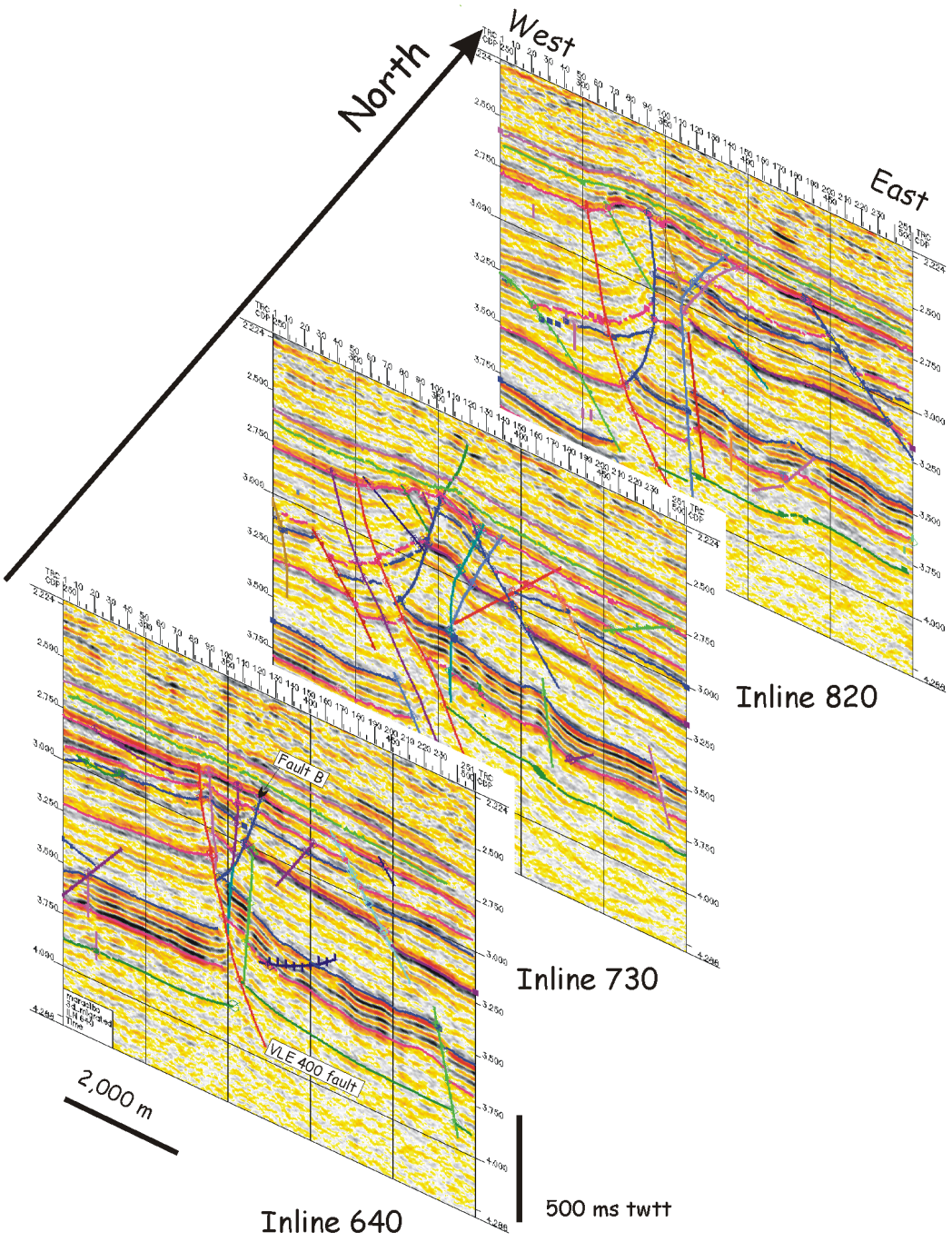

Figure 3-36b. Three seismic inlines of 640, 730 and 820 with interpretation showing development of the VLE 400 fault family from south to north within the study area. See Figure 3-24 for the location.

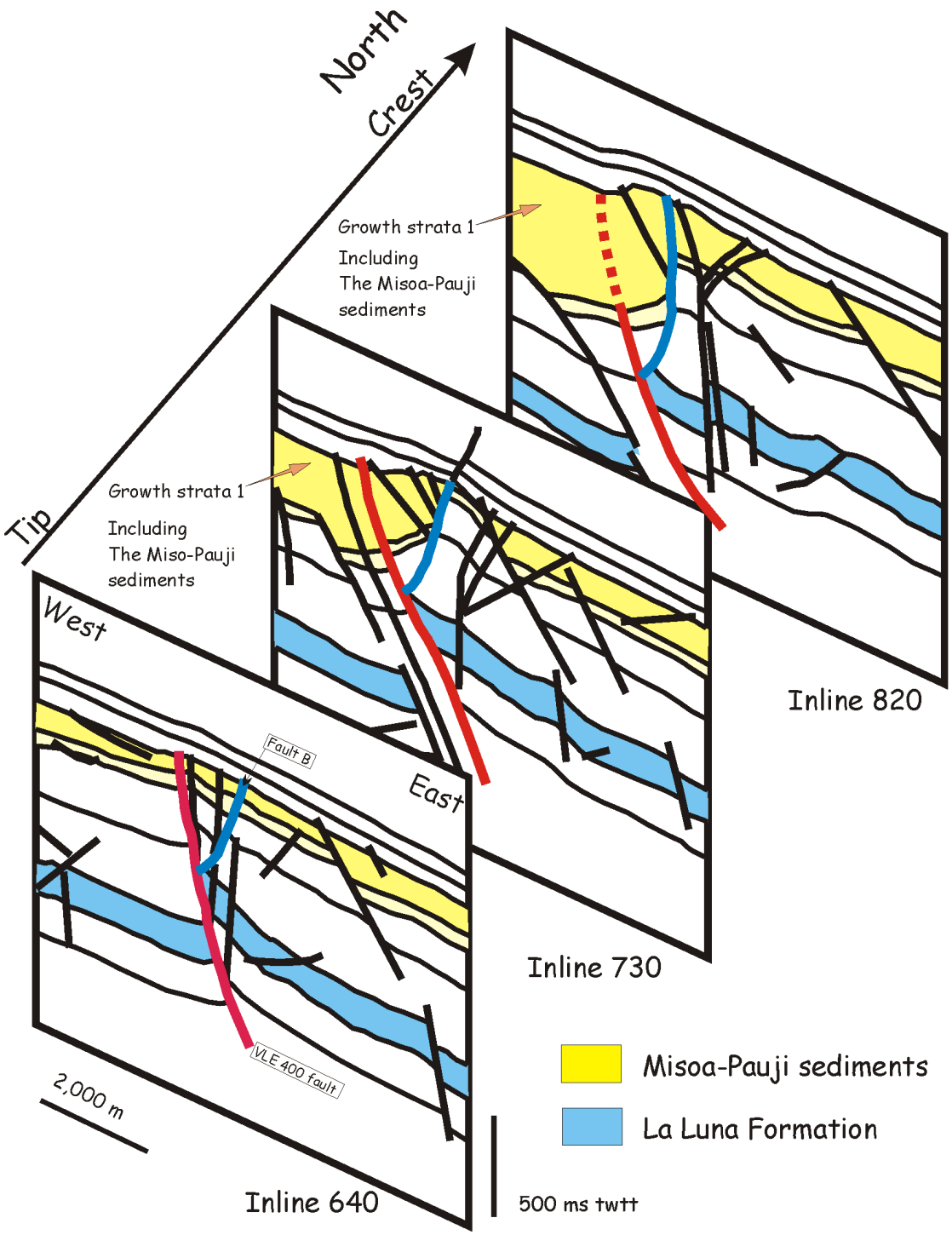

Figure 3-36c. Three geoseismic inlines of 640, 730 and 820 showing development of the VLE 400 fault family from south to north within the study area. See Figure 3-24 for the location.

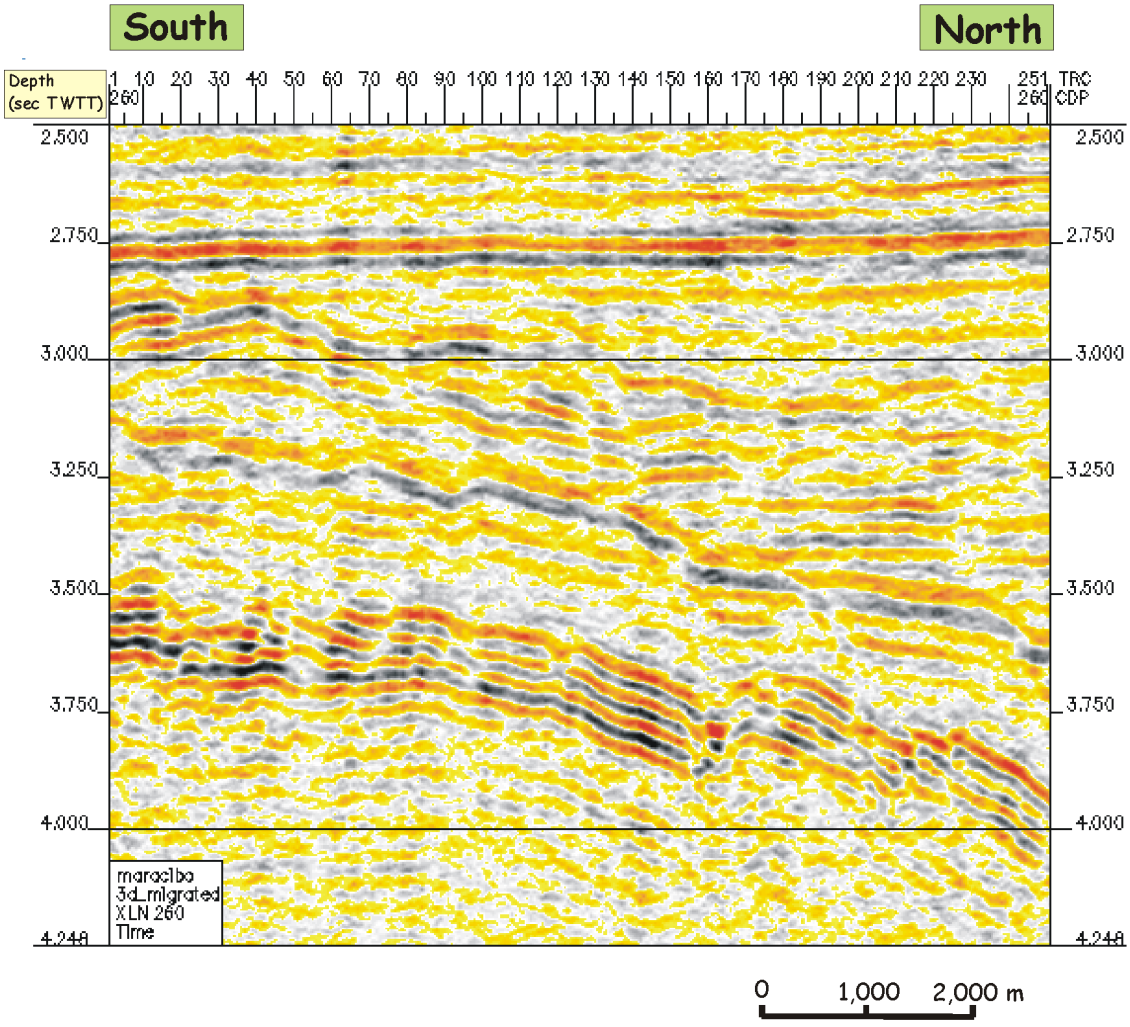

Figure 3-37a. Seismic profile crossline 260. See Figure 3-24 for the location.

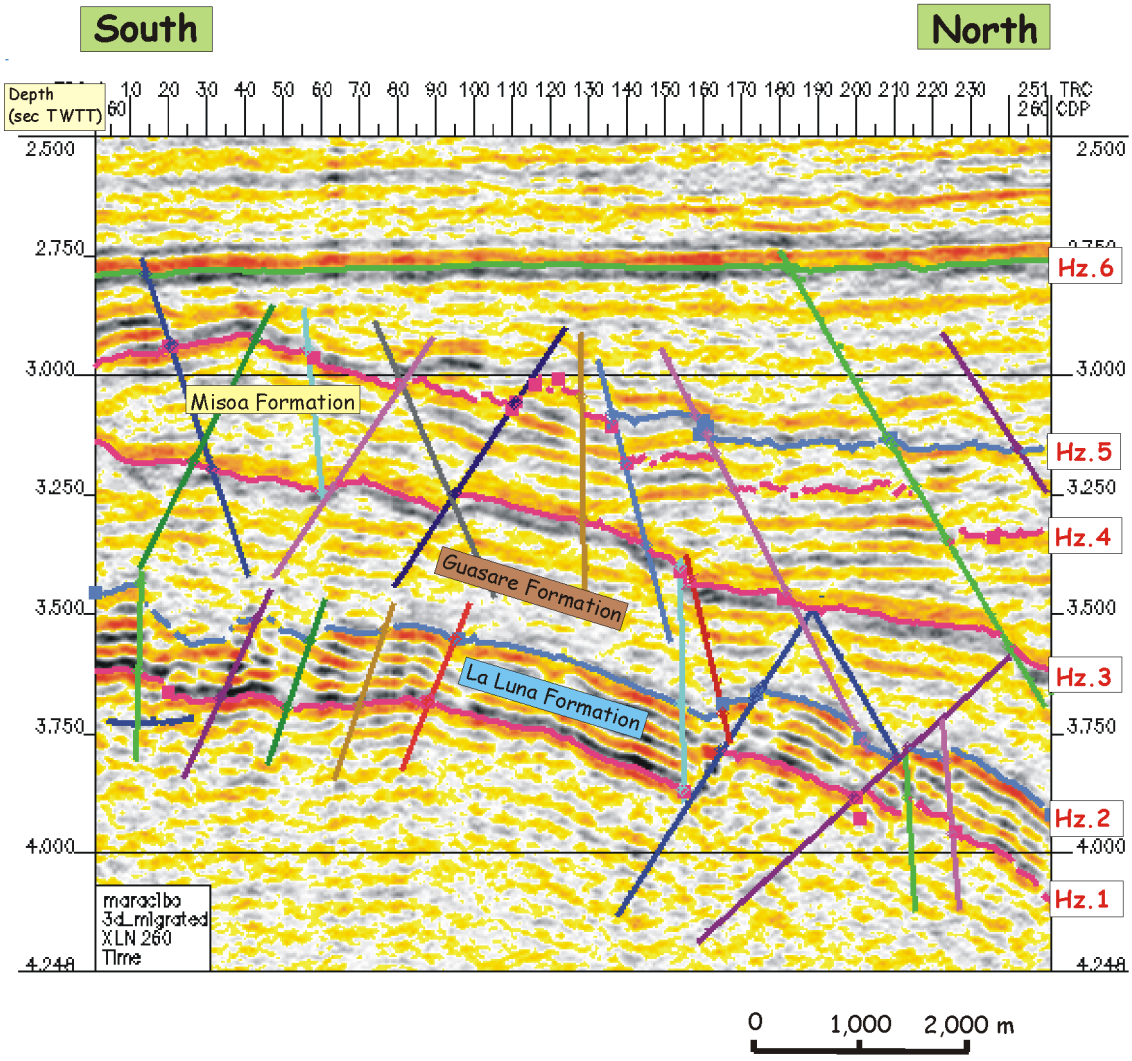

Figure 3-37b. Seismic profile crossline 260 with interpretation. See Figure 3-24 for the location.

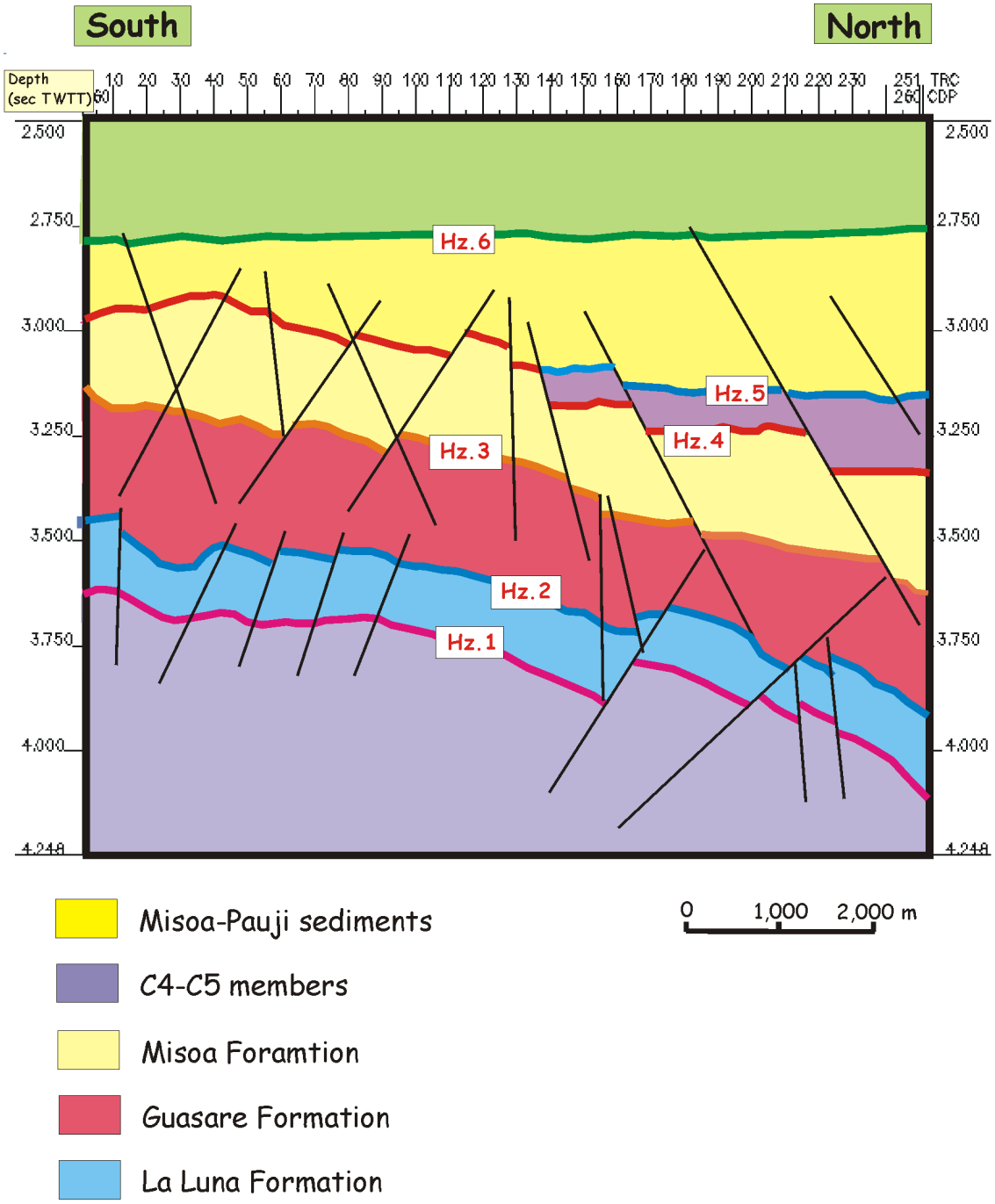

Figure 3-37c. Geoseismic profile crossline 260 with interpretation. See Figure 3-24 for the location.

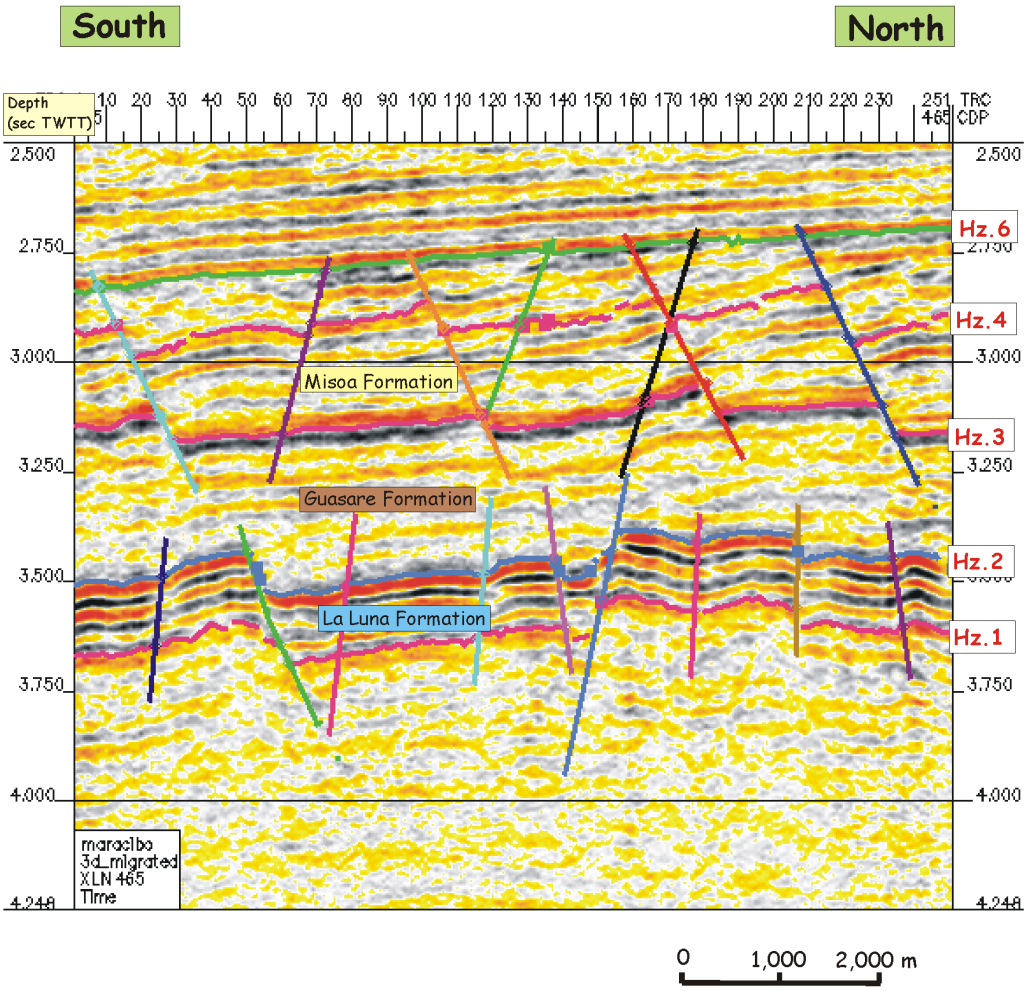

Figure 3-38a. Seismic profile crossline 465 with interpretation. See Figure 3-24 for the location.

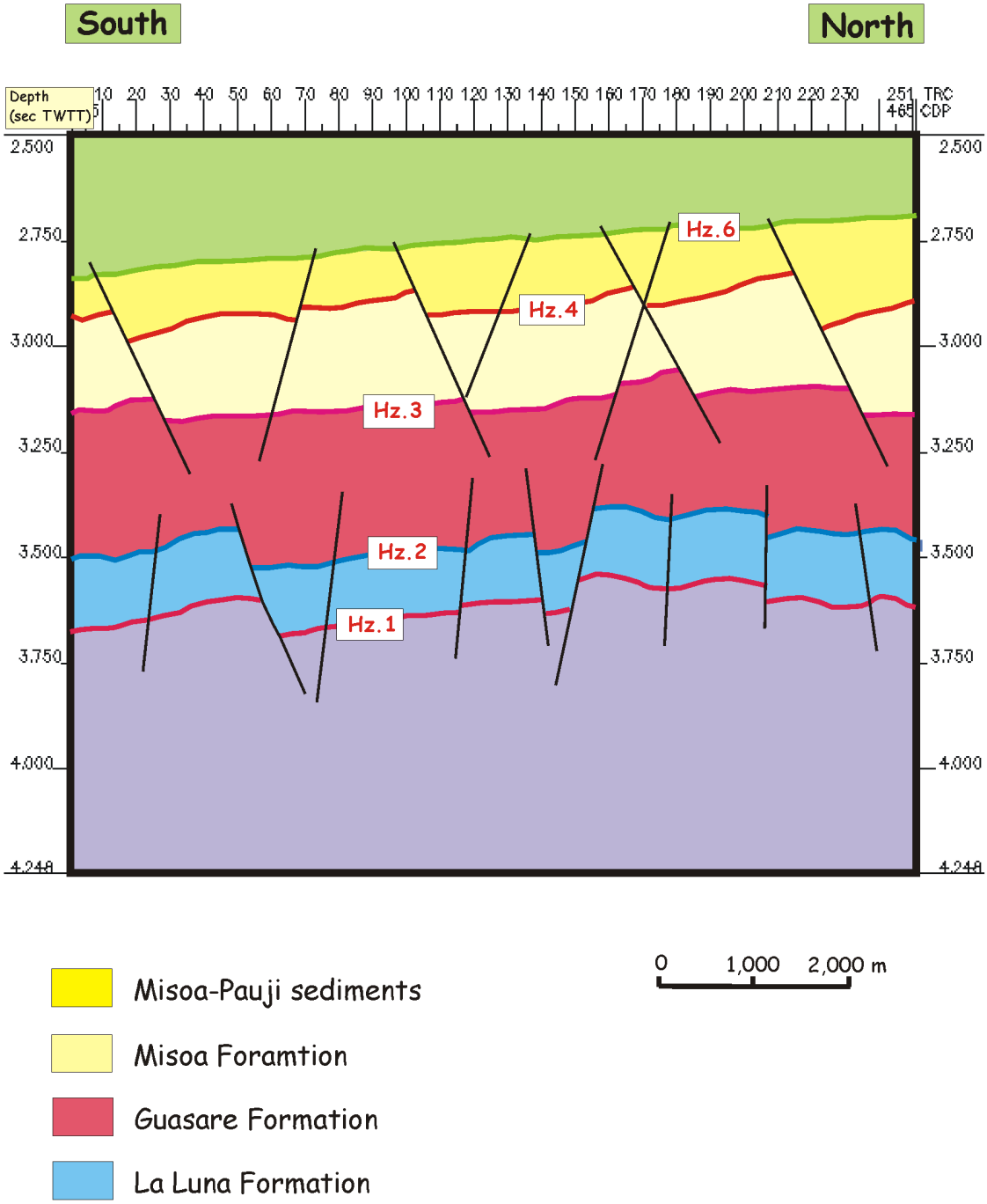

Figure 3-38b. Geoseismic profile crossline 465 with interpretation. See Figure 3-24 for the location.

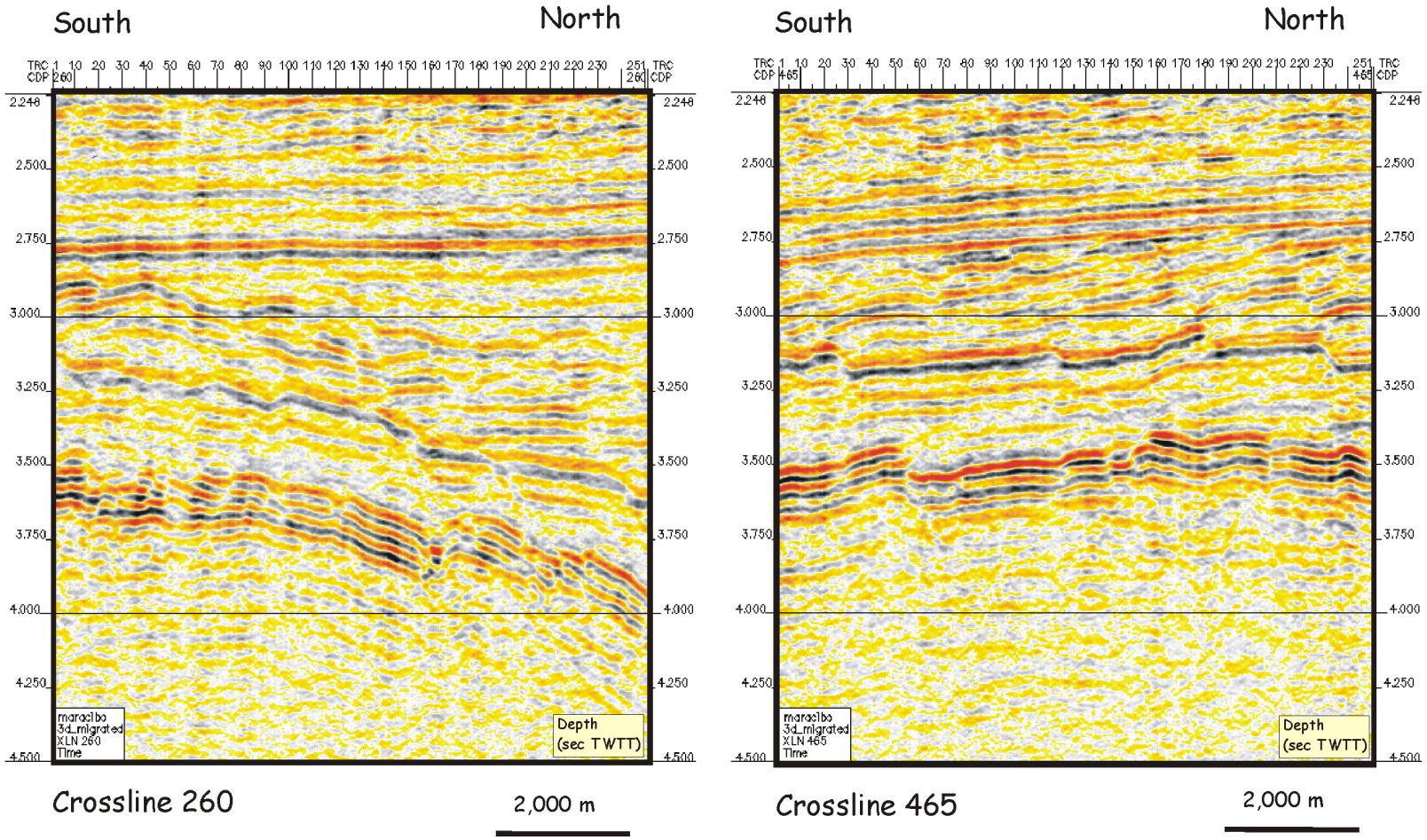

Figure 3-39a. Two seismic crosslines of 260 and 465 showing development of the Misoa-Pauji sediments in the western block of the VLE 400 fault. See Figure 3-24 for the location.

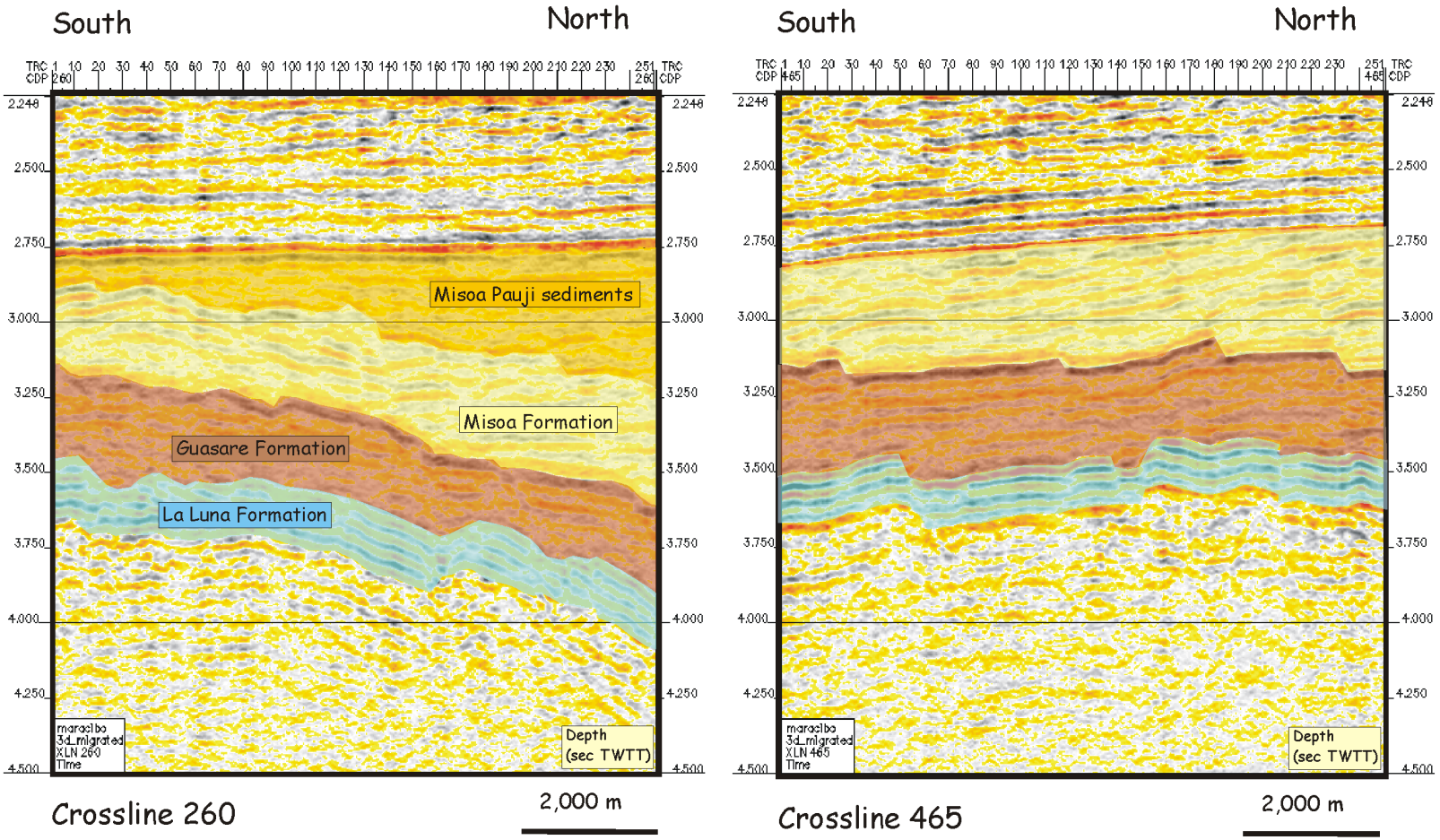

Figure 3-39b. Two seismic crosslines of 260 and 465 with interpretation showing development of the Misoa-Pauji sediments in the western block of the VLE 400 fault. The bottom, green-colored formation is the La Luna, red is the Guasare Formation and light yellow is the Misoa Formation. The yellow formation in line 260 is the Misoa-Pauji sediment. See Figure 3-24 for the location.

block (Figure 3-24). Seismic horizons below the Hz.6 (the Eocene unconformity) in the western block gently dip to the north. Seismic reflectors within the sediments are horizontally parallel, showing onlap seismic facies. Sediments were deposited by tectonic movements when the Oca fault acted as a subduction zone between the South American plate and the Carribean plate. Compression generated thrust faults through the existing VLE 400 fault zone. Compressional stress uplifted the eastern block of the field and provided accommodation space in the western block which was filled by a part of the sediments.

An isochron map between Hz.6 (the Eocene unconformity) and Hz.5 (top of the C-4 member) shows the thickness by growth strata 1 (Figure 3-24). To describe the sediments in detail, a seismic horizon defined as “Inter 1” was selected within the section. Interpretation and mapping of the horizon were limited to the western. They are missing in the eastern block. A time-structure map of the inter1 horizon shows a trend similar to that of Hz.6 (the Eocene unconformity, Figure 3-40). Two isochron maps were generated using the Inter 1 horizon: one between Inter 1 and Hz.5 (top of the C-4 member, Figure 3-41), and the other between Inter 1 and Hz.6 (the Eocene unconformity, Figure 3-42). Both isochron maps show the thickness increase abruptly across northwest-southeast normal faults. This implies that the area was extended by the northwest-southeast normal faults, and the VLE 400 fault family acted as a kind of boundary fault or possible transfer fault.

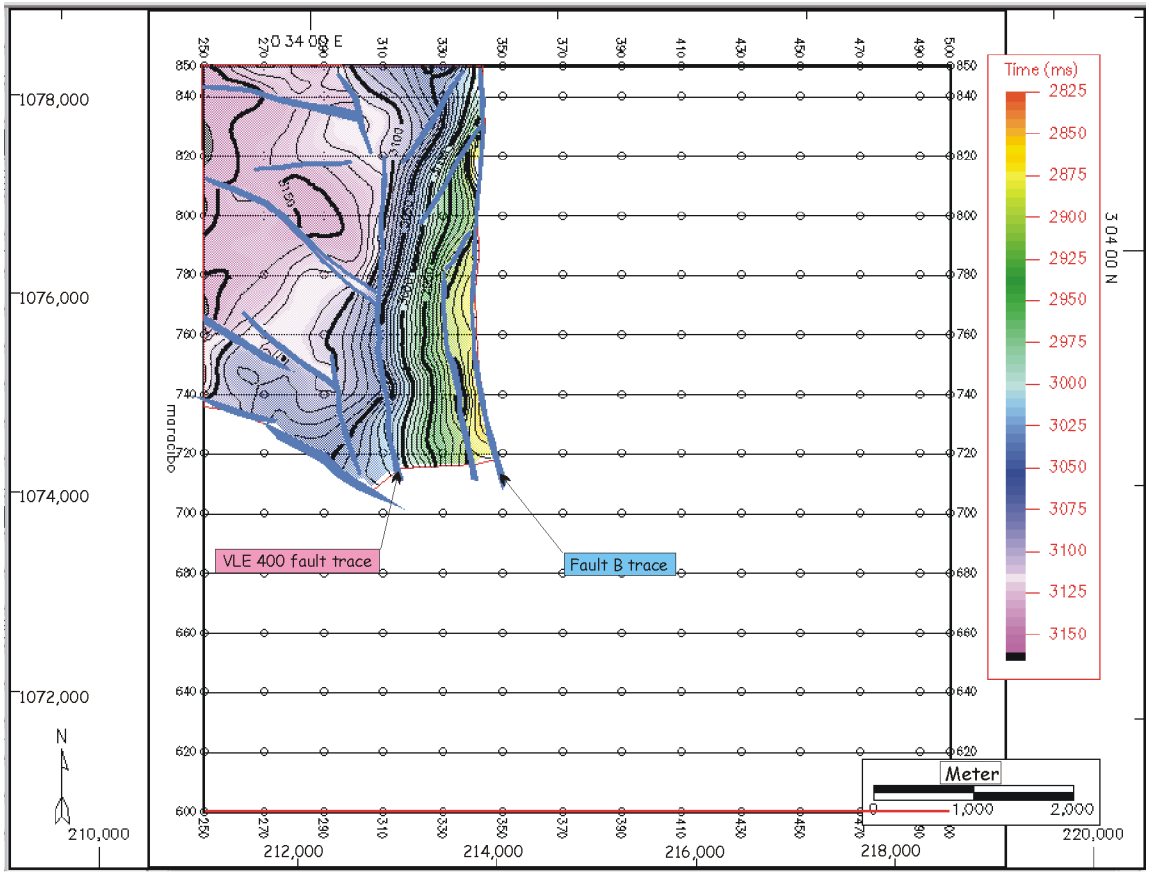

Faults (blue)

Sea Level Datum
C.I. = 10 ms twtt
Scale 1:75,760

Figure 3-40. Time structure of Inter 1.

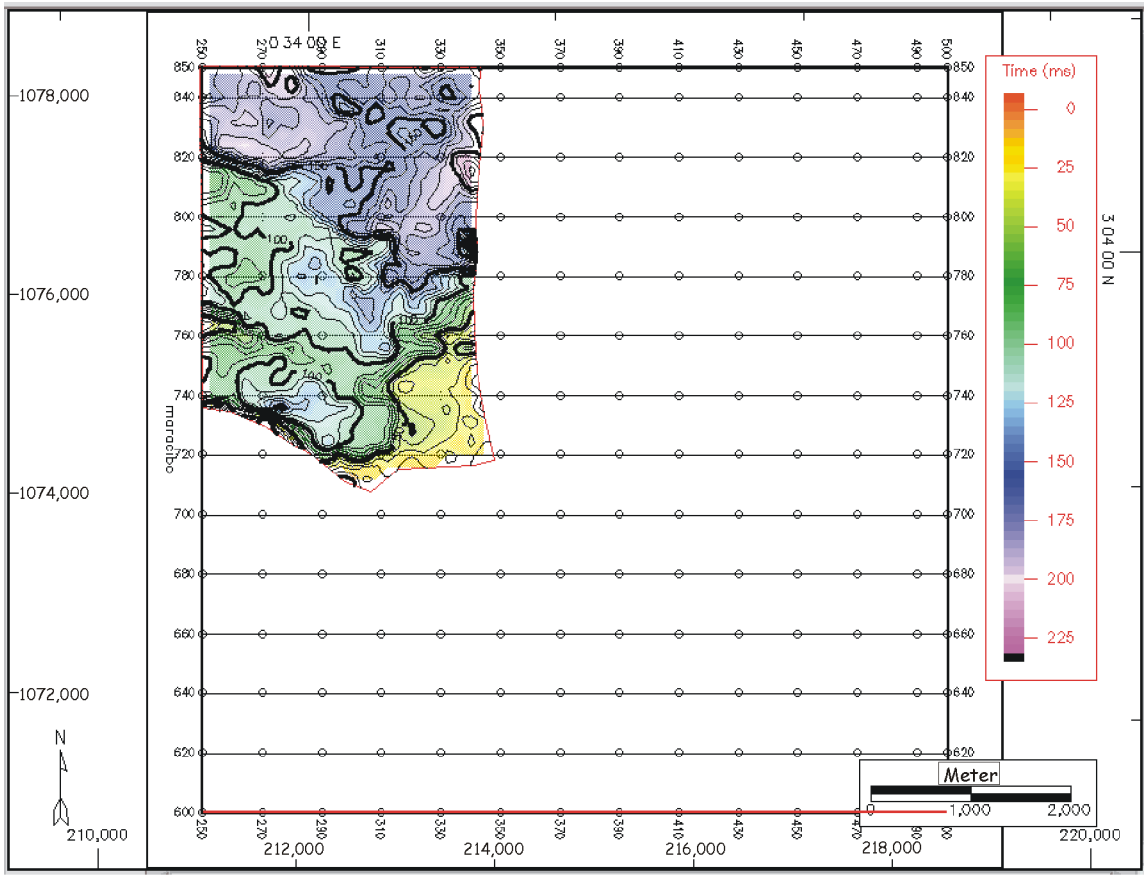

West

East

Sea Level Datum
C.I. = 10 ms twtt
Scale 1:75,760

Figure 3-41. Isochron between Inter 1 and C-4 member.

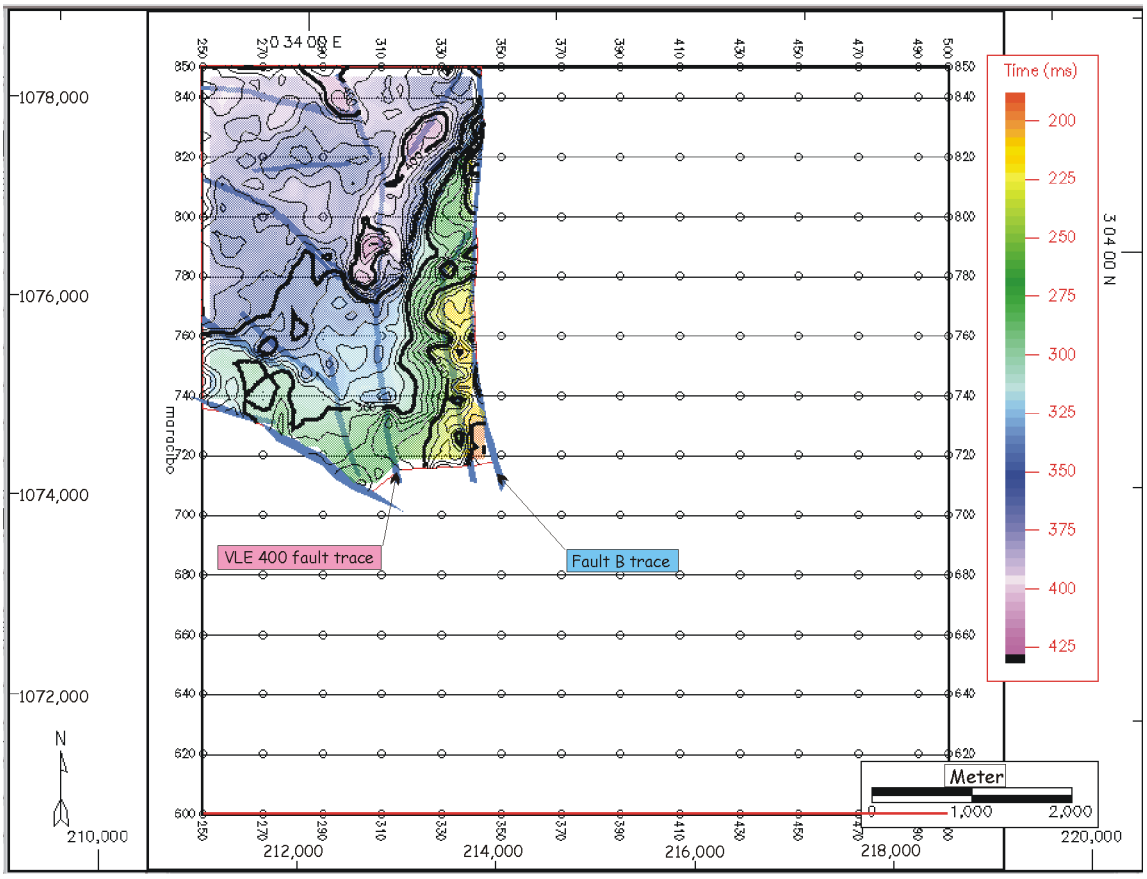

Figure 3-42. Isochron between Hz.6 (Eocene unconformity) and Inter 1.

4. CONTROLS ON HYDROCARBON DISTRIBUTION

It is essential to understand hydrocarbon systems and find the major controls on hydrocarbon accumulation in order to predict undiscovered hydrocarbon resources. Hydrocarbon systems including a migration history from sources to traps and trapping mechanisms are major considerations for the hydrocarbon distribution, but analysis of hydrocarbon systems is difficult because of the time factor. Therefore, the first step is to establish a structural development model according to tectonic evolution stages. The next step is to identify stratigraphic features as a pattern of sedimentary filling within the established structural framework. Understanding the role of structure and stratigraphy in hydrocarbon accumulation is not only important for the hydrocarbon exploration in a practical way but also useful as a tool to confirm precision of the established structural and stratigraphic models. Tectonic movements between the South American and Caribbean plates controls the structural development in the Maracaibo basin. The structural development with a pattern of sedimentary filling contributes to the hydrocarbon distribution in the field.

4.1. Tectonic movements

Tectonic movements are major controls on hydrocarbon distribution in the basin. Figure 1-1 shows oil fields discovered along the tectonic lines such as the northnortheast-southsouthwest strike-slip and thrust faults. Tectonic controls on hydrocarbon distribution of the Lamar VLE 196 field are predominantly described on the structural maps of the main reservoirs. Hydrocarbons are trapped only on the eastern block of the VLE400 fault, possibly because of migration path permeability and/or closure by the fault.

The VLE 400 fault family has had three different stress orientations during tectonic evolution of the Maracaibo basin (Figure 4-1). In the Jurrasic, extension stress created normal faulting and rifting. Synrift sediments are not well-defined within the study area because the wells don't penetrate the sediments, but regional basin studies (Kulke, 1995) suggest their deposition on the study area (Figure 4-1, A). Tectonic movement had little significant influence on the deposition of the La Luna, the Guasare and the Misoa Formations within the study area (Figure 4-2, B). Isochrons of the formations generated by 3-D seismic data interpretation and analysis of faults show that depositional features were not deformed during deposition. Tensional stress changed to compression during the middle Eocene. Compression across the plate boundary between

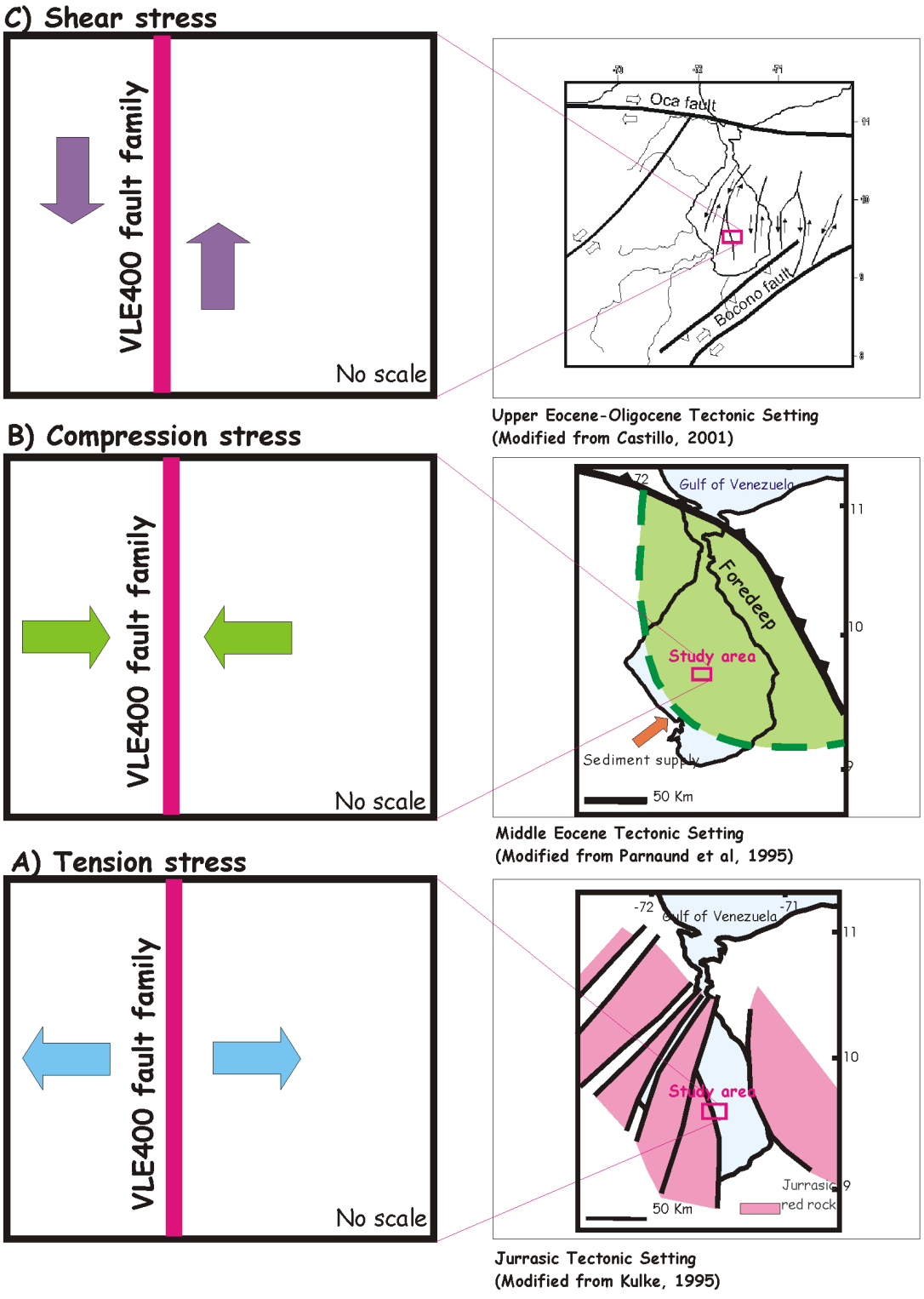

Figure 4-1. The VLE 400 fault family stress variation through the tectonic evolution of the Maracaibo basin.

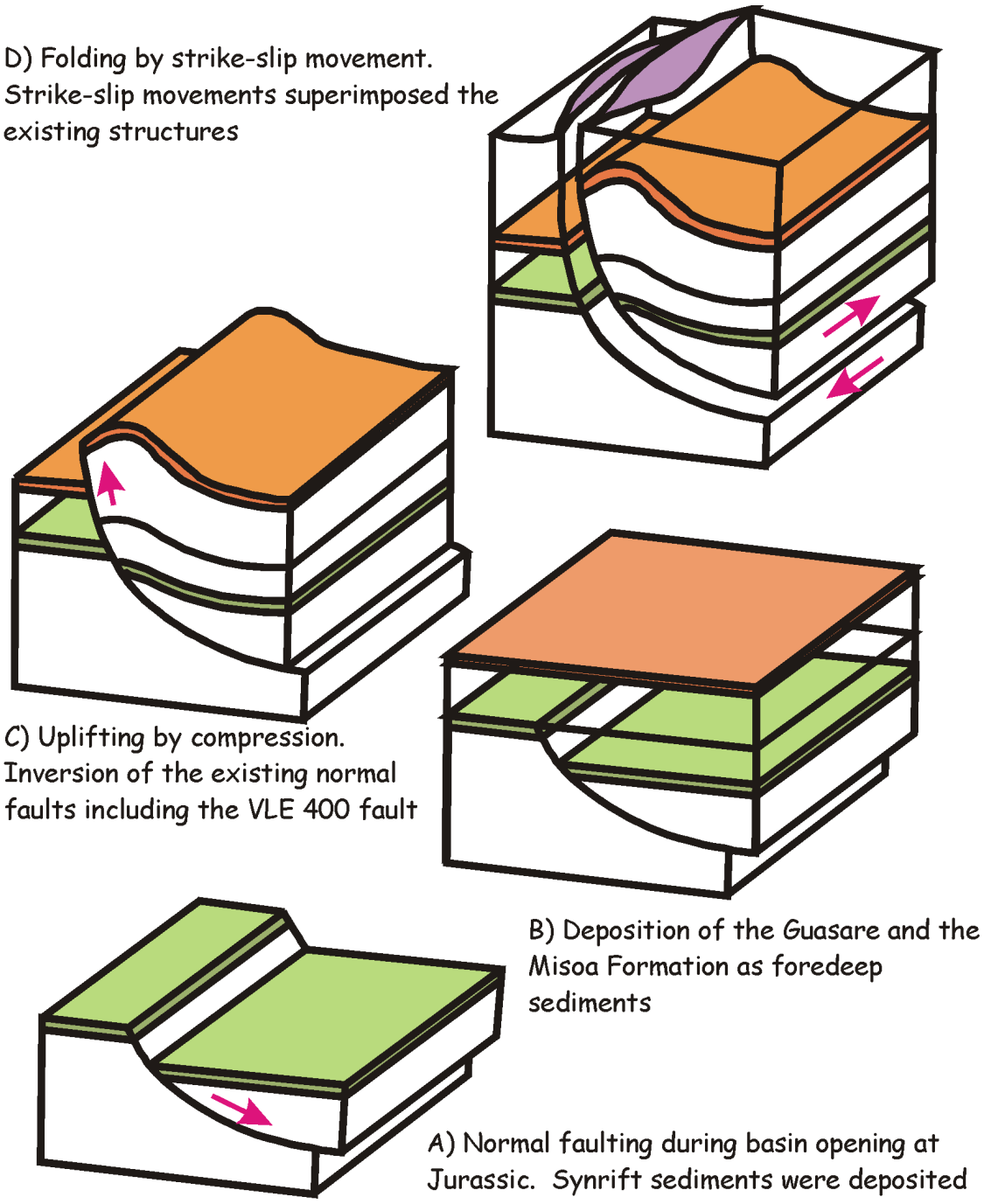

Figure 4-2. Basin evolution model of the Maracaibo basin according to the tectonic movement of the VLE 400 fault family.

the South American and Carribean plates to the north-east (Figure 4-1, B). Simplified depositional features during evolution of the VLE 400 fault family are illustrated at four different stages in Figure 4-2. Synrift sediments were deposited during rifting (Figure 4-2, A). The La Luna, Guasare and Misoa Formations deposited in the study area without severe deformation, though the Misoa Formation was deposited in an active tectonic setting (Figure 4-2, B). Absence of deformation may be due to the distance from the collision boundary of the study area, so compression was not effective in the VLE 400 fault during deposition of the Misoa Formation. After deposition of the Misoa Formation, compression prevailed in the study area (Figure 4-2, C). Compression generated additional accommodation space to the western block of the VLE 400 fault family. Previous studies did not clearly describe the sediments deposited in the accommodation space, but probably they are correlated to the Misoa or Pauji Formation (Misoa-Pauji sediments). The left-lateral strike-slip movement of the VLE 400 fault family was generated by interaction of two overall east-west trending, right-lateral strike-slip faults, the Oca fault to the north and the Bocono fault to the south (Figure 4-3, A). The Icotea and associated faults formed rotated blocks between the Oca and Bocono faults and provided localized uplifts and subbasins along the northeast-southwest left-lateral strike-slip faults, such as the VLE 400 fault family (Figure 4-3, B). This model explains why the VLE 400 fault family has left-lateral movements whereas the Oca and the Bocono faults have right-lateral movements.

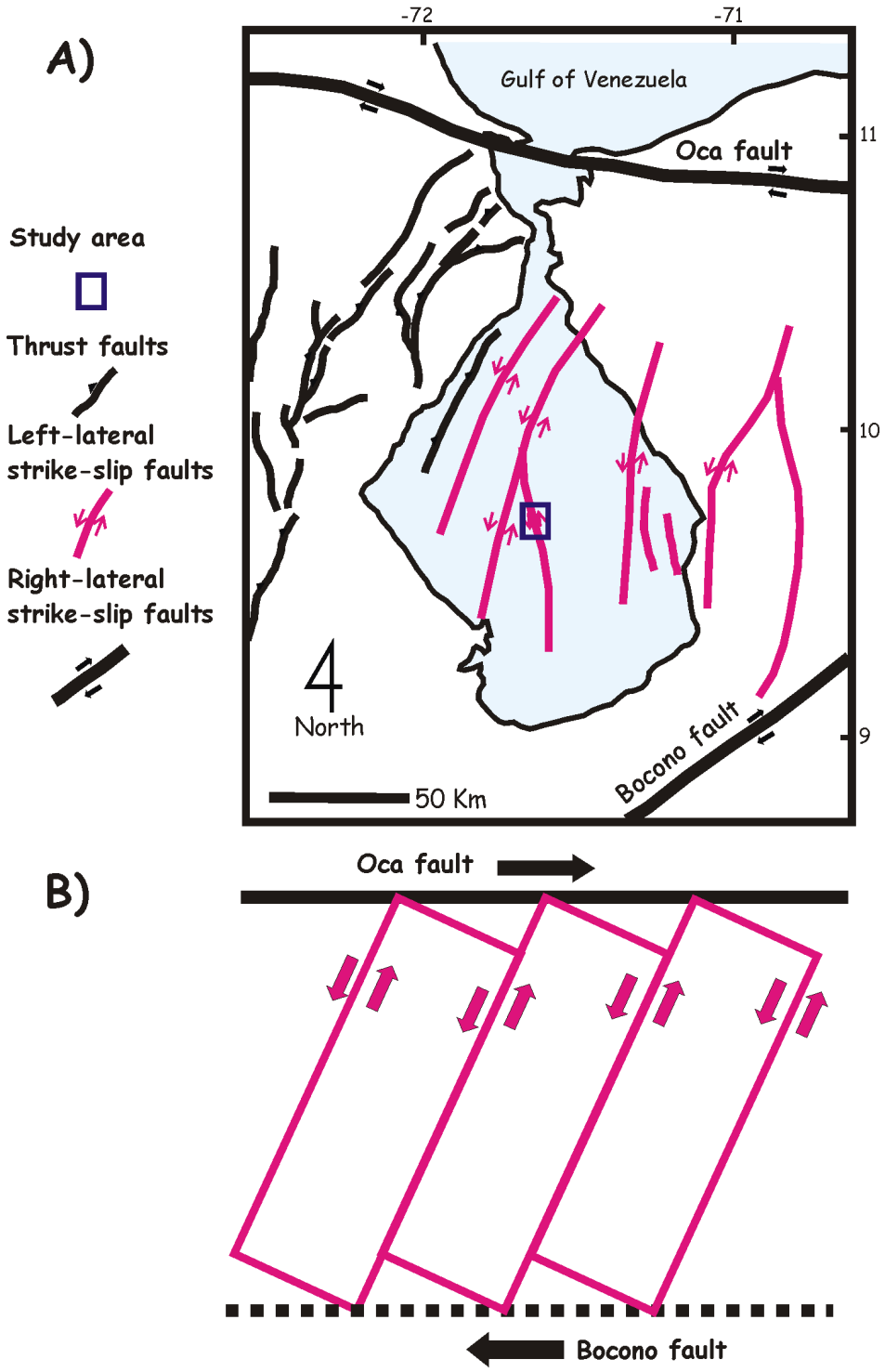

Figure 4-3. Right-lateral strike-slip movements of Oca fault created block rotations with left-lateral strike-slip faults between blocks. A) Modified from Castillo, 2001.

I have developed a basin evolution model of the Maracaibo basin based on observation from the 196–Lamar field, subtle tectonic movement analysis using a growth strata concept, and integrated interpretation of seismic and well data as illustrated in Figure 4-2. Although the model depends on movements of VLE 400 fault family and localized observation, it fits the hydrocarbon distribution and explains the origin of the “pop-up” structure.

4.1.1. Subtle tectonic movements interpreted by growth strata using isochrons across faults

The growth strata concept is useful to reveal complex tectono-stratigraphy features constructed by interaction between growing structures and deposition (Verges et al., 2002), and the petroleum industry uses it because of hydrocarbon potential within the growth strata (Bischke, 1994). Subtle movements below conventional seismic resolution can be interpreted by the growth strata concept using isochron analysis. The VLE 400 fault family actively developed up to the Eocene unconformity, and then it became inactive. Some movements should appear below the conventional seismic resolution, so the activities and rejuvenation of the faults are reviewed by a growth strata concept. Under the tension stress, if Fault B was reactivated, the growth strata would be deposited in the western block from Fault B, and if the VLE 400 fault was reactivated, the growth strata would be deposited in the eastern block from the VLE 400 fault.

4.1.2. Tectonic movements detected by integration of seismic and well data

The top of the C-4 member near the Eocene unconformity pinches out toward the west and more or less sub-parallel to the Eocene unconformity. A seismic unit between the top of the C-4 member and the Eocene unconformity appears to lap over the top of the C-4 member (Figure 4-4). Pinch-out and on-lap are observed in most of the west-east seismic lines, including the arbitrary cross-lines of well-to-well correlation (Figure 4-5). Because the pinch-out shape seismic unit has a different dipping angle than the C-4 and C-5 members, sub-parallel to the Eocene unconformity and on lapping to the top of C-4 member, it is possible to interpret the boundary between the C-4 and C-1~3 members as an unconformity. The unconformity between the top of the C-4 and C-1~3 members may be a localized event within the study area; however, it is generally not accepted in the viewpoint of regional geology, in spite of the seismic characteristics. A model has been considered to solve the apparent disagreement between the regional geology and the seismic characteristics. Deposition of the C-5, C-4 and C-1~3 members had been interpreted conformable. After deposition of the C-1~3 member, the southwestern part of the study area was uplifted by reverse faults, and the uplifted area was eroded out. The erosion surface became the Eocene regional unconformity. This model matches the regional geology well. Well-to-well correlation using the model provides consistency of electronic well logs. The unconformity is not clearly identified between two wells, but well logs of the VLE1063 correlate

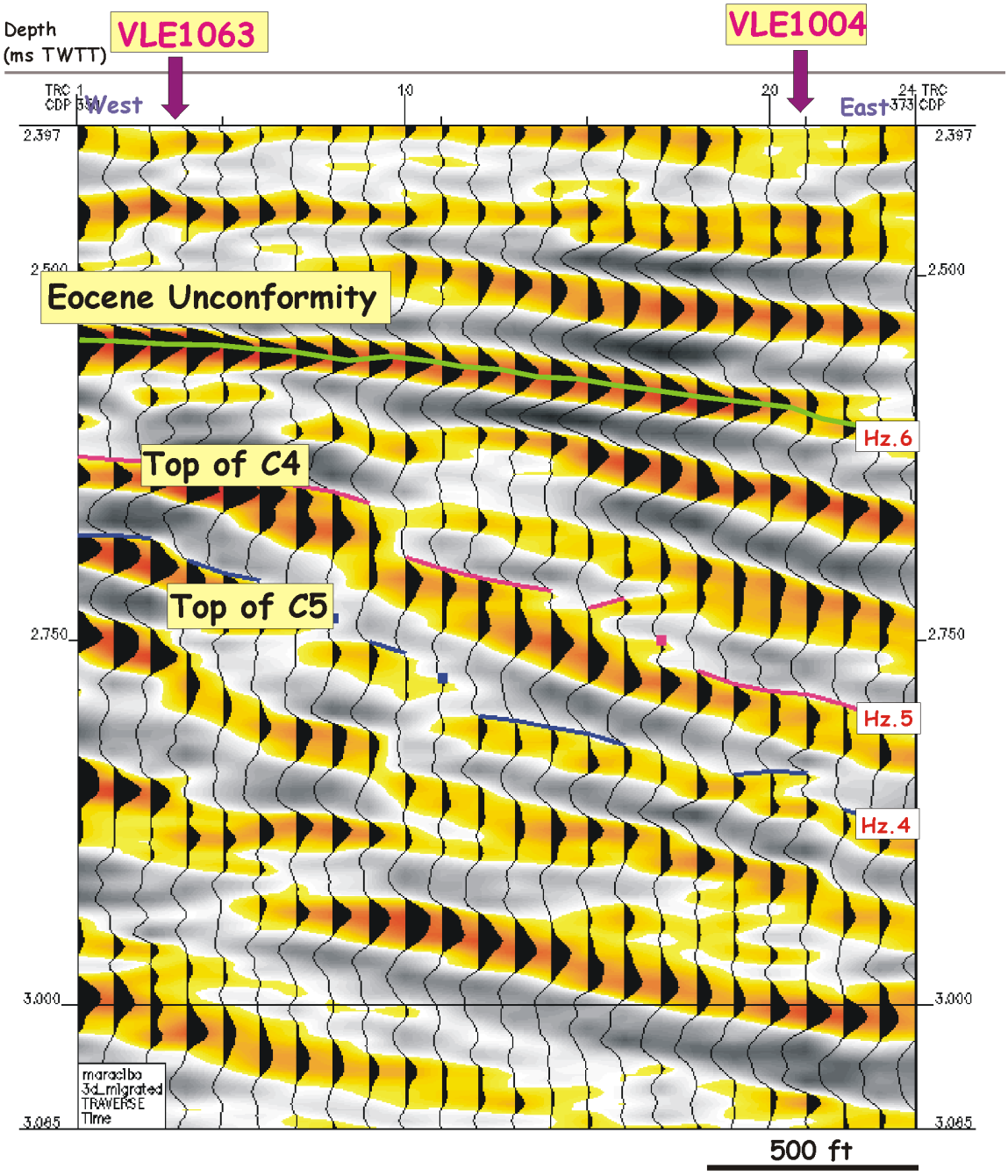

Figure 4-4. Arbitrary seismic line between wells VLE 1063 and 1004 showing top-lap seismic configuration toward the Eocene unconformity. See Figure 4-5 for the location.

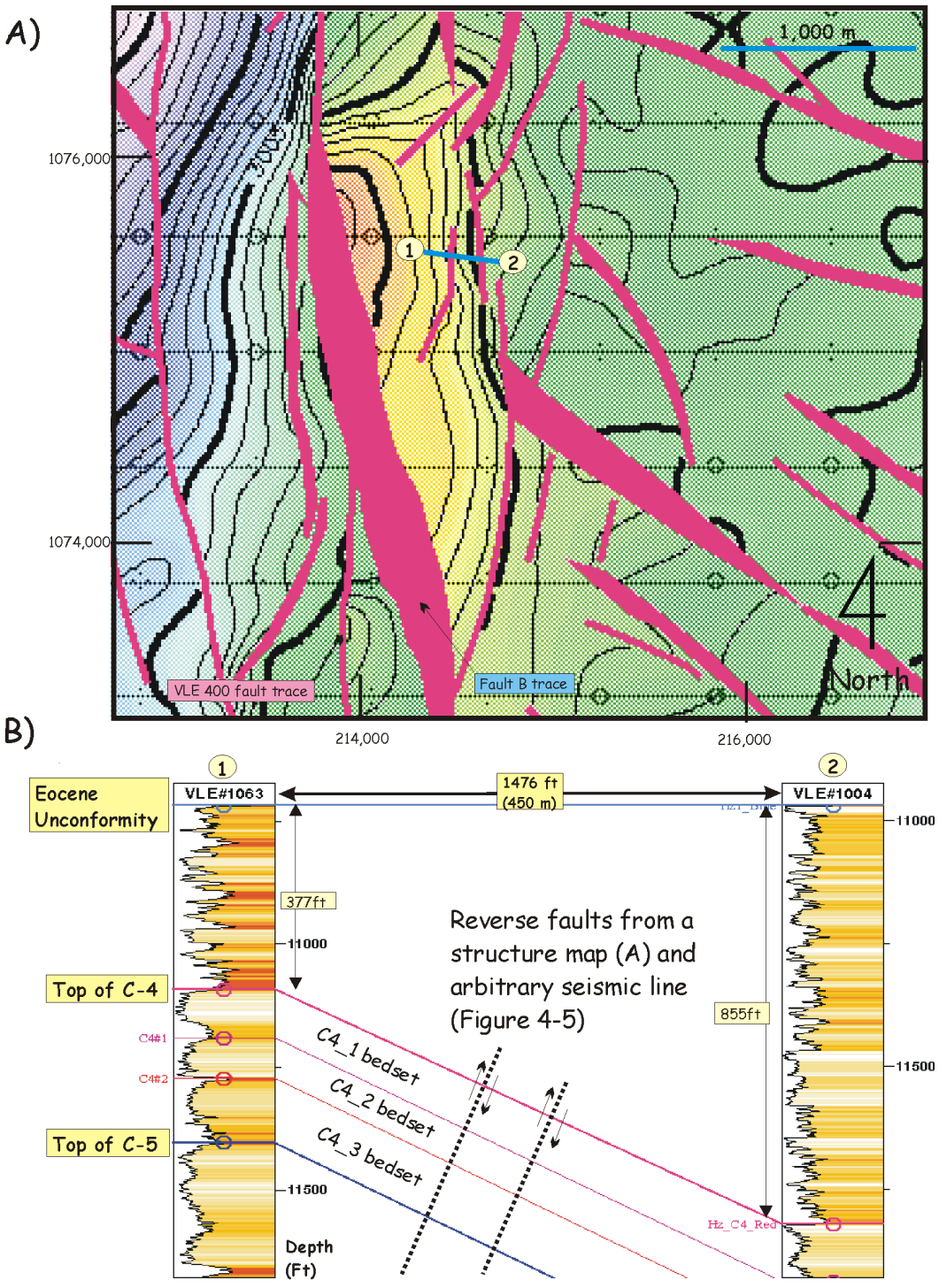

Figure 4-5. Well-to-well correlation of wells VLE 1063 and 1004 with time structure map of the top of the C-4 member.

better in the bottom parts of VLE1004 well (Figure 4-5). Thickness differences from the top of the C-4 member to the Eocene unconformity between the two wells are obvious; the thickness from the top of the C-4 member to the Eocene in the VLE1063 well is 377 ft (115 m), and in VLE1004 well it is 855 ft (260 m). The distance between the two wells is 1,476 ft (450 m).

Integration of well-to-well correlations, seismic facies and regional tectonics suggests uplift and erosion after conformable depositions of the C-5 through C-1~3 members (Figure 4-6). More than 478 ft (146 m) of sediments of the C-1~3 member in VLE 1063 were removed by the Eocene erosion. Regional progradation followed the transgression but progradation deposits are not recorded in the study area. More than 1,300 ft. (396 m) of the prograding "B" sandstones are reported in the basin (Antonio, 1998). Figure 4-7 shows an interpreted seismic profile including wells VLE1063 and 1004 with a conceptual process of uplift and erosion. Two possible reverse faults are suggested according to the concept, consistent with the VLE400 fault family movements. The two reverse faults are subtle, but they can be traced from seismic profile (Figure 4-4) with careful observation of the termination of seismic reflectors.

4.2. Role of structure and stratigraphy in hydrocarbon accumulation

Construction of structural and stratigraphic framework by evaluation of the orientation and distribution of structures and characteristics of depositional

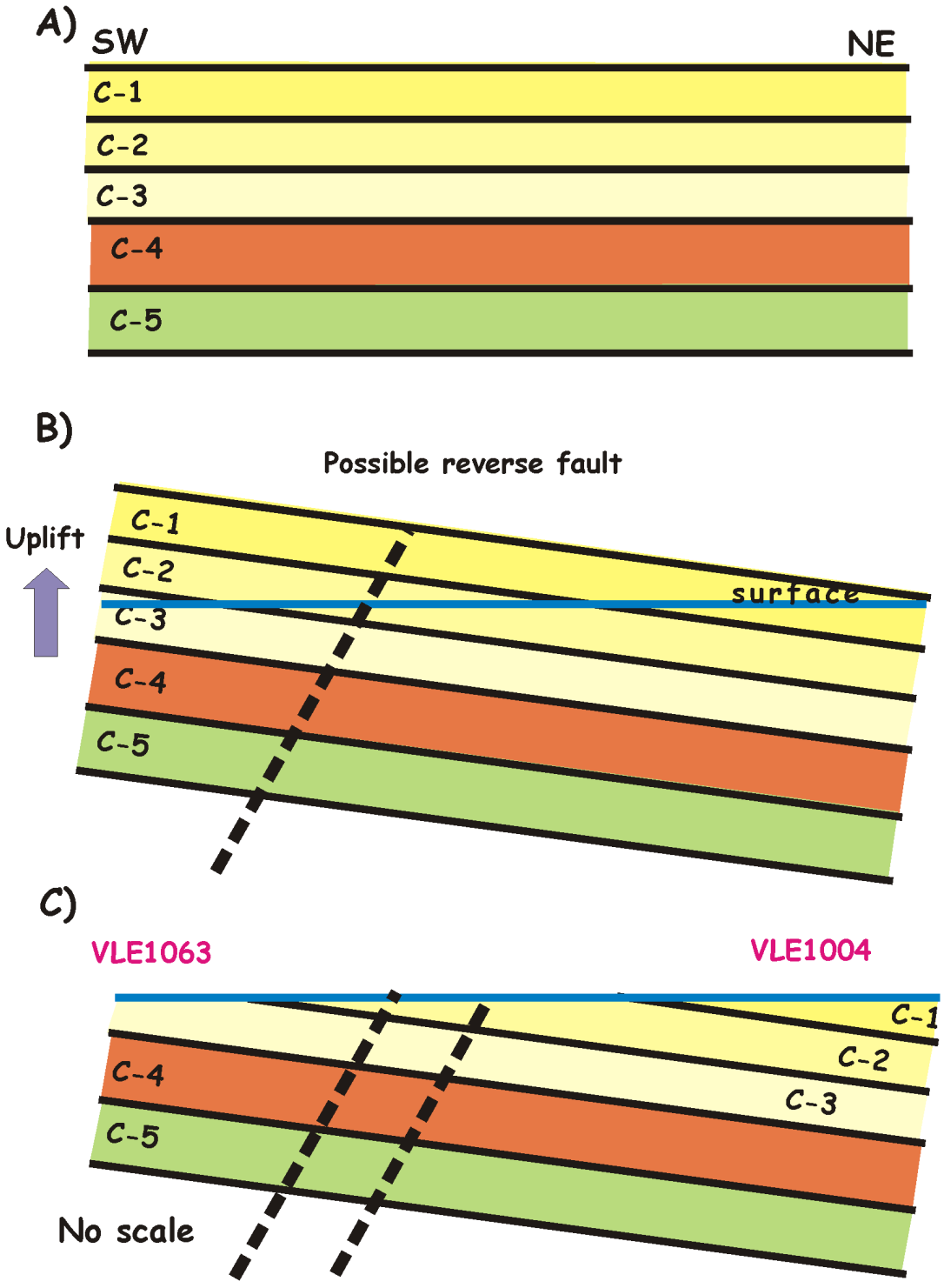

Figure 4-6. A thinning model generated by uplift and erosion of the C-1~3 member.

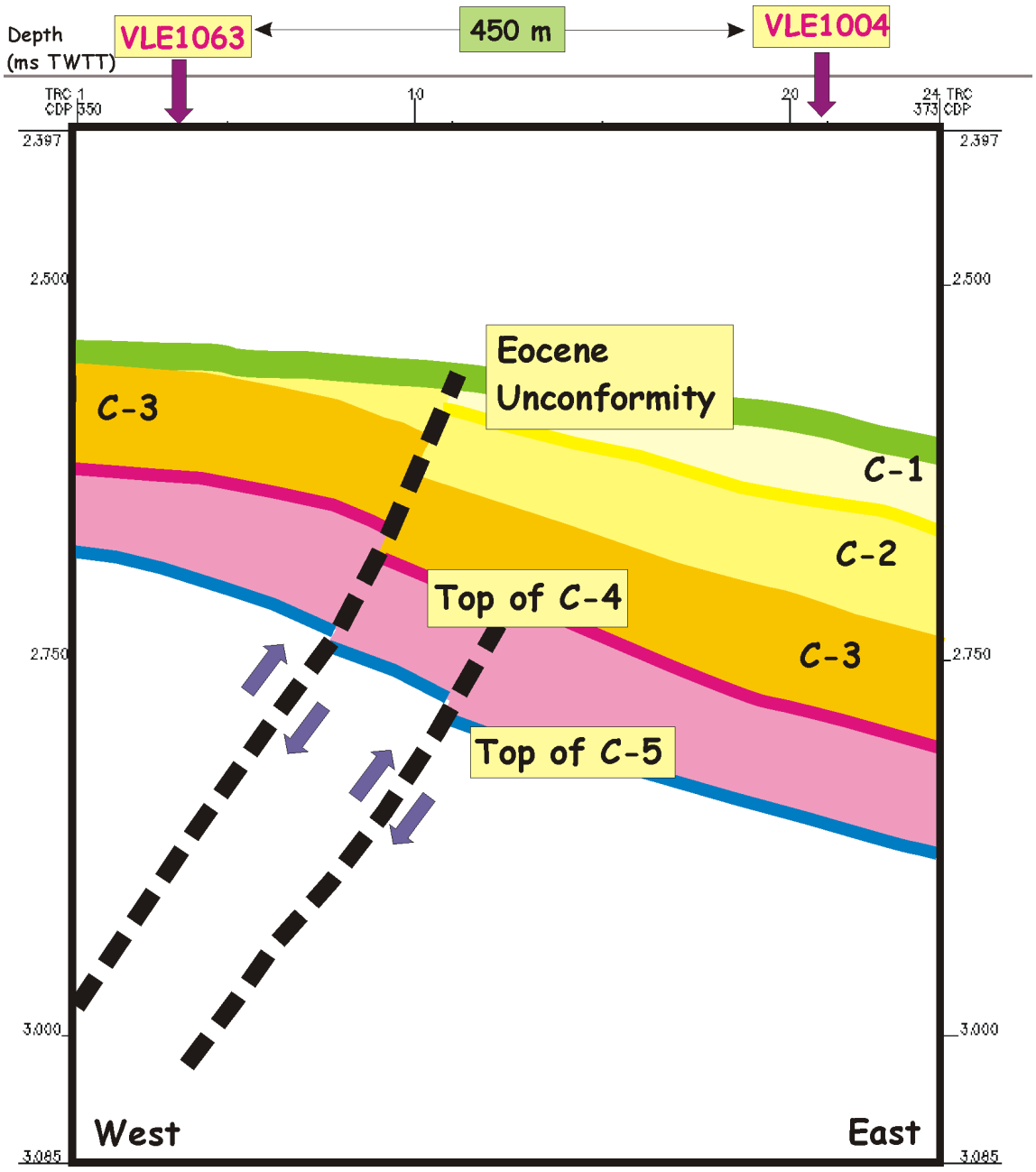

Figure 4-7. An interpreted seismic profile displays wells VLE 1063 and 1004 showing thickness variation from the top of the C-4 member to the Eocene unconformity. See Figure 4-5 for the location.

features is a basic step for understanding hydrocarbon accumulation trends, especially in a complex tectonic setting like the Maracaibo basin. The geologic structures and the stratigraphy in the field interacted closely and provided genetically integrated frameworks.

4.2.1. Reactivation of the VLE 400 fault family

The development of the thick Guasare marine shale on top of the La Luna Formation prevents vertical and lateral fluid flows from source to reservoirs except along faults. The VLE400 fault family, especially the northwest-southeast, en echelon normal faults, penetrates the reservoir and source rocks vertically and acts as a migration path. As it is recognized, the VLE 400 fault family has a multiple tectonic history including normal, reverse and strike-slip movements. During rejuvenation of the existing fault plane, it is expected that the fractured zone of the fault plane was increased, and then the quality and quantity of the permeable migration paths through the fault system improved. Fluid migration pathways are mainly controlled by the development of the faults and played an important role for hydrocarbon distribution in the field.

4.2.2. “Pop-up” structure

A prominent anticline developed on the regional Eocene unconformity in the field. The anticline has a four-way dip closure and appears to be fault-sealed on the west; producible hydrocarbons occur only in the eastern block. I

compared four different anticlinal modes : 1) A strike-slip restraining bend, 2) A scissors fault, 3) A fault-propagation fold and 4) Ductile flow of the Guasare Formation, a shale between the Misoa and La Luna, because of increased thickness of the Guasare in the uplifted area.

The basin has a long and complex tectonic history (Miller et al., 1958; James, 1990). The Eocene unconformity resembles a positive flower structure, whereas Misoa and Guasare structures suggest a mixture of strike-slip and scissors-like faulting. The structure of the La Luna is similar to a fault-propagation fold.

Evaluation of the structural and stratigraphic framework of the field shows that no single mode can explain the complicated structures. Therefore, I suggested a four-step basin evolution model of the field (Figure 4-2). The present complicated structures are mainly products of the evolution of the VLE400 fault family and incidentally to the ductile movement of the Guasare (Choi and Watkins, 2004). The ductile movement of the Guasare might cause the gaps during 2-D structural reconstruction, especially through the VLE400 fault family area. Even though 2-D structural reconstruction has a limitation for strike-slip movements, the gaps usually occur with the Guasare Formation instead of with distortion of all formations.

4.2.3. Misoa-Pauji sediments

The Misoa-Pauji sediments, which overlie the reservoir rocks in the western block of the VLE400 fault family, look like growth strata (Medwedeff, 1989) in the foreland basin system (Verges et al., 2002). The origin of the Misoa-Pauji sediments that developed in the western block of the VLE400 fault family was likely a combination of the uplift of the eastern block and strike-slip movements of the VLE400 fault system. Generally, a transgressive and regressive (T-R) cycle is controlled by eustatic, tectonic subsidence and sediment supply rate mainly related to climate and uplift. In a foreland basin system, the T-R cycle is closely related to changes in subsidence rate and uplift by tectonic loading. Using the characteristics of the basin, a typical T-R cycle is suggested by flexural subsidence and uplift (Castle, 2001). The Misao/Pauji sediments appear to be transgressive and might contain maximum flooding surfaces between the transgressive and regressive depositions. The Misoa-Pauji sediments covered the top of the C-1~3 member while the VLE 400 fault family was active from compression to shear stress. The thicker sediments in the western block remained in the strata, but the thinner sediments in the eastern block eroded out during the uplift and regional unconformity development (Figure 4-2).

4.2.4. Ductile movements of the Guasare Formation

A 2-D reconstruction of the interpreted seismic profiles shows missing volumes of the Misoa, Guasare and La Luna Formations within the VLE 400 fault family. Significant volumes of the Misoa Formation (Figure 4-8) disappeared through uplift and erosion, strike-slip movements of the VLE 400 fault, and partly ductile movements of the Guasare Formation. Reconstruction in 2-D by restoration and balancing is a useful technique in evaluating seismic data interpretation and understanding the tectonic movements through geological time. The method is based on a principal assumption: area is preserved (constant) before and after deformation. That means that bed thickness and bed length must be conserved, so volumes remain constant during deformation, and implies that the orientation of the cross-section is perpendicular to the direction of the stress (Rowan and Kligfield, 1989). Strike-slip movements dominated from the late Eocene to early Miocene, causing horizontal movements of the Misoa Formation. Ductile movement of the Guasare Formation through the VLE 400 fault family caused volume shifts in various directions. As the Guasare and the Misoa Formations clearly show, unusual thicker parts appear through the VLE 400 fault. Because the isochrons are generated by simple calculations between two horizons, a thinning area appears through the normal-fault polygons. This thinning area is not a depositional feature, but the computer generated contours because of normal faulting geometry. The thicker parts follow the VLE 400 fault and Fault B trend

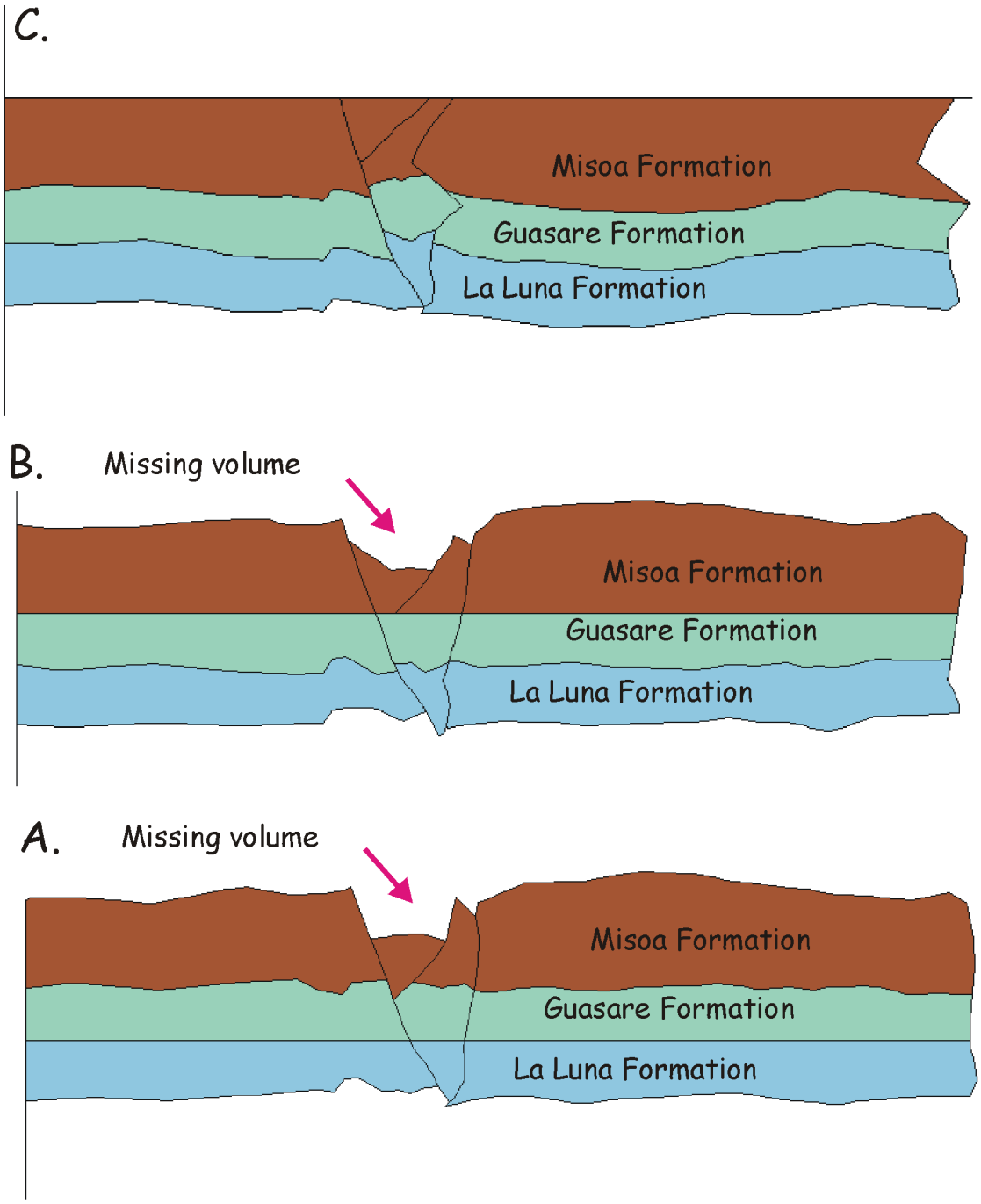

Figure 4-8. Reconstruction of seismic profile 640 using three different formation tops of the La Luna, Guasare and Misoa Formation from C to A. The missing volume may be caused by uplift and erosion, ductile movements, and strike-slip movements.

in the two isochrons and additional thicker parts appear through the normal faults in the western block of the Misoa Formation (Figure 4-9). Uplift and erosion, strike-slip movements of the VLE 400 fault family, and ductile movements of the Guasare Formation prevent precise generation of a balanced cross-section of the interpreted seismic profiles using 2-D reconstruction.

4.2.5. Retrogradational geometry by stacking of aggradation strata

The C members of the Misoa Formation penetrated by hydrocarbon production wells record aggradtional geometries of fluvial (upper), fluvial-marine (middle) and marine (lower) delta deposits through transgressive progresses controlled by tectonic flexural subsidence during the early Eocene. The Misoa Formation is one of a very few ancient examples of tide-dominated deltaic sandstones in the foreland basin system (Maguregui and Tyler, 1991). Foreland basin deposits typically have a large-scale transgressive and regressive cycle controlled by tectonic flexural subsidence, orogenic unloading and basin rebounds. During a thrust event, rapid flexural subsidence caused a fast relative sea level rise in the basin, and during quiescent times, sea level fluctuation by eustacy and sediments influx from orogenic belts created stacked depositional patterns such as aggradation. The primary controls for the cycle are flexural subsidence, and eustatic sea-level variations contribute to the stacking patterns of the reservoir sandstones during quiescent times.

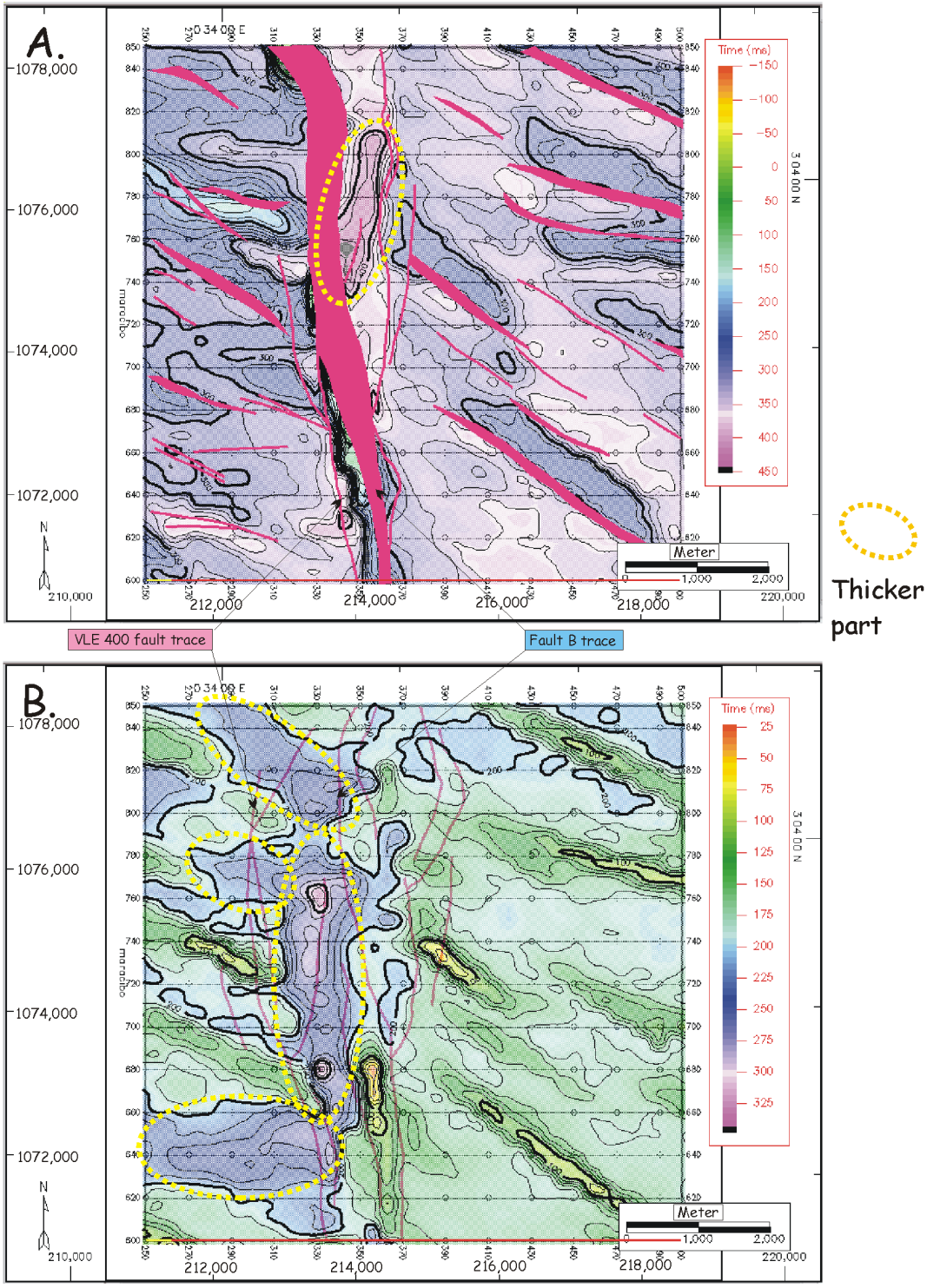

Figure 4-9. Possible ductile movements of the Guasare Formation. A) Isochron of the Guasare Formation. B) Isochron between the top of the Guasare Formation and the top of the C-5 member.

Specific stacking patterns of sedimentary packages such as progradation, aggradation and retrogradation can vary hierarchically. Individual staking patterns of the C-1~3, C-4 and C-5 members are aggradation; however, the overall stacking pattern of those members together is retrogradation. Thus, the stacking of three aggradational sedimentary packages makes the overall retrogradational geometry.

4.3. Discussion

The Maracaibo basin is famous as a giant oil field but it is not clear what makes the basin prolific. The tectono-sedimentary model, presented here for the petroleum system of the field, suggests three distinct factors: thick reservoir and source rocks; juxtaposition sealing by the growth strata, and development of efficient migration paths, not dispersed by carrier beds but controlled and concentrated by faults.

Transgressive deposits are usually thin because of their depositional characteristics developed during the rapid migration of shoreline landward and comparatively less sediment supply than when a volume of new accommodation space is created. The thick members of the Misoa Formation, informally called “C-sandstones” are well-known transgressive deposits which thickness has been reported as 2,300 to 16,000 ft (700 to 5,000 m) (Talukdar and Marcano, 1994) and recorded as more than 1,500 ft (460 m) in the field. The Misoa Formation

is unusually thick for a transgressive deposit. The proposed “retrogradtional geometry by stacking of aggradation strata” explains the unusual thickness of the formation well. Sediments flowed into the accommodation space created by tectonic loading during episodic transgression and generated aggradational strata. The following tectonic loading event provided new accommodation space for another aggradation strata deposition. Between the aggradation strata, thin transgressive sediments may have been eroded out by channelized cut-and-fill depositions of the aggradation strata above. Consecutive tectonic loadings created a series of aggradation strata and a retrogradational geometry higher in the hierarchy. Through the depositional processes, thick clastic sediments that developed in the basin act as excellent reservoirs in quality and quantity. Because of the stepping, consecutive tectonic loading, the Misoa Formation of the study area changed its depositional environment from fluvial (upper), to fluvial-marine (middle) to marine (lower) delta. Frequently, transgressive deposits can be good quality reservoir rocks because reworking processes provide mature clastic sediments (Snedden and Dalrymple, 1999; Posamentier, 2002). The Misoa Formation has a good quality and quantity due to the episodic transgression.

The thick, good quality reservoir rocks are suitable for accumulation of hydrocarbon, but they have a different aspect in the viewpoint of sealing, especially in case of sealing including faults. Without juxtaposition sealing by the growth strata, the thick Misoa Formation could not have a thick hydrocarbon

column. The growth strata of the Misoa-Pauji sediments, which have not been paid significant attention, play an important role in the sealing of the accumulated hydrocarbon in the trap including the VLE 400 fault family. Growth strata 1, which shows significant thickness, developed on top of the reservoir rocks in the western block. It may be related in some way to few hydrocarbon accumulations in deeper formations that have the same structural features as the Misoa Formation. The faulted anticlines are the common trapping style in the basin. The northeast-southwest trending faults including the VLE 400 fault family have a multi tectonic history and have few chances to act as sealing faults. Therefore, the growth strata on top of the reservoir rocks play an important role for lateral sealing of the reservoir. The VLE 400 fault family cannot be a lateral sealing fault, but could provide vertical migration paths. Compared to the migration by carrier beds, which dispersed hydrocarbon widely, the migration through fault planes provides hydrocarbon to the trapped area more efficiently in a vertical direction.

5. HYDROCARBON EXPLORATION POTENTIAL

Analysis of controls on hydrocarbon distribution based on the integrated evaluation of the VLE196 Lamar field provides conceptual and practical new hydrocarbon exploration potentials of the field. Although the field has a long exploration and production history, it has concentrated mainly on the Eocene Misoa Formation. Compared to the Misoa Formation, the new hydrocarbon exploration potentials may be insignificant; however, the new potential can be applied not only for the field but also for the basin, and can provide additional economic benefits.

There are three new exploration leads: Miocene faulted anticlines, Cretaceous sinkholes and sediments below source rock (Figure 5-1). The existing production wells didn't penetrate the Cretaceous sinkholes and sediments below source rock because they underlie the main reservoir, the Eocene Misoa Formation, and their crests are located in different areas.

5.1. Miocene faulted anticlines

Strike-slip movements of the VLE 400 fault family prevailed from the late Eocene to Pliocene and generated an anticline of the Eocene unconformity and similar structures of Miocene sediments. Two of the Miocene faulted anticlines were mapped by seismic horizons of Hz.7 and Hz.8 within the Miocene

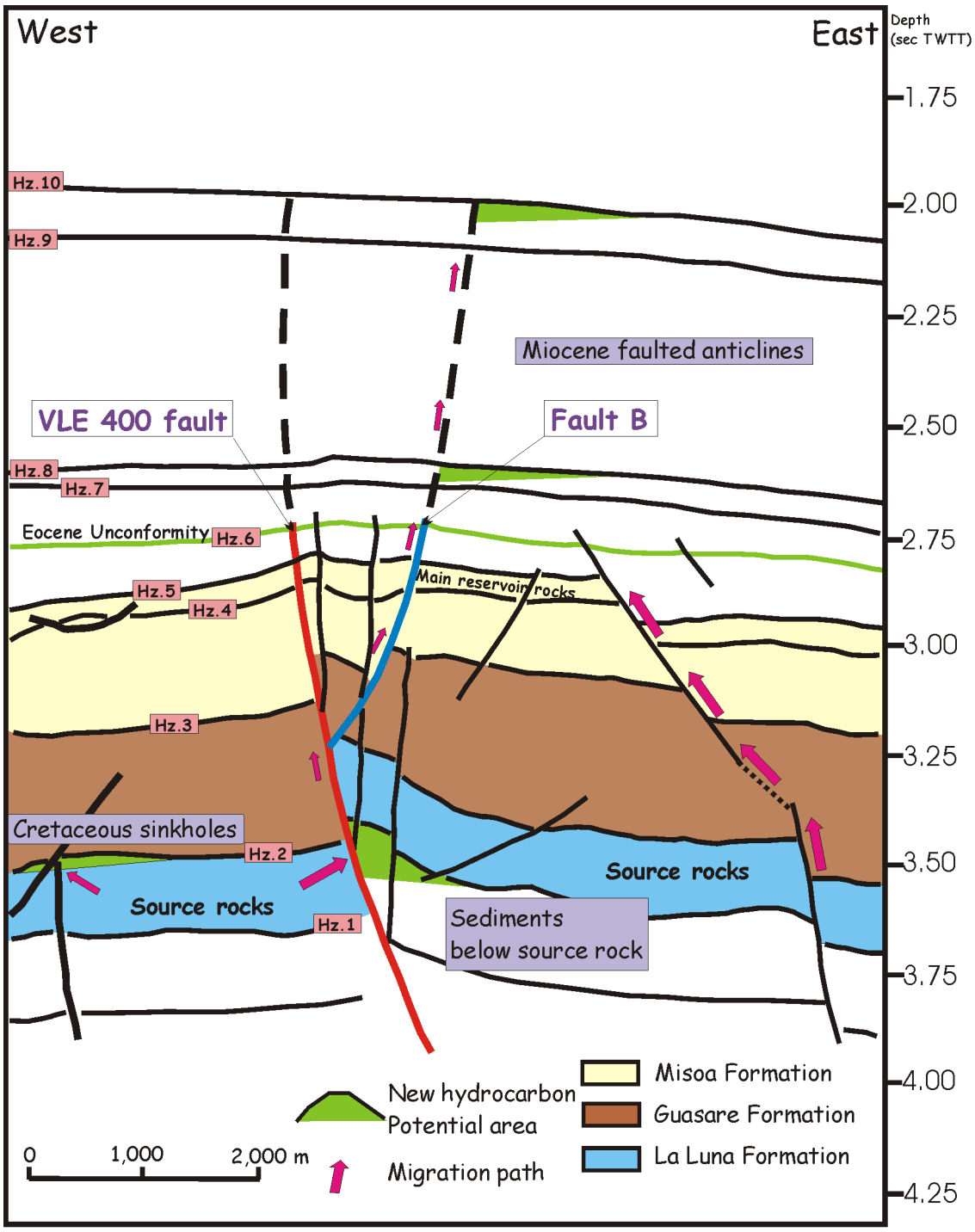

Figure 5-1. New hydrocarbon leads in Miocene faulted anticlines, Cretaceous sinkholes and sediments below the source rocks.

sediments (Figures 5-2). The structures of the two horizons are similar to the structure of the Eocene unconformity except for fault traces which were generated by early Miocene strike-slip movement. Faulted anticlines in the basin have an advantage of hydrocarbon migration because thick marine shales on top of the La Luna source rocks prevent hydrocarbon migration through carrier beds; therefore, fault planes connected with source rocks are favorable path ways.

5.2. Cretaceous sinkholes

Analysis of seismic facies from vertical profiles and horizontal time slices discloses several possible sinkholes of the Cretaceous La Luna Formation in the study area. Most of the possible sinkholes are associated with faults, and some are in accordance with the northwest-southeast trending normal faults developed by strike-slip movements of the VLE 400 fault family (Figure 5-3). The possible sinkholes are not penetrated by production wells, as illustrated in Figure 5-4. They represent favorable conditions for hydrocarbon migration from the La Luna Formation, the main source rocks. The overlying Guasare Formation can act as excellent seals for the sinkholes because of its thick shale sediments. The possible sinkholes are stratigraphic traps developed not by lithology but by reservoir property changes. The main exploration concern for the La Luna Formation is the reservoir quality. A permeable reservoir is more

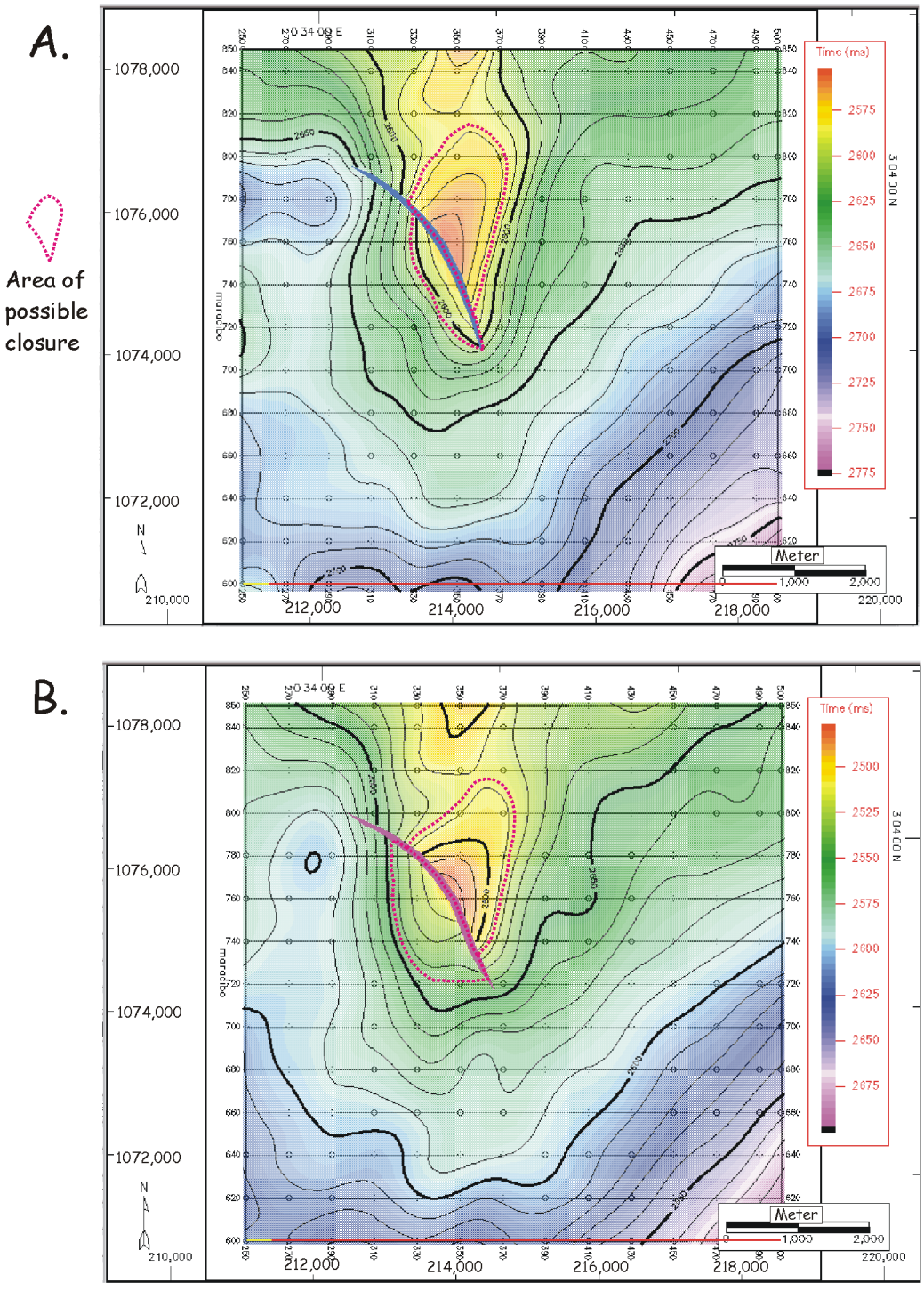

Figure 5-2. Miocene faulted anticlines. A) Time structure of Hz. 7. B) Time structure of Hz. 8. Contour interval is 10 ms twtt.

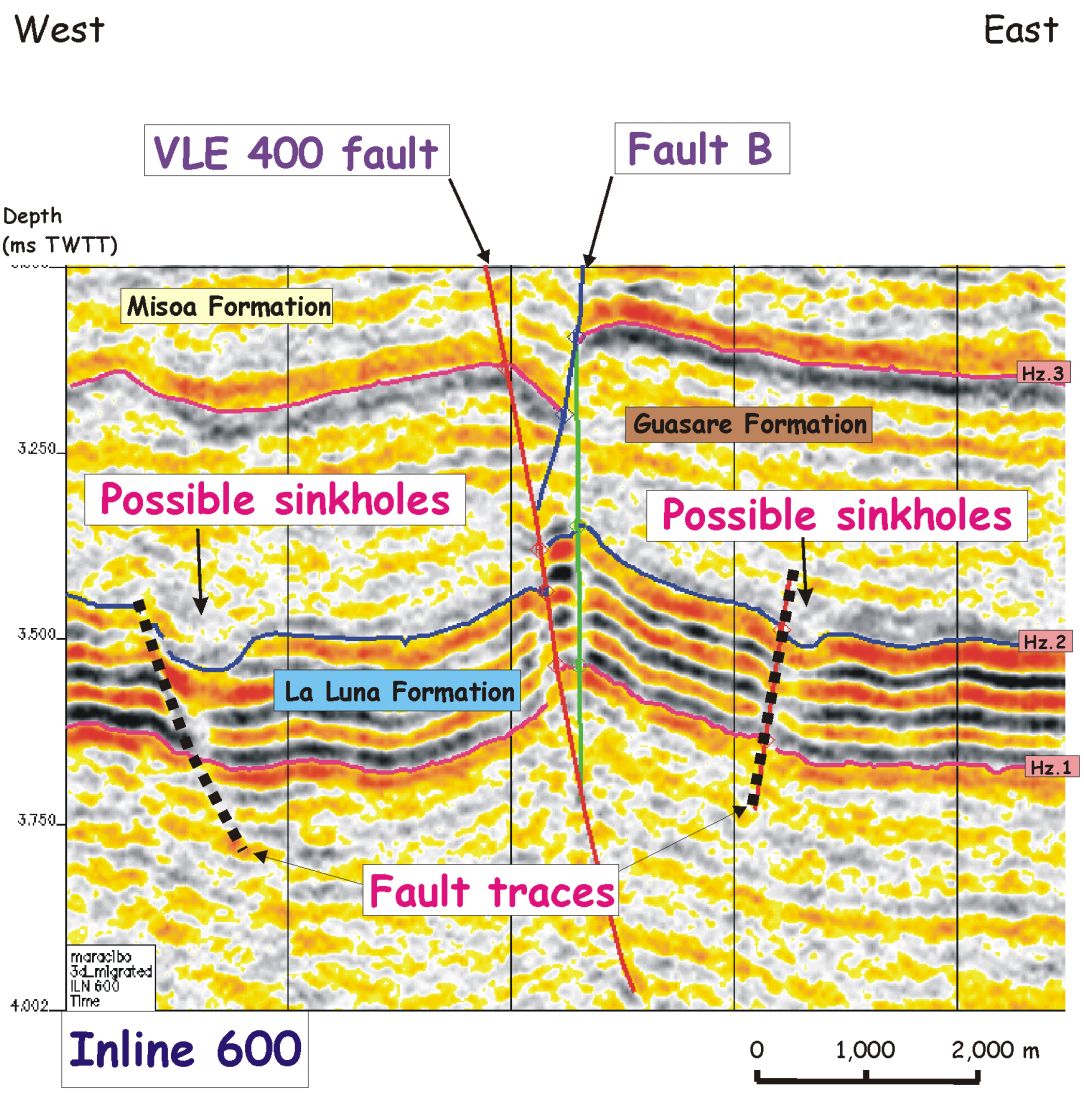

Figure 5-3. Seismic inline 600 showing the possible sinkholes through the fault traces. See Figure 5-4 for the location.

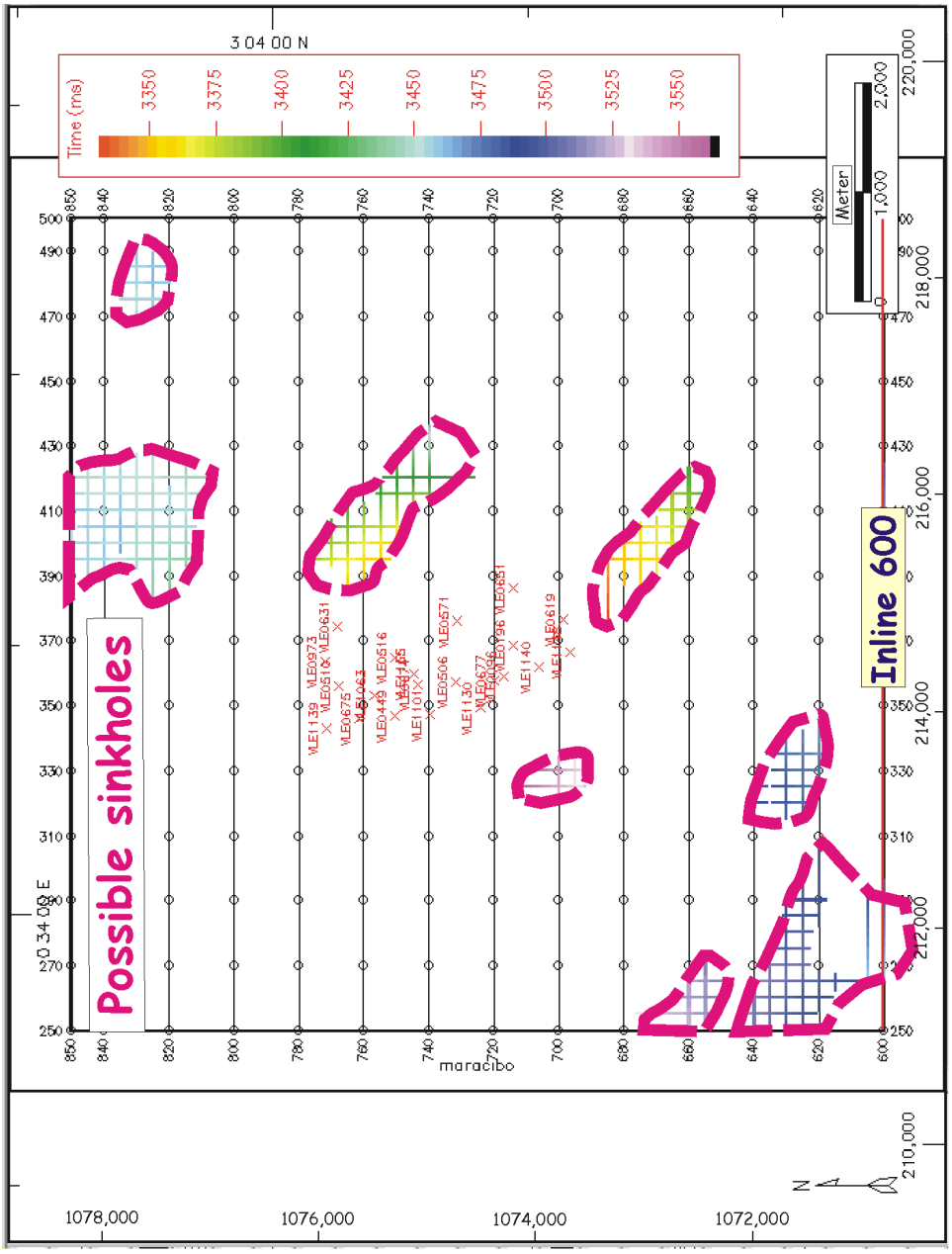

Figure 5-4. Possible sinkholes and production-well locations.

important than a structural closure in this formation, because the overlying Guasare Formation provides top seals and stratigraphic traps. The La Luna Formation is not likely to be a reservoir rock without secondary porosity and permeability. Fractured features caused mainly by faulting and surface weathering provided favorable reservoir rock conditions within the impermeable source rocks (Figure 5-3). In this regard, the possible sinkholes of the Cretaceous La Luna Formation are conceptually the most favorable conditions for hydrocarbon migration from the source rock. The area of possible sinkholes is not large, but there are many possible areas within the field and expected in the basin.

5.3. Sediments below source rocks

Below the La Luna Formation, sedimentary rocks in the basin are not well-defined by seismic data and well controls. No well data are available within the field, and very few well controls are apparent for the sediments below the source rocks in the basin. However, sedimentary rocks are expected below the La Luna Formation according to the 3-D seismic data, regional geology and tectonic evolution of the basin. Although some sedimentary rocks are reported below the La Luna Formation, they have not received any attention because they are under the main source rocks of the La Luna Formation. Structural closures of the sediments below the source rock are defined as illustrated in

Figure 3-1; it is clear that the closures of formations are not in the same location but separated from each other, as closures of deeper formations moving southward (Figure 5-5). The separation of closures among different depths may be caused by ductile movements of the Guasare Formation, mainly consisting of shale. Usually, formations below source rocks have some difficulties as hydrocarbon exploration targets because of the migration path. In the field, uplifting of the eastern block from the VLE 400 fault family provides direct contacts to the main source rocks as described in the Figure 5-1. Therefore, potential closure area of the sediments below the source rock have migration paths from the source rocks via juxtaposition due to faulting.

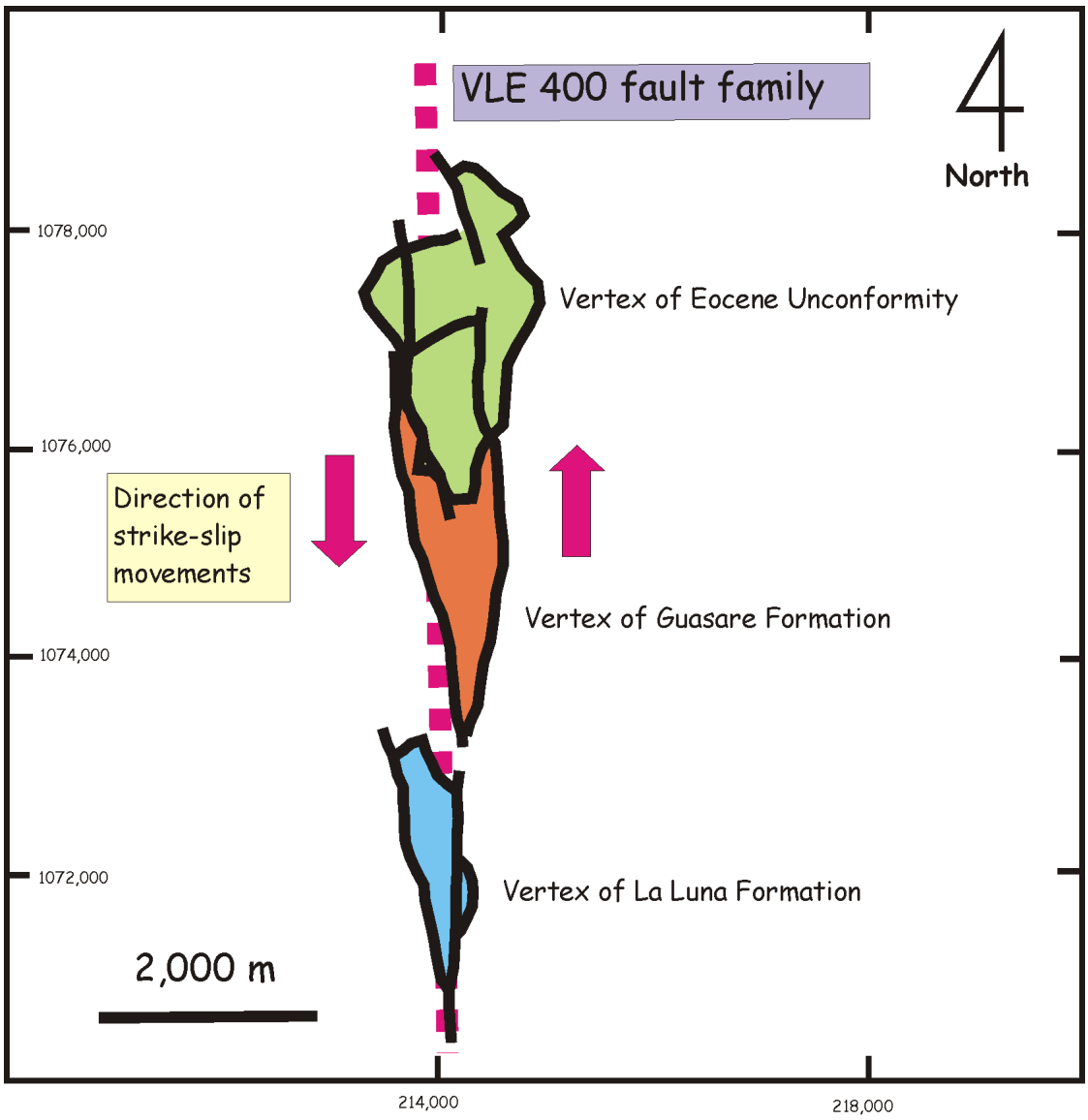

Figure 5-5. Structural highs of the La Luna, Guasare and Misoa Formation showing different locations.

6. CONCLUSIONS

Integrated evaluation of 3-D seismic data in the VLE 196 Lamar field, Maracaibo basin with well-log data using a growth strata concept reveals the complicated VLE 400 fault family evolution from normal, reverse and strike-slip movements, including subtle reactivation. Structural and stratigraphic interpretation of the field discloses controls of hydrocarbon distribution, especially the reason that hydrocarbons are trapped only in the eastern block.

Tectonic controls on the sedimentation shaped the characteristics of the Misoa Formation. Flexural subsidence generated transgressive deposition as a form of tide-dominated deltaic sediments in the basin. Abrupt sea level rises caused by sudden flexural subsidence provided distinct depositional environment changes for the C-5, C-4 and C-1~3 members of the Misoa Formation representing fluvial (upper), fluvial-marine (middle) and marine (lower) delta environments of depositions, respectively. The Misoa Formation shows retrogradational geometry with aggradational components. At least 480 ft (146 m) of the C-1 and C-2 bedsets, and probably some part of the C-3 bedset, eroded out near the VLE 400 fault family during uplift and truncation of strata, now below the Eocene unconformity.

Left-lateral strike-slip movements of Oca and Bocono faults generated block rotations between the two faults and created right-lateral movements of

northeast-southwest trending strike-slip faults including the VLE 400 fault family, which developed almost perpendicular to the two faults.

Subtle tectonic movements are evaluated by isochron maps with a growth strata concept. Five isochron maps below and above the Eocene regional unconformity are used for analysis of reactivation of the VLE 400 fault family. The VLE 400 fault family consisted of two groups: dipping east and dipping west. Because the VLE 400 fault family has a multi evolution history, identifying the stress through time is complicated. Isochron maps of the five formations show distinct features between two blocks across the fault family. Using a growth strata concept to analyze the isochron maps determined which faults were active during deposition of the certain formations. Of the Misoa-Pauji sediments analyzed by growth strata 1 (between the top of the C-4 member and the Eocene regional unconformity), the western block from Fault B (dipping west) is thicker. The Misoa-Pauji sediments, which developed in the western block, act as a juxtaposition sealing against the reservoir rocks in the eastern block. Due to the Misoa-Pauji sediments, hydrocarbon accumulated only in the eastern block. The growth strata concept is useful for evaluation of subtle tectonic movement analyses, especially those caused by rejuvenation of the existing fault, which is not easily detected by conventional seismic data interpretation. Evaluation of growth strata developed across the fault system provides stress orientations of tectonic movements. The advantage of subtle tectonic movement analysis using a growth strata concept is to identify subtle

movements beyond conventional seismic resolution. Another advantage is to classify different stress orientations of the same fault through geologic time.

Shales of the Guasare Formation mobilized through the VLE 400 fault family, especially north-south trending thrust and normal faults, and en echelon northwest-southeast trending normal faults in the western block. Ductile movements of the Guasare Formation along the north-south trending faults created a seal against the reservoir rock in the eastern block. Shale mobilization during transpressional movements of the VLE 400 fault family contributed to forming of the pop-up structure in the Eocene unconformity.

New hydrocarbon exploration potentials are identified after evaluation of depositional response to tectonic movements and controls on the hydrocarbon distribution in the field. The new potential areas are based on the existing petroleum system analysis, especially migration paths and trapping mechanisms. Miocene faulted anticlines are identified as one of the potential areas because they are attached with the VLE 400 fault family, which is classified as one of the migration paths. Cretaceous sinkholes are located favorably to serve as migration paths because they developed on the source rock. Sediments below the source rock have not been considered as hydrocarbon resources because they underlie the source rocks. However, the uplift of the sediments below the source rock in the VLE 400 fault family is high enough to make lateral contact with source rocks.

REFERENCES

Ambrose, W. A., E. R. Ferrer, S. P. Dutto, F. P. Wang, A. Padron, W. Carrasquel, J. S. Yeh, and N. Tyler, 1995, Production optimization of tide-dominated deltaic reservoirs of the lower Misoa Formation (Lower Eocene, LL-652 Area, Lagunillas Field, Lake Maracaibo, Venezuela: University of Texas at Austin, Bureau of Economic Geology Report of Investigations No. 226, 46 p.

Antonio, F.D., 1998, Architecture of a shore-zone reservoir system in Barua field, Maracaibo basin Western Venezuela: M.S. thesis, University of Texas at Austin, Austin, Texas, 130 p.

Audemard, F.M., 1992, Tectonics of western Venezuela: Ph.D. dissertation, Rice University, Houston, Texas, 763 p.

Berg, R.R., 1975, Capillary pressure in stratigraphic traps: AAPG Bulletin, v. 59, p. 939-956.

Bischke, R. E., 1994, Interpreting sedimentary growth structures from well log and seismic data (with examples): AAPG Bulletin, v. 78, p. 873-892.

Blaser, R., and C. White, 1984, Source rock and carbonization study, Maracaibo Basin, Venezuela: AAPG Memoir 35, p. 229-254.

Burke, K., 1988, Tectonic evolution of the Caribbean: Annual Review of Earth and Planetary Sciences, v. 16, p. 210-230.

Cant, D.J., and G. S. Stockmal, 1989, The Alberta foreland basin: relationship between stratigraphy and Cordilleran terrane-accretion events: Canadian Journal of Earth Sciences, v. 26, p. 1964-1975.

Castillo, M.V., 2001, Structural analysis of Cenozoic fault systems using 3D seismic data in the southern Maracaibo Basin, Venezuela: Ph.D. dissertation, University of Texas at Austin, Austin, Texas, 235 p.

Choi, B., and J. S. Watkins, 2004, Thrust tectonic movement provided hydrocarbon traps through the VLE 400 fault in the Maracaibo basin, Venezuela (abs.): AAPG Annual Meeting Program and Abstracts.

Dalrymple, R. W., 1992, Tidal depositional systems, *in* R.G. Walker and N.P. James, eds., Facies models: response to sea-level change: St. John's, Newfoundland, Geological Association of Canada, p. 195-218.

DeCelles, P.G., and K.A. Giles, 1996, Foreland basin systems: Basin Research, v. 8, p. 105-123.

Demaison, G., and B. J. Huizinga, 1994, Genetic classification of petroleum systems using three factors: charge, migration, and entrapment, *in* L.B. Magoon and W.G. Dow, eds., The petroleum system – from source to trap: AAPG Memoir 60, p. 73- 89.

Escalona, A., and P. Mann, 2003, Three-dimensional structural architecture and evolution of the Eocene pull-apart basin, central Maracaibo basin, Venezuela: Marine and Petroleum Geology, v. 20, p. 141-161.

Gurnis, M., 1992, Rapid continental subsidence following the initiation and evolution of subduction: Science, v. 255, p. 1556-1558.

Harding,T.P., and A. C. Tuminas, 1989, Structural interpretation of hydrocarbon traps sealed by basement normal block faults at stable flank of foredeep basins and at rift basins: AAPG Bulletin, v. 73, p. 812-840.

Holditch, S. A. & Associates Inc., 1997, Reservoir characterization of C-4 and C-5 intervals, VLE 196 Area, Block V, Lamar Field, Lake Maracaibo, Venezuela Volume 1, (unpublished) Report, 40 p.

James, K., 1990, The Venezuelan hydrocarbon habit, *in* J. Brooks, ed., Classic petroleum provinces: Geological Society of London, Special Publication, no. 50, p. 9-35.

Klemme, H.D., 1994, Petroleum systems of the world involving upper Jurassic source rocks, *in* L.B. Magoon and W.G. Dow, eds., The petroleum system – from source to trap: AAPG Memoir 60, p. 51-72.

Knott, S. D., 1993, Fault seal analysis in the North Sea: AAPG Bulletin, v. 77, p. 778-792.

Kulke, H., 1995, Regional petroleum geology of the world, Part II Africa, America, Australia and Natratica: Stuttgart, Germany, Gebr. Borntraeger Verlagsbuchhandlung, p. 489-515.

Link, M.H., C. K. Taylor, N. G. Munoz, J. E. Bueno, and P. J. Munoz, 1996, 3-D seismic examples from central lake Maracaibo, Maraven's block I field, Venezuela, *in* P. Weimer and T.L. Davis, eds, AAPG Studies in

Geology No. 42 and SEG Geophysical Developments Series No. 5: AAPG/SEG, Tulsa, p. 69-82.

Lugo, J., 1991, Cretaceous to Neogene tectonic control on sedimentation : Maracaibo Basin, Venezuela: Ph.D. dissertation, University of Texas at Austin, Austin, Texas, 219 p.

Lugo, J., and P. Mann, 1995, Jurassic Eocene tectonic evolution of Maracaibo basin, Venezuela, *in* A.J. Tankard, R. S. Suarez, and H.J. Welsink, eds., Petroleum basins of South America: AAPG Memoir 62, p. 699-725.

Maguregui, J. A., 1990, Evolution and reservoir properties of Middle Eocene Tide-dominated deltaic sandstones in eastern Lagunillas Field, Maracaibo basin, Venezuela: M.S. thesis, University of Texas at Austin, Austin, Texas, 171 p.

Maguregui, J.A., and N. Tyler, 1991, Evolution of middle Eocene tide-dominated deltaic sandstones, Lagunillas field, Maracaibo basin, western Venezuela, *in* A.D. Miall and N. Tyler, eds., The three-dimensional facies architecture of terrigenous clastic sediments and its implications for hydrocarbon discovery and recovery: SEPM concepts in sedimentology and paleontology, v. 3, p. 233-244.

Medwedeff, B. A., 1989, Growth fault-bend folding at southeast Loat Hills, San Joaquin Valley, California: AAPG Bulletin, v. 73, p. 54-67.

Miller, J. B., K. L. Edwards, P. P. Wolcott, H. W. Anisgard, R. Martin, and H. Anderegg, 1958, Habitat of oil in the Maracaibo basin, Venezuela: AAPG Bulletin, v. 42, p. 601-640.

Ostos R, M., 1990, Tectonic evolution of the south-central Caribbean based on geochemical data: Ph.D. dissertation, Rice University, Houston, Texas, 459 p.

Parnaund, F., Y. Gou, J. C. Pascaul, M. A. Capello, I. Truskowski, and H. Passalacqua, 1995, Stratigraphic systhesis of western Venezuela, *in* A.J. Tankard, R. S. Suarez, and H.J. Welsink, eds., Petroleum basins of South America: AAPG Memoir 62, p. 681-698.

Posamentier, H. W., 2002, Ancient shelf ridges – a potentially significant component of the transgressive systems tract: case study from offshore northwest Java: AAPG Bulletin, v. 86, p. 75-106.

Rowan, M. G., and R. Kligfield, 1989, Cross section restoration and balancing as aid to seismic interpretation in extensional terranes: AAPG Bulletin, v. 73, p. 955-966.

Royden, L. H., 1993, The tectonic expression of slab pull at continental convergent boundaries: Tectonics, v. 12, p. 303-325.

Skerlec, G.M., 1999, Evaluating top and fault seal, *in* E. A. Beaumont and N. H. Foster, eds., Treatise of petroleum geology/handbook of petroleum geology: exploring for oil and gas traps: AAPG Bulletin, p. 10-94.

Smith, D.A.,1980, Sealing and non-sealing faults in Louisiana gulf coast salt basin: AAPG Bulletin, v. 64, p.145-172.

Snedden, J. W., and R. W. Dalrymple, 1999, Modern shelf sand ridges: from historical perspective to a unified hydrodynamic and evolutionary model, *In* K. M. Bergman and J. W. Snedden, eds., Isolated shallow marine sand bodies: sequence stratigraphic analysis and sedimentological interpretation: SEPM Special Publication, v. 64, p. 3-28.

Talukdar, S.C., and F. Marcano, 1993, Petroleum systems of the Maracaibo basin, Venezuela (abs.): AAPG Bulletin, v. 77, p. 361.

Talukdar, S.C., and F. Marcano, 1994, Petroleum systems of the Maracaibo basin, Venezuela, *in* L.B. Magoon, and W.G. Dow, eds., The petroleum system – from source to trap: AAPG Memoir 60, p. 463-481.

Van Wagoner, J.C., H.W. Posamentier, R.M. Mitchum, P.R. Vail, J.F. Sarg, T.S. Loutit, and J. Hardenbol, 1988, An overview of the fundamentals of sequence stratigraphy and key definitions. *In* C.K. Wilgus, B.S. Hastings, C.G.St.C. Kendall, H.W. Posamentier, C.A. Ross, J.C. Van Wagoner, eds., Sea-level changes: an integrated approach. Society of Economic Paleontologists and Mineralogists Special Publication No. 42, p. 39-45.

Verges, J., M. Marzo, and J. A. Munoz, 2002, Growth strata in foreland settings: Sedimentary Geology, v. 146, p. 1-9.

Watkins, J. S., B. Choi, S. Arzuman, and S. Leveque, 2004, Shale mobilization and contributions to hydrocarbon accumulation in compressional tectonic regime, Lake Maracaibo region, Venezuela (abs.): AAPG European Region Conference with GSA Technical program.

Watts, N.L.,1987, Theoretical aspects of cap-rock and fault seals for single- and two-phase hydrocarbon columns: Marine and Petroleum Geology, v. 4, p. 274-307.

VITA

Name:	Byeonggoo Choi
Address	Myeongryoon-dong 1ga 31-2, Jongro-goo, Seoul, Korea.
Email Address:	bgchoi@knoc.co.kr

Education:	B.S., Geology, Korea University, 1986 M.E., Mineral &Petroleum Engineering, Hanyang University, 2001 M.S., Petroleum Geology, University of Aberdeen, 1994 Ph.D., Geology, Texas A&M University, August 2005.
Doctoral Dissertation:	Eocene Tectonic Controls on Reservoir Distribution in VLE196, Block V, Lamar Field, The Maracaibo Basin, Venezuela.
Experience:	March 1986 to present – Korea National Oil Corporation. January 2001 to May 2004 – Teaching Assistant, Department of Geology & Geophysics, Texas A&M University.